



Spring 2008

Timing and Nature of Post-Collapse Sedimentation in Kulshan Caldera, North Cascades, Washington

Dennis M. (Dennis Martin) Feeney
Western Washington University, d_m_feeney@yahoo.com

Follow this and additional works at: <https://cedar.wwu.edu/wwuet>



Part of the [Geology Commons](#)

Recommended Citation

Feeney, Dennis M. (Dennis Martin), "Timing and Nature of Post-Collapse Sedimentation in Kulshan Caldera, North Cascades, Washington" (2008). *WWU Graduate School Collection*. 654.
<https://cedar.wwu.edu/wwuet/654>

This Masters Thesis is brought to you for free and open access by the WWU Graduate and Undergraduate Scholarship at Western CEDAR. It has been accepted for inclusion in WWU Graduate School Collection by an authorized administrator of Western CEDAR. For more information, please contact westerncedar@wwu.edu.

**TIMING AND NATURE OF POST-COLLAPSE
SEDIMENTATION IN KULSHAN CALDERA,
NORTH CASCADES, WASHINGTON**

by

Dennis M. Feeney

Accepted in Partial Completion of the Requirements for the Degree
Master of Science

Moheb A. Ghali Dean of the Graduate School

ADVISORY COMMITTEE



Chair, Dr. Scott Linneman, Associate Professor




Dr. Chris A. Suczek, Associate Professor

Dr. Bernie Housen, Associate Professor

MASTER'S THESIS

In presenting this thesis in partial fulfillment of the requirements for a master's degree at Western Washington University, I agree that the Library shall make its copies freely available for inspection. I further agree that copying of this thesis in whole or in part is allowable only for scholarly purposes. It is understood, however, that any copying or publication of this thesis for commercial purposes, or for financial gain, shall not be allowed without my written permission.


Signature _____

Date June 10, 2008

MASTER'S THESIS

In presenting this thesis in partial fulfillment of the requirements for a master's degree at Western Washington University, I grant to Western Washington University the non-exclusive royalty-free right to archive, reproduce, distribute, and display the thesis in any and all forms, including electronic format, via any digital library mechanisms maintained by WWU.

I represent and warrant this is my original work, and does not infringe or violate any rights of others. I warrant that I have obtained written permissions from the owner of any third party copyrighted material included in these files.

I acknowledge that I retain ownership rights to the copyright of this work, including but not limited to the right to use all or part of this work in future works, such as articles or books.

Library users are granted permission for individual, research and non-commercial reproduction of this work for educational purposes only. Any further digital posting of this document requires specific permission from the author.

Any copying or publication of this thesis for commercial purposes, or for financial gain, is not allowed without my written permission.

Dennis Feeney
February 28, 2018

**TIMING AND NATURE OF POST-COLLAPSE
SEDIMENTATION IN KULSHAN CALDERA,
NORTH CASCADES, WASHINGTON**

A thesis Presented to
The faculty of Western Washington University

In Partial fulfillment of the Requirements for the Degree
Master of Science

by

Dennis M. Feeney
May 2008

Abstract

Sedimentary rocks found in the 4.5 x 8 km Kulshan caldera of the Mount Baker volcanic field in the North Cascades, WA, indicate that the post-collapse basin hosted a lacustrine environment shortly after the initial collapse at 1.149 Ma (Hildreth, 1996). The sedimentary rocks of the 14 Goat area in Kulshan caldera are well-preserved in 124 meters of stratigraphic exposure. Blocks of wall rock debris in the lower stratigraphy show instability in the caldera wall. Intermediate and late stages are mainly turbidites composed primarily of sediments derived from extra-caldera ignimbrite. From these I interpret the 14 Goat area of Kulshan to have been a steep and deep depositional basin for most of its history. Additional sedimentary structures found in Kulshan caldera reveal a complex environmental history. Trough cross-bedding within a well sorted sandstone indicates channelized flow. Clastic dikes resulted from the overburdening of wet sediments. Dropstones found throughout the stratigraphy indicate an active ice field. Outside the stratigraphic section but within the 14 Goat area oscillation ripples indicate shallow water and raindrop imprints show drying. Paleomagnetic analysis of 12 sites spanning the entire stratigraphic column failed to show that any magnetic transition was recorded in the Kulshan sediments. Anisotropy of magnetic susceptibility results confirm that grain settling from quiet water produced the most prominent magnetic fabric and confirm secondary alteration was likely the cause of scatter in the remanent magnetization signal. A conservative estimate for the duration of the lacustrine environment at Kulshan caldera is 157 ka leading to a minimum rate of sedimentation of 79 cm/ka. A shorter estimate suggests duration of 22 ka and rate of sedimentation of 560 cm/ka. The sedimentary environments of Kulshan caldera are similar to other calderas with post-collapse depositional records. Kulshan caldera compares favorably to depositional models for small calderas (less than 10 km).

PREFACE

This thesis is written as a journal article for submission. I will be submitting a version of this thesis that will be edited for content, space, and figures to the Canadian Journal of Earth Sciences. Appendices attached to this thesis will not be included in the article submission.

The Data Repository for this thesis is included as an attached CD, containing three folders: Paleomagnetism, $^{40}\text{Ar}/^{39}\text{Ar}$ dating, Plagioclase composition. The paleomagnetic section contains AMS results, .asc files, .fit files, .bdi files, .mea files, .loc files, .tau files, .lnp files, intensity measurements, and the randomness survey. The $^{40}\text{Ar}/^{39}\text{Ar}$ section contains the data retrieved from the noble gas mass spectrometer by Dr. Tom Ullrich at the Pacific Centre for Isotopic and Geochemical Research at the Department of Earth and Sciences, University of British Columbia. The plagioclase composition contains all microprobe data collected from thin sections analyzed at the Washington State University GeoAnalytical lab by Dr. Scott Cornelius.

ACKNOWLEDGEMENTS

First and foremost I would like to thank Scott Linneman. My experience as a graduate student would have been made great because of the great amount of support, knowledge and patience you gave me. I know that your time is valuable and I appreciate you sharing so much of it with me. Thanks also to my committee members Chris Suczek and Bernie Housen. Your edits, time in the field, and ability to be sounding boards proved to be valuable assets to this thesis.

This project would not have been possible without the following people. The interest in the topic and idea behind the thesis came from Kevin Scott of the USGS. I appreciate his entrusting me with this project. Russ Burmester spent countless hours helping calculate, interpret, explain the data, recalculate, reinterpret, re-explain the data, re-recalculate, re-interpret, and re-re-explain the data. Though I left many of our meetings in a complete stupor, I would be nowhere without his help. Thanks to George Mustoe who always seemed to be there when I needed some obscure tool or operation manual. Thanks to Dave Tucker for our 'informal' meetings and being a great sounding board. Additionally, thanks to all the faculty and staff of the WWU Geology Department. Your questions, comments, support and ideas have kept me on my toes for three years.

My wife, Chelsea, put up with many lonely nights not knowing if her man would return from slaying the dragons found inside the p-mag box. From the bottom of my heart, you are my favorite wife.

Financial support was provided by a fellowship from the NSF GK-12 program and grants from the WWU Geology Department and the Office of Research and Sponsored Programs.

TABLE OF CONTENTS

ABSTRACT	iv
PREFACE	v
ACKNOWLEDGEMENTS	vi
INTRODUCTION	1
GEOLOGIC BACKGROUND	2
Location and geographic setting	2
Geologic setting	2
Previous work	6
<i>Kulshan caldera</i>	6
METHODS	8
Stratigraphy and sedimentology	8
Magnetic stratigraphy	8
SEDIMENTOLOGY	9
Lithofacies and petrofacies	9
STRATIGRAPHY AND INTERPRETATION	12
Stratigraphic succession at 14 Goat area	12
Section 1	14
<i>Section 1 interpretation</i>	18
Section 2	20
<i>Section 2 Interpretation</i>	20
Section 3	23
<i>Section 3 Interpretation</i>	23
Section 4	23
<i>Section 4 Interpretation</i>	29
Additional sedimentary structures	30
MAGNETIC STRATIGRAPHY	30
ANISOTROPY OF MAGNETIC SUSCEPTIBILITY	32
AGE	35
DISCUSSION	36
REFERENCES	49

APPENDICES

Appendix A: Magnetic Stratigraphy	52
Appendix B: Plagioclase analysis	57
Appendix C: Petrography	62
Appendix D: $^{40}\text{Ar}/^{39}\text{Ar}$ date attempt	76
Appendix E. Maps	79

DATA REPOSITORY

1. Paleomagnetic files, folders and applications
2. $^{40}\text{Ar}/^{39}\text{Ar}$ files
3. Plagioclase compositions data

LIST OF TABLES

In text

Table 1. Randomness and Paleomagnetics	36
Table 2. Anisotropy of magnetic susceptibility	37

In appendices

Table B 1. Plagioclase compositions at 21 meters	58
Table B 2. Plagioclase compositions at 31 meters	59
Table B 3. Plagioclase compositions at 88 meters	60
Table B 4. Plagioclase compositions at 100 meters	61
Table D 1. $^{40}\text{Ar}/^{39}\text{Ar}$ data from the andesite sill	77
Table E 1. UTM coordinates	81

LIST OF FIGURES

In text:

Figure 1. Kulshan caldera location and geology	3
Figure 2. Kulshan caldera sedimentary unit and geographic points	5
Figure 3. Kulshan sedimentary cross section	6
Figure 4. Y shards found in tuffaceous sediments	10
Figure 5. Composition of plagioclase grains found throughout the section	11
Figure 6. Kulshan ignimbrite compared to tuffaceous sediments found in lake deposits	12
Figure 7. Stratigraphic Section	13
Figure 8. Section I	15

Figure 8. Section 1 photos	16
Figure 9. Section 2	21
Figure 9. Section 2 photos	22
Figure 10. Section 3	24
Figure 10. Section 3 photos	25
Figure 11. Section 4	27
Figure 11. Section 4 photos	28
Figure 12 Raindrops and ripples photos	31
Figure 13. Orthogonal plots	33
Figure 14. High temperature paleomagnetic directions	34
Figure 15. AMS data	44
Figure 16. AMS and Remanent magnetizations	45

In appendices

C Pks015-2 PPL & XPL photos	62
C Pks24-5-b PPL & XPL photos	63
C Pks031-3-t PPL & XPL photos	64
C Pks039-4 PPL & XPL photos	65
C Pks058-3 PPL & XPL photos	66
C Pks066-2 PPL & XPL photos	67
C Pk1066-3 PPL & XPL photos	68
C Pks073-5-t PPL & XPL photos	69
C Pks073-5-m PPL & XPL photos	70
C Pks093-4 PPL & XPL photos	71
C Pks099-3-b PPL & XPL photos	72
C Pks110-2-b PPL & XPL photos	73
Figure D 1. Plateau age	78
Figure E 1. Trail map of Kulshan caldera	79
Figure E 2. Location of stratigraphic column and an important site	80

INTRODUCTION

Kulshan caldera in the North Cascades of Washington has over 120 meters of well-lithified and outcropping sedimentary deposits, making it one of the few calderas with an exposed history of post-collapse sedimentation. The list of continental calderas worldwide with excellent stratigraphic records detailing the post-collapse depositional environment is brief: Crater Lake, Oregon USA (Nelson et al., 1994), Creede caldera, Colorado USA (Heinken et al., 2000; Larson and Crossey, 1996; Larson and Nelson, 2000), Lake Atitan, Guatemala (Newhall et al., 1987), Whitehorse caldera, Oregon, (Rytuba et al., 1981), Laguna de Ayarza, Guatemala (Poppe et al., 1985), and Lake Taupo, New Zealand (Riggs et al., 2001; Smith, 1991). Each caldera represents a different depositional environment due to factors that include preexisting topography (pre-existing lakes), type of bedrock, eruption size, caldera basin shape and size, and post-collapse eruption frequency. This study interprets the post-collapse sedimentation history of the Pleistocene Kulshan caldera in the North Cascades of Washington.

Analysis of the Kulshan caldera sediment package not only provides a rare example of post-collapse sedimentation but also sheds some light on the debate about the nature and duration of the transitional field states related to paleomagnetic reversals. Using $^{40}\text{Ar}/^{39}\text{Ar}$ dating methods on known transitional lavas, Singer et al. (2005) determined that the paleomagnetic field instabilities (including paleomagnetic excursions) begin 18 ky before the onset of a complete polarity reversal. These estimates of duration of the transitional field period are at odds with paleomagnetic studies of deep sea sediments, which determined that the full reversal process takes around 7000 years (Clement, 2004). The results from Clement (2004) were determined using 5.8 to 10.4 cm of sediments. $^{40}\text{Ar}/^{39}\text{Ar}$ plagioclase dates from Hildreth et al. (2004) limit the age of

Kulshan era volcanism from 1.149 ± 0.010 to 0.992 ± 0.014 Ma. Paleomagnetic results from Hildreth et al. (2004) show that samples from pre- and post- collapse lavas span the Jaramillo normal subchron. The Jaramillo normal subchron is constrained to 1.072 - 0.988 Ma. (Gradstein et al., 2004). Caldera basins with their abundant sediment supply and steep ring-faulted walls should experience high rates of sedimentation, from 7 cm/ka to 1000 cm/ka (Nelson et al., 1994), far greater than the deep sea sediment used in the Clement (2004) study. In this study I test whether a paleomagnetic analysis of Kulshan caldera sediments could contribute to the debate about the duration of magnetic reversals.

GEOLOGIC BACKGROUND

Location and Geographic Setting

Kulshan caldera is located on the northeast slopes of Mount Baker in the North Cascades of Washington (Figure 1). Kulshan caldera resulted from the largest eruption of the Mount Baker volcanic field. The oldest recorded eruption from the Mount Baker volcanic field formed Hannegan caldera 3.7 Ma (Tucker et al., 2007). After the Hannegan eruption the magmatic focus migrated to the southwest, and it currently resides beneath the active stratovolcano of Mount Baker (0.1 Ma) (Hildreth et al., 2003).

Geologic Setting

Kulshan caldera is one of only three Quaternary calderas located along the 1100 km Cascade volcanic range (Hildreth, 1996; Hildreth et al., 2004). Kulshan caldera is located at the junction of the North Cascades metamorphic complex, the Pliocene Lake Ann granodiorite pluton, and the late Pleistocene and Holocene andesitic Mount Baker edifice. The rim of Kulshan caldera is constructed of three pre-existing rock types

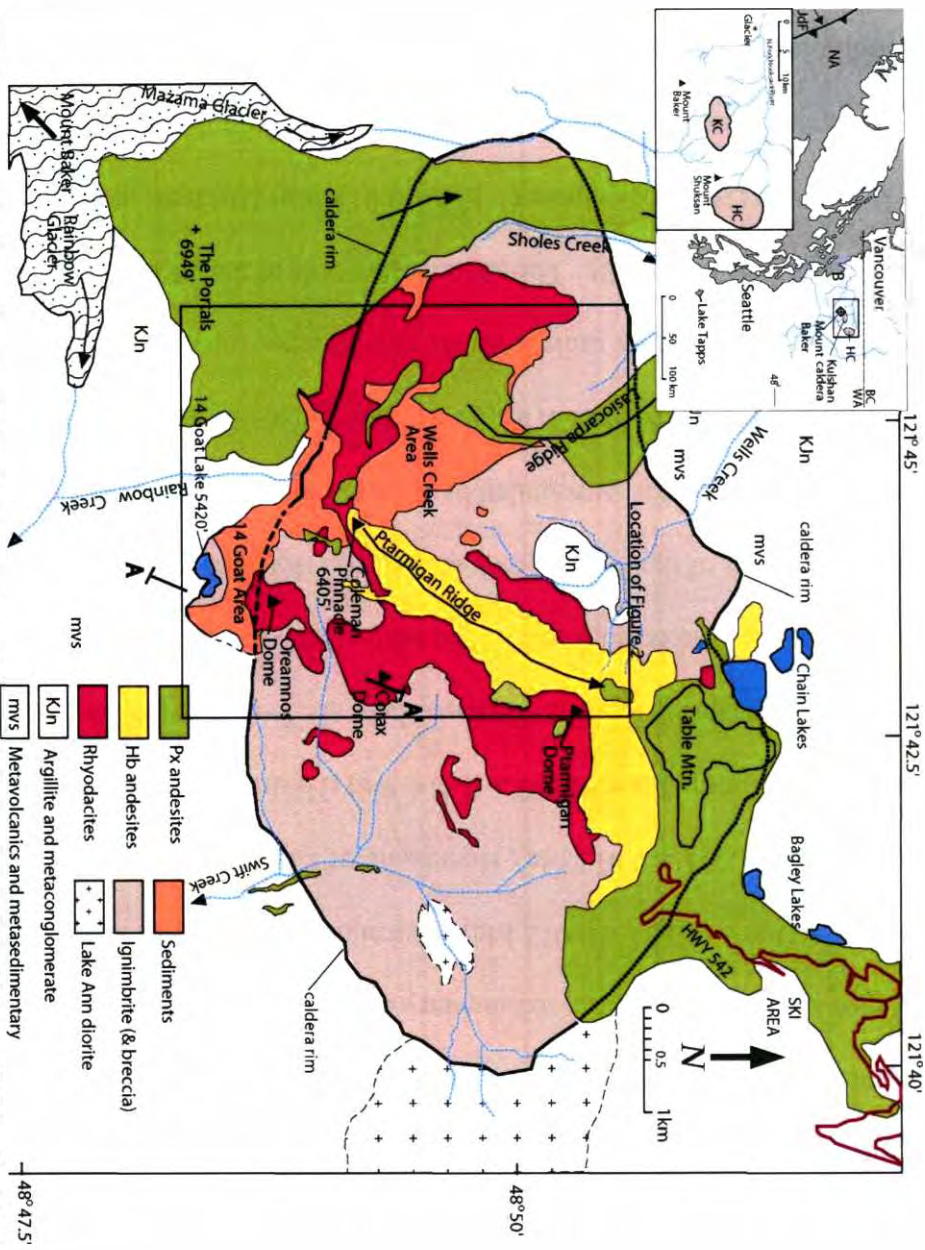


Figure 1. Pleistocene Kulshan caldera (KC) (1.149 ± 0.010 Ma) is located in the north Cascades of Washington, USA. Kulshan caldera is the second phase of Mount Baker's three stages of volcanism (First- Hannegan caldera (HC) 3.2 Ma, Third- Mount Baker proper, 100,000 to present.) Kulshan ignimbrite is rimmed by Paleozoic Chilliwack metasedimentary/metavolcanics (southern and northern rim), Pliocene Lake Ann stock granodiorite (east rim) and Jurassic/Cretaceous Nooksack argillite, sandstone, and conglomerate (northern and western rim). Kulshan era lavas include hornblende and pyroxene andesites, rhyodacite domes and ridges and ignimbrite. The focus of this study is the sedimentary rocks located on the southern rim. (modified from Hildreth, 1996)

(Figure 1). The northern and western rim is Jurassic-Cretaceous Nooksack argillite, conglomerate, and sandstone. The southern and northeastern rims are Paleozoic Chilliwack metasedimentary and metavolcanic rocks (Figure 1). The eastern rim of Kulshan caldera cuts a small portion of Pliocene Lake Ann granodiorite (Hildreth, 1996).

Kulshan caldera is most easily recognized by the rhyodacite ignimbrite, which represents the initial fill of the caldera. The ignimbrite is upwards of 1000 m thick. Post-collapse lavas relevant to the sedimentary environment at Kulshan caldera are: rhyodacite Oreamnos Dome (1.127 ± 0.012 Ma), Ptarmigan Dome (1.013 ± 0.009 Ma), rhyodacite Corax Dome (1.111 ± 0.012 Ma), rhyodacite of Lasciocarpa ridge (undated) and rhyodacite of Camp Kiser (0.992 ± 0.014 Ma) (Hildreth et al. 2004).

The lacustrine deposits discussed here are found in two zones off the southeast slopes of Mount Baker (Figure 2). The northernmost is in the Wells Creek area. The sedimentary unit of the Wells Creek area sits on rhyodacite ignimbrite from the initial Kulshan eruption and is surrounded by several post-collapse lavas. The 1.008 ± 0.008 Ma (post-collapse) (Hildreth et al., 2004) rhyodacite of Ptarmigan ridge separates the Wells Creek sedimentary units from the southern portion of the study area referred to as the 14 Goat area (Figure 2). The sedimentary unit of the 14 Goat area is located between the rhyodacite Oreamnos Dome (1.127 ± 0.012 Ma) (Hildreth et al., 2004) and Paleozoic Chilliwack metasedimentary rim rock (Figure 3). Though the lacustrine rocks are presently located in two separate areas, I presume these areas are remnants of what was originally a single basin.

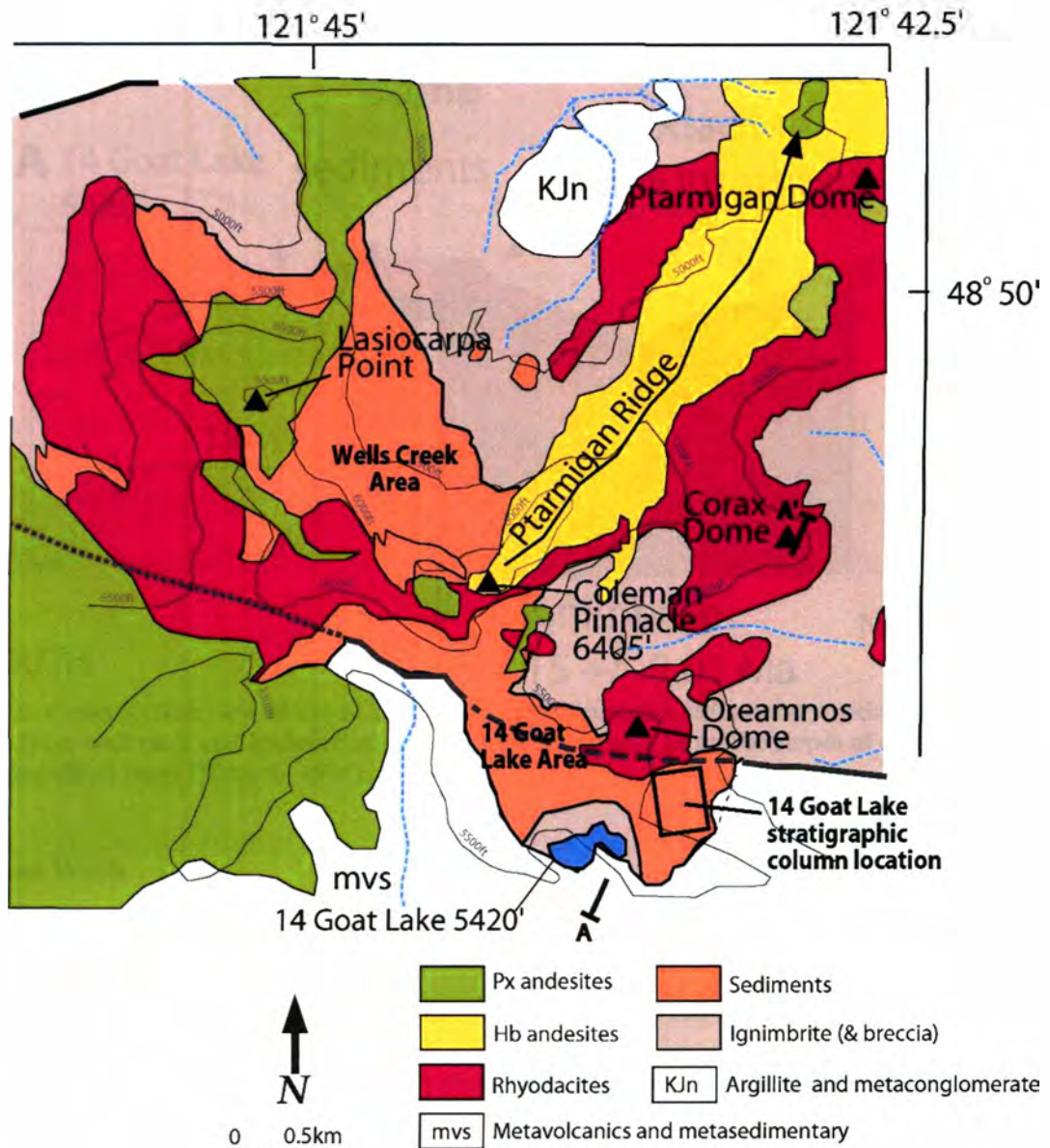


Figure 2. The orange areas represent the sedimentary units of Kulshan caldera. The northern most unit is referred to as the Wells Creek area. The southern most unit is referred to as the 14 Goat area (The name comes from the lake, the lake is officially unnamed but the locals call it 14 Goat lake). The rocks in the Wells Creek area are too hydrothermally altered; therefore, this study focuses on the rocks of the 14 Goat area. (modified from Hildreth, 1996)

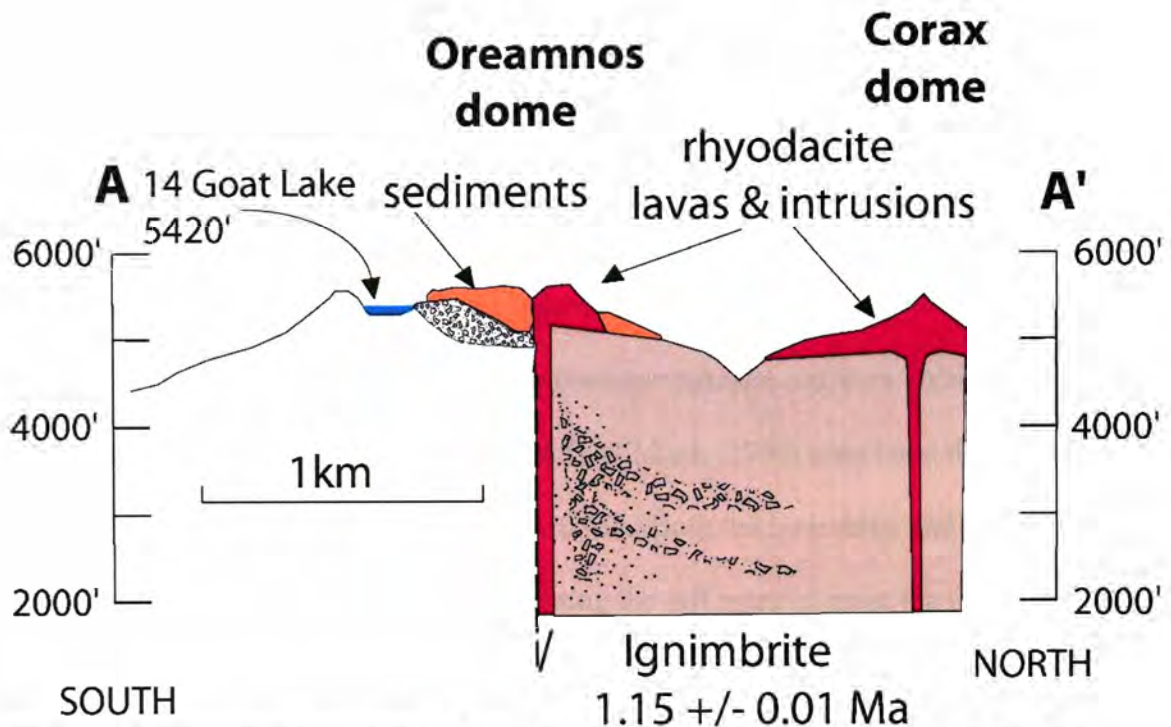


Figure 3. Cross section view of the 14 Goat area. The lacustrine sedimentary rocks sit on breccia from wall rock and ignimbrite. The sedimentary rocks lie on the slopes of Oreamnos dome. (modified from Hildreth, 1996)

Previous Work

Kulshan Caldera

Hildreth (1996) described the Kulshan sediments as ash-dominated muds, wall rock clasts, and breccia. Hildreth (1996) observed no evidence of fluvial channels, deltas, beaches, or ice contact. He noted that the unit shows evidence of ripples and bedding but no signs of mudcracks, fluvial processes, or pro-glacial processes are found. He indicated the general dip of the strata is 10 - 20° towards the center of the caldera. Hydrothermal alteration is found in various degrees throughout the strata, pyrite, calcite and clays occur in some locations.

Hildreth (1996) determined that Kulshan caldera was formed by a subglacial eruption. Hildreth noted two reasons for this interpretation, irregularities in the

ignimbrite and the nature of the Lake Tapps tephra. The ignimbrite lacks welding, has anomalously fine vesicularity and grades from lower layers that are pumice rich and poor in fines to upper layers rich in fines and poor in pumice. The Lake Tapps tephra, found in the lower Puget Sound region (Figure 1), was first described by Westgate et al. (1987). They noted thick bubble walls, low vesicularity, and vitric dust filling the vesicle walls of the Lake Tapps tephra as signs for a hydro-phreatomagmatic eruption. Although the origin was unknown to Westgate et al. (1987), Hildreth (1996) correlated the Lake Tapps tephra to the Kulshan eruption 1.149 ± 0.010 Ma. Both the ignimbrite and the tephra show signs of interaction with water, indicating the influence of more than just groundwater. Stratigraphy surrounding the Lake Tapps tephra (Westgate et al., 1987) indicates that the eruption occurred during a period of deglaciation and shortly following a period of glaciation in the lowlands; however, Westgate et al. (1987) indicate that, though the Puget Sound lowlands may have been temporarily denuded of ice, the ice caps of the Cascades and Olympics may have remained. Marine isotope stages also indicate the Kulshan eruption occurred during a warming phase (stage 35) (Gibbard and van Kolfschoten, 2004).

This study includes a petrographic description and stratigraphic interpretation of Kulshan caldera as a depositional basin. In addition to traditional field methods, Anisotropy of Magnetic Susceptibility (AMS) assisted in the interpretation of grain settling patterns. I used magnetic stratigraphy to approximate rates of sedimentation and the age of the lacustrine environment at Kulshan caldera.

METHODS

Stratigraphy and Sedimentology

Stratigraphy was measured on open outcrops. The sections were selected because of the 120 meters of continuous stratigraphy. Two of the sections were offset along strike due to the heavily eroded and steep terrain, and important stratigraphic features. Samples for plagioclase compositions were collected at 21 meters above the stratigraphic base, 30 meters, 88 meters and 99 meters. Compositions were determined on the Cameca Automated Electron Microprobe at the Washington State University GeoAnalytical Laboratory. Plagioclase crystals were randomly sampled to negate any compositional zoning differences.

Magnetic Stratigraphy

Seventy six coherent field-oriented samples from 15 different sites were collected from the lacustrine sediments. These blocks represent 13 stratigraphic horizons and 2 dike related sites. The blocks were taken to the Pacific Northwest Paleomagnetism Laboratory (PNPL) at Western Washington University, individually cored with a nonmagnetic bit and marked according to PNPL standards. The cores were then cut with a nonmagnetic diamond saw blade into individual specimens and labeled to match paleomagnetic standards set by PNPL. Anisotropy of magnetic susceptibility (AMS) of samples was analyzed on an AGICO KLY3-S Magnetic Susceptibility Bridge. AMS results determine the degree and orientation of mineral fabrics in the rocks being tested. Analyses of the remanent magnetization were performed using standard paleomagnetic techniques involving step-wise thermal demagnetization. Resulting magnetizations were measured with a 2-G 755 Cryogenic magnetometer.

SEDIMENTOLOGY

Lithofacies and Petrofacies

The complex interaction between subaqueous depositional processes in a volcanically active basin and a wide variety of volcaniclastic and nonvolcaniclastic sediments gives Kulshan caldera a wide range of lithofacies in the sedimentary sequence. Grains from Kulshan caldera range in size from clay and silt to clasts more than a meter in diameter. There are four primary components to the Kulshan caldera sedimentary units: fine vitric ash, lithic fragments, sand-sized crystals, and pumice. The fine vitric ash is predominantly microscopic shards of pumice that have been winnowed to silts; some have been altered to clay. The fine vitric ash presents itself as shards formed from broken walls of vesicles in pumice (Figure 4). The term lithic fragments refers to clasts derived from surrounding wall rock. The lithic fragments range in size from block up to 1.5 meters in diameter to sand and can vary in composition from metaconglomerate and argillite to granodiorite and blocks of welded tuff. The lithic fragments are largely angular to subangular. The sand sized crystals includes angular grains of plagioclase, hornblende, biotite and to a small degree oxides. An analysis of plagioclase grain compositions indicates the primary source of plagioclase is the rhyodacite ignimbrite from the initial Kulshan caldera eruption 1.149 ± 0.010 Ma (Figure 5) (Appendix B). Finally pumice describes the pieces of reworked rhyodacite ignimbrite from the initial Kulshan caldera-forming eruption. The pieces of pumice are subangular compared to original ignimbrite (Figure 6). As described by White et al. (2001) the factors that determine settling rates for pumice are density, vesicularity, and vesicle inter-

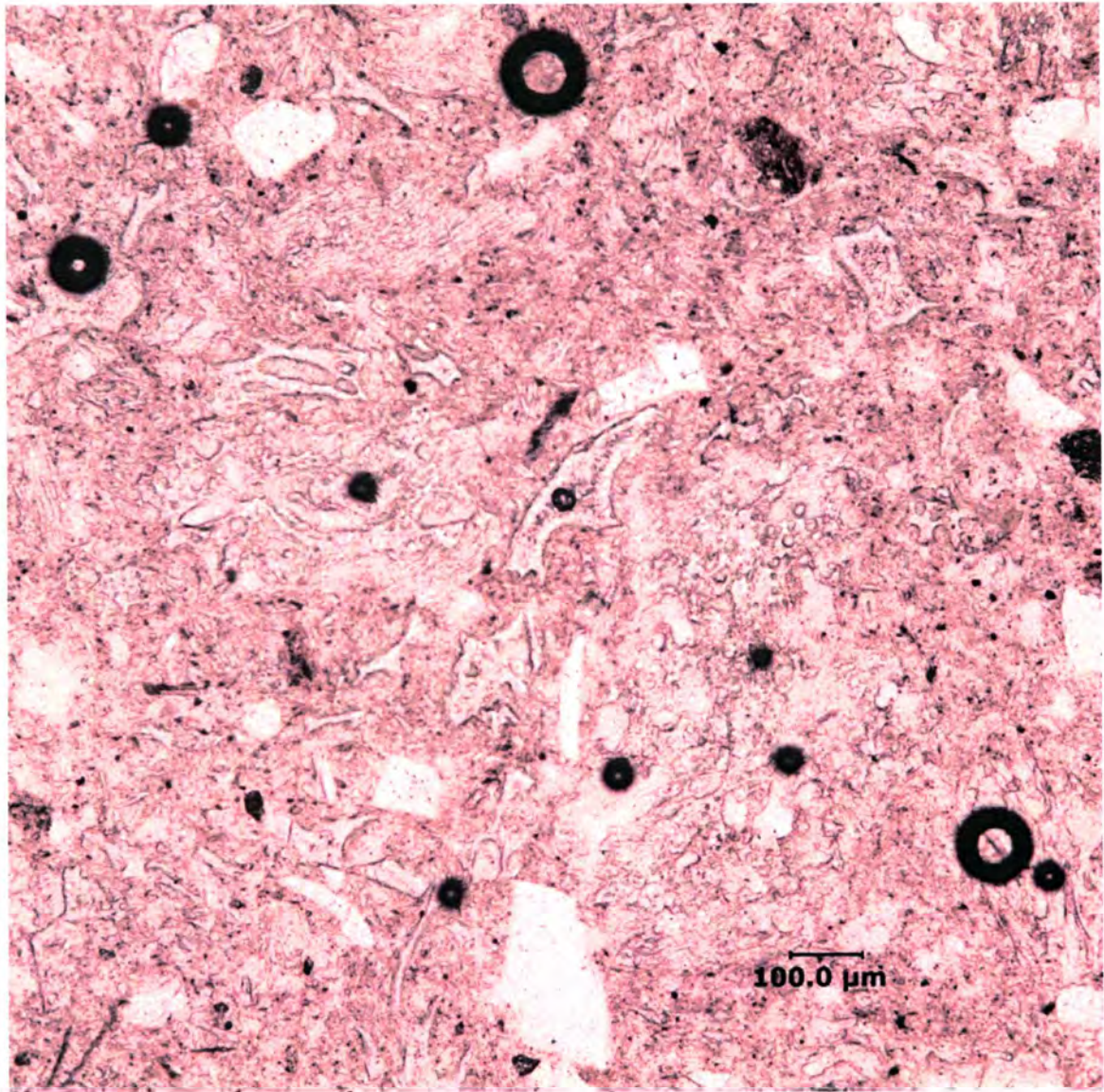


Figure 4. Pumice and pumice shards in a glass matrix in plain polarized light. The glassy matrix contains several examples of bubble Y-shards from weathered pumice. This micro-picture is taken from a sample found 24 meters up section in a tuffaceous unit, however, similar matrices can be found throughout the sequence.

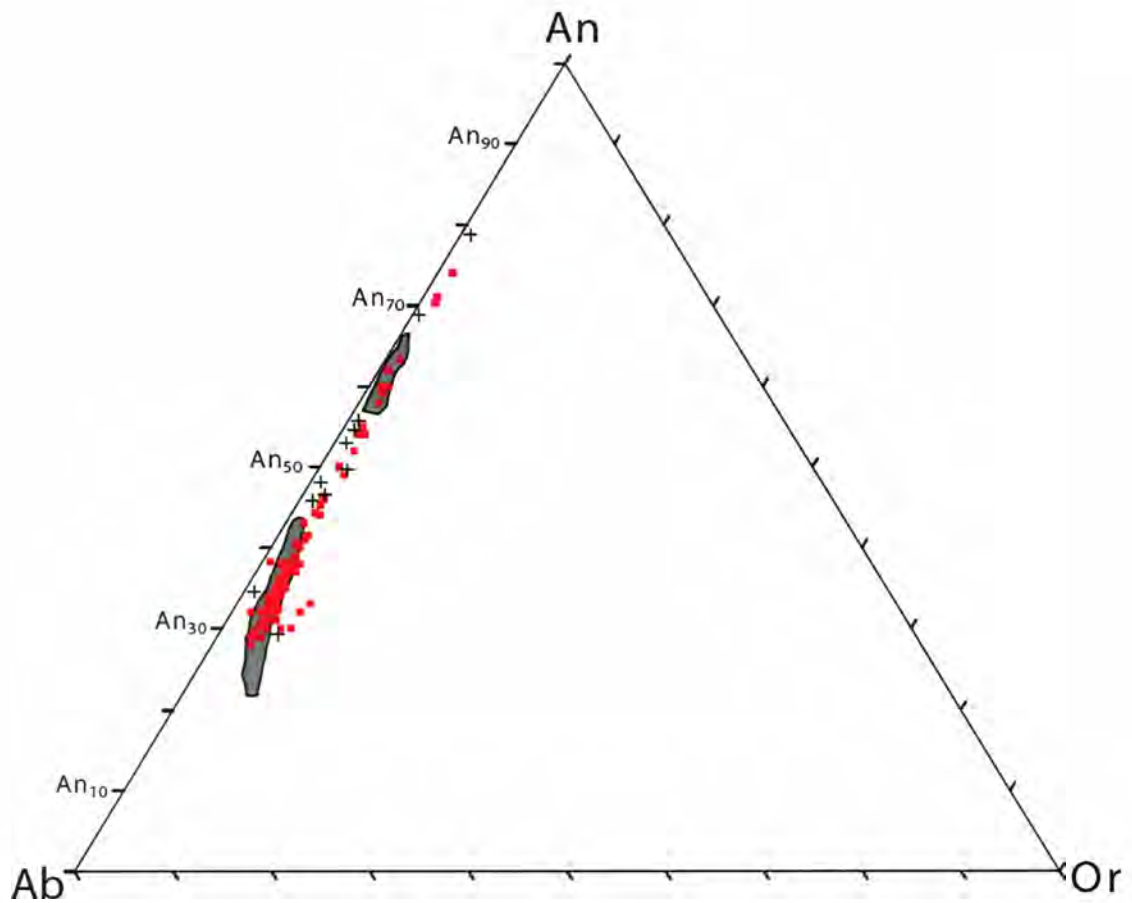


Figure 5. Plagioclase compositions from sand grains in Kulshan caldera (boxes) fit well with compositions from ignimbrite (grey areas and crosses indicating outliers) (Hildreth et al., 2004). The composition for all but five crystals fell in the andesine range (30 – 50% anorthite). The plagioclase crystals come from units 20 meters, 30 meters, 82 meters and 99 meters above the stratigraphic base. The plagioclase crystals are zoned, and sampling within the crystals was random.

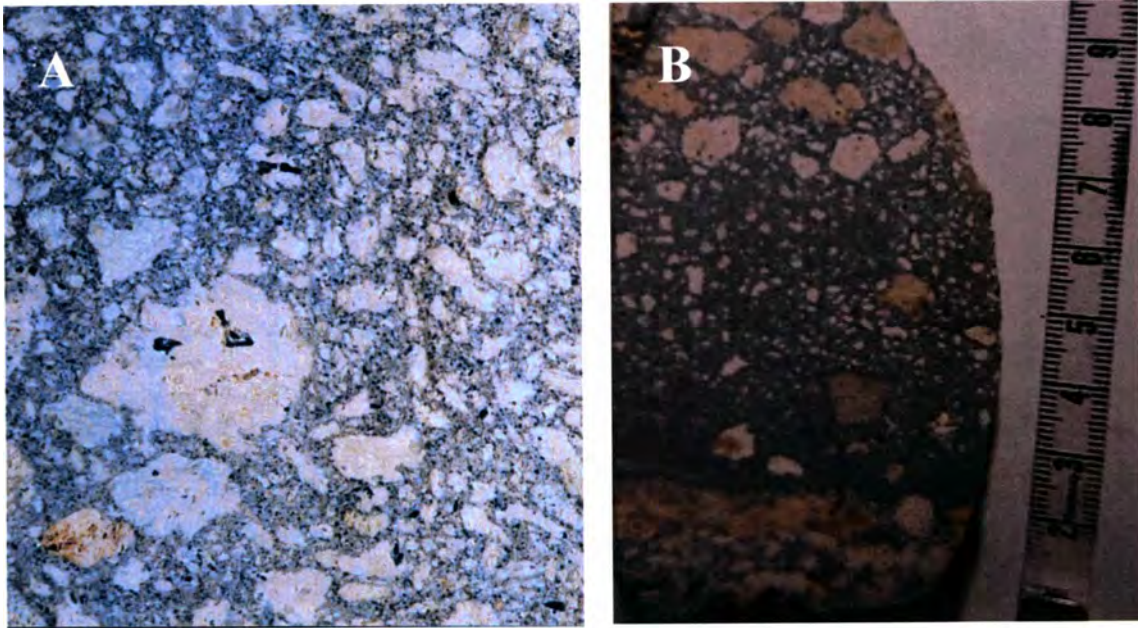


Figure 6. A. Close-up view of welded ignimbrite from the original Kulshan caldera eruption. Note the irregular pumice pieces and high angularity. The largest piece of pumice in the frame is 1.6 X 1.2 cm. (Hildreth, 1996). B. Pumice in fine ash as seen in Kulshan sedimentary sequence. Note the rounder edges compared to the original ignimbrite. This type of pumice is seen throughout the sedimentary sequence.

connectedness. These factors cause pumice to have erratic settling rates with normal or reverse grading or no grading at all.

STRATIGRAPHY AND INTERPRETATION

Stratigraphic succession at 14 Goat area

The stratigraphy of the sedimentary rocks at Kulshan caldera can be viewed in one complete column (Figure 7); however for discussion purposes the stratigraphy is split into four sections. Section 1 (the lowest section) starts southeast of Oreamnos Dome near the headwaters of the southern fork of Swift Creek (Figures 1 & 2). Section 1 is from 0 to 43 m. Section 2 begins 110 m southwest along strike at 20 m with Section 1. Section 2 is from 20 to 31 m, I repeat meters 20 to 43 due to vastly different stratigraphies.

Stratigraphic Column of 14 Goat area Kulshan Caldera

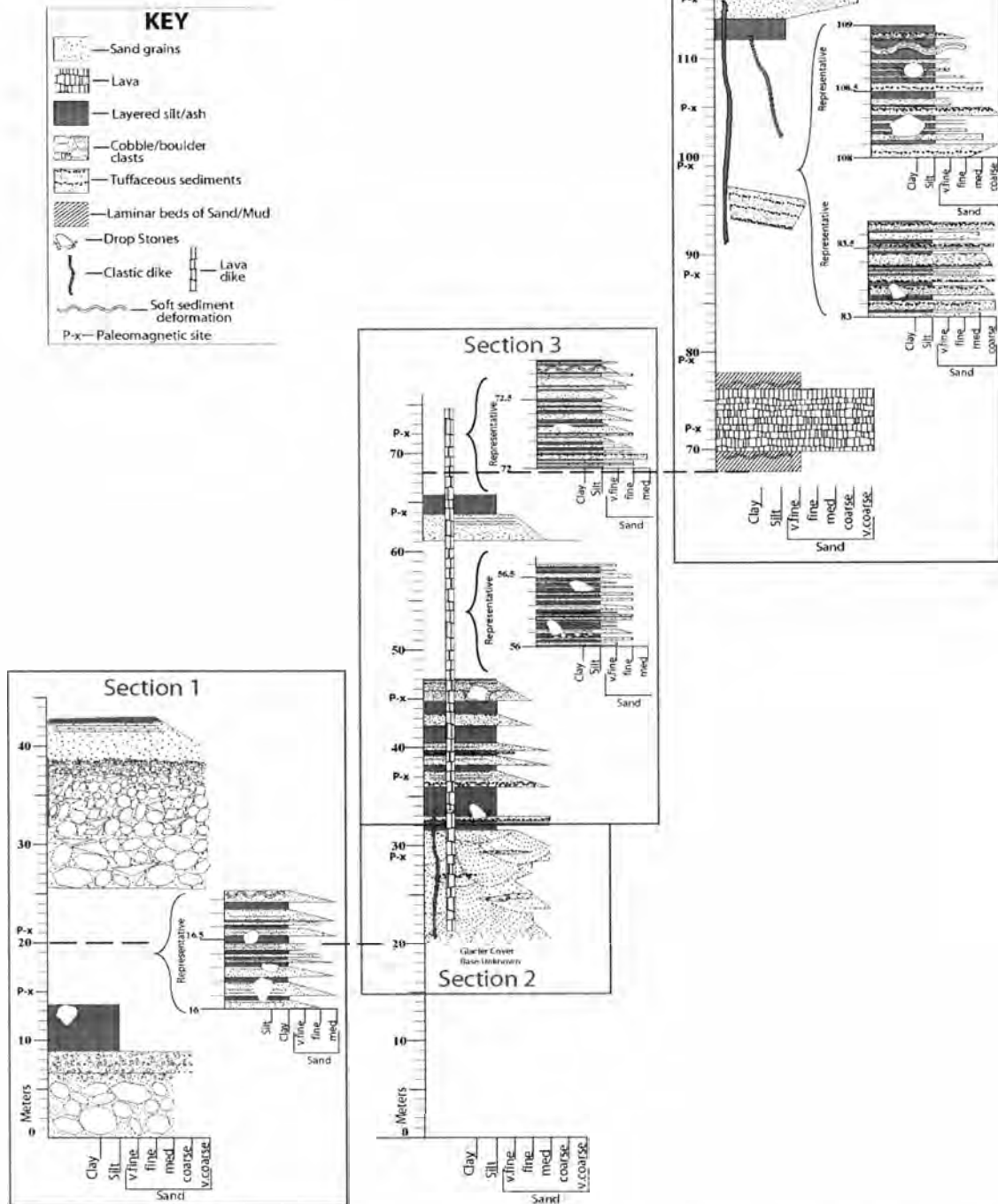


Figure 7. The entire stratigraphic column is 123 meters. Sections 1 and 2 have 23 meters of overlap in stratigraphy. The overlap is due to significant stratigraphic differences found around 24 meters in Section 2. Section 2 is located 110 meters southwest of Section 1. There is an overlap of 8 meters between Sections 3 and 4. This is due to the andesite sill that is discontinuous through the sequence. Section 4 is 20 meters west of Section 3.

Section 3 continues the sedimentary record above Section 2 from 31 to 75 m. Finally Section 4 is 40 m west along strike with the rhythmic turbidites in Section 3 at 70 m. I repeat meters 70 to 75 due to vastly different lithologies. The sedimentary rocks of Kulshan caldera are dipping anywhere from 0° to 16° to the north and northwest. Small-scale post-depositional deformation has caused some of the sedimentary rocks to dip to the south or southeast (sections up to 4 meters). This variation in dips is inconsistent and there is no large-scale pattern. The strike and dip measurements imply that post-volcanic subsidence was not great enough in Kulshan caldera to offset small-scale deformation caused by regional dome emplacement (Hildreth et al., 2004).

Section 1

Section 1 is the basal deposits from 0 to 43 meters. Section 1 (Figure 8) begins with the deposition of a six meter thick megabreccia primarily composed of Paleozoic Chilliwack Formation metaconglomerate. This sequence is deposited directly on the Paleozoic Chilliwack Formation metaconglomerate basement/rim-rock. Unlike the sedimentary sequence in the Wells Creek area, which begins on Kulshan caldera ignimbrite, the sedimentary rocks in the 14 Goat area are deposited on a shelf of Chilliwack metaconglomerate. Clasts range in size from more than one meter to sand-sized matrix. The unit is clast-supported. Sitting atop the megabreccia is a 2.5 m thick section of bedded, poorly indurated breccia. The contact between the megabreccia and the breccia is a thin bed (less than 5 cm) of sand. The clasts of the breccia are pebble to cobble sized and are composed of the same metaconglomerate as the megabreccia below. The grains in the matrix are sand. Sand makes up 35% of the unit. This section is clast supported.

Figure 8 Section 1 0 - 43 meters

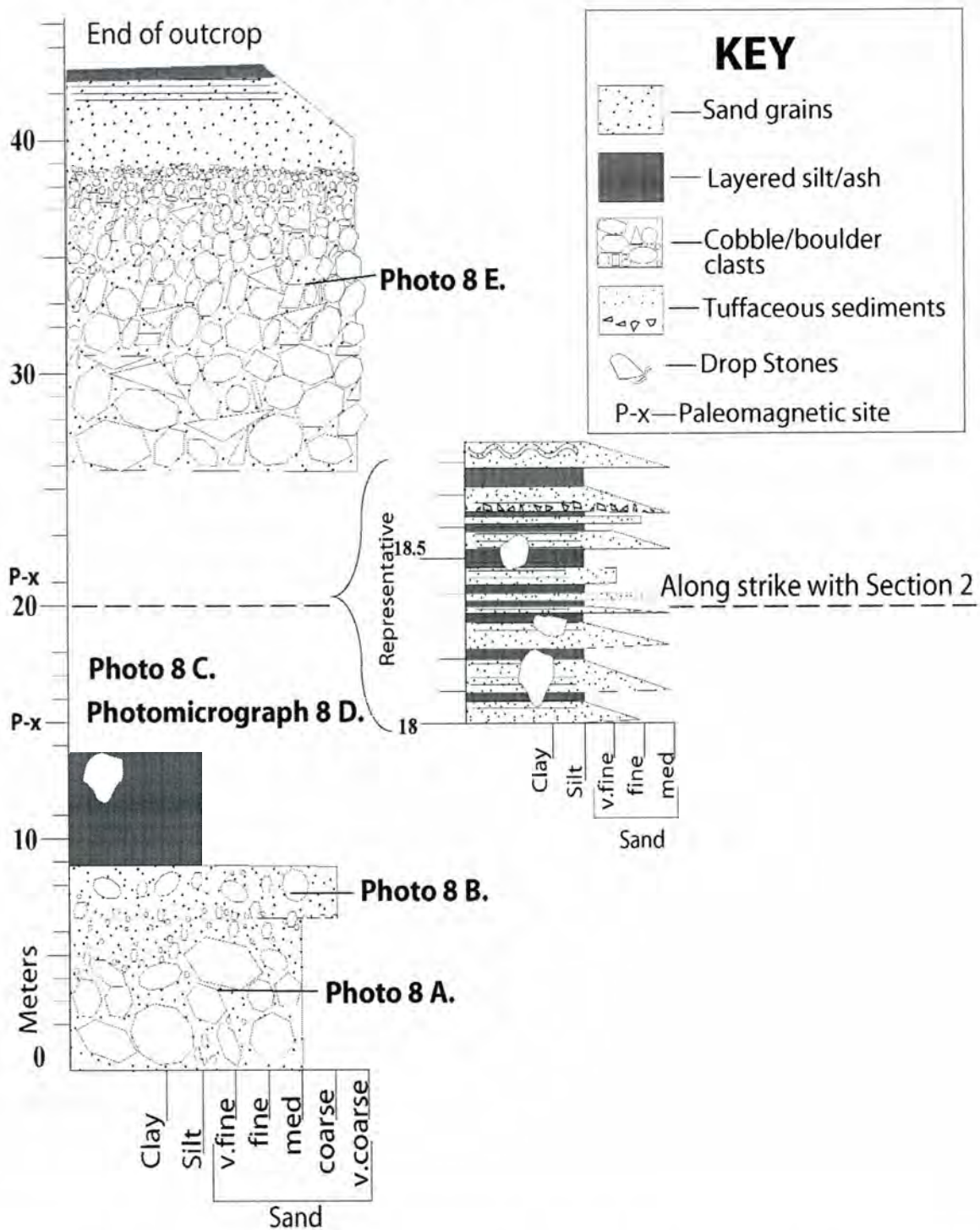


Figure 8. Section 1 (0 to 43 Meters) is dominated by breccias and debris flows. Rhythmic turbidites are found from 13-25 meters and contain the lowest exposed tuffaceous sediments at 17 meters. Photographs are found on the next page.

Figure 8. Section 1 photographs

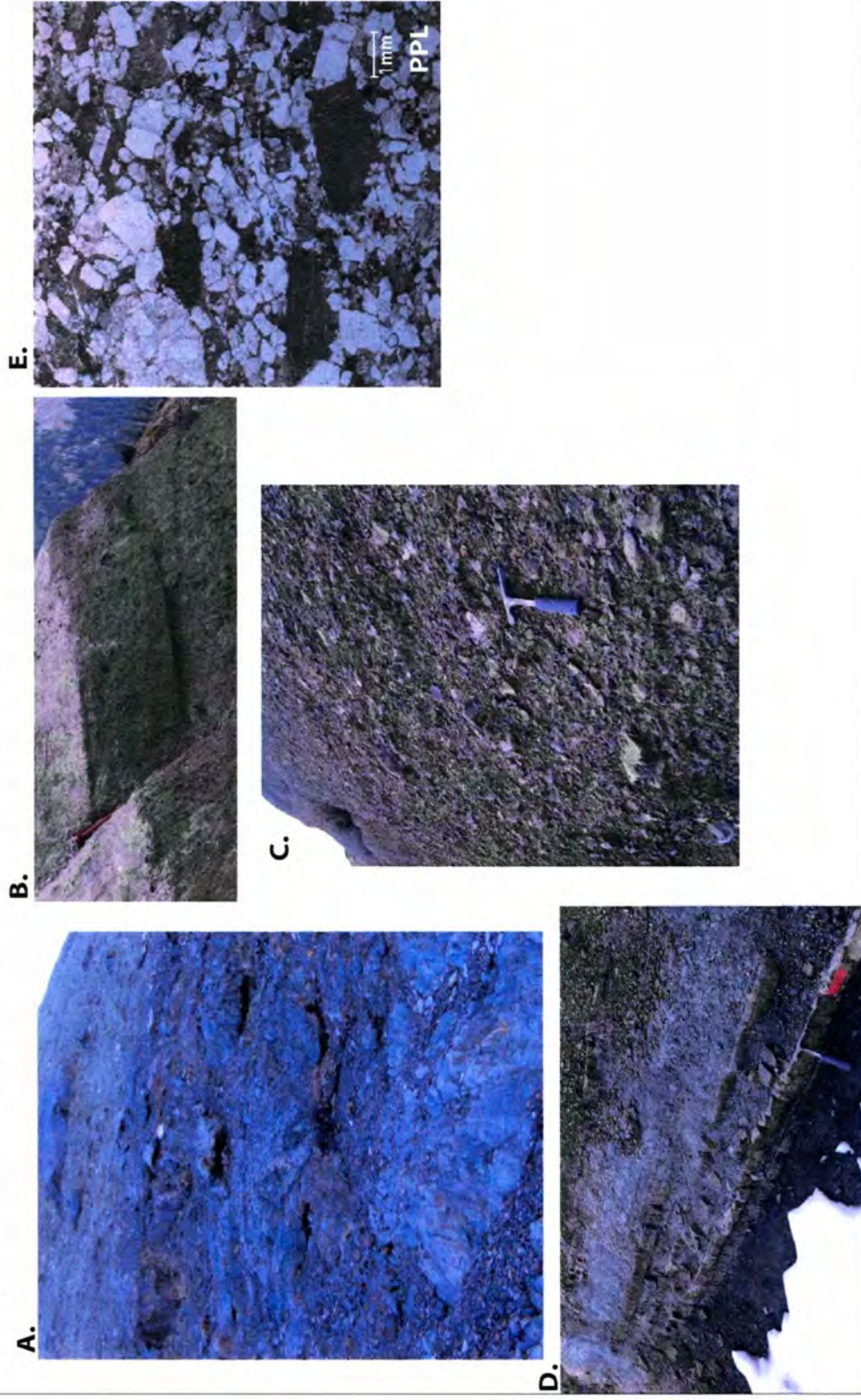


Figure 8 Section 1 photographs. A. is taken at 9 meters; B. is taken from the base (looking up); C. is of the debris flow at 27 meters; D. is of turbidites at 15 meters; E. is a plane polarized light microphotograph from the sandstone at 15 meters.

Directly above the pebble breccia is a 5 m thick silt unit. This unit is inconsistent in thickness along strike. The finer grained units in Kulshan caldera tend to be less indurated than sandy units; therefore, these large slopes are interpreted as silt.

Sitting atop the five meters of silt, the next 14 meters on the stratigraphic column is a sequence of rhythmically deposited turbidites. These turbidites are the first of a series of turbidites that dominate the Kulshan sedimentary unit. The turbidites are found from 14 to 27 meters in the stratigraphic column. The rhythmites are lithic/feldspathic arenite that grade to silt. The sand beds are as thick as 30 cm and as thin as 3cm, and the silt beds are 1 to 15 cm thick. The lithic material is granule to sand sized (4 mm to 0.5 mm in diameter) and angular. Mineral compositions from nonlithic clasts are predominantly plagioclase with a small trace of hornblende and oxides. Secondary calcite is present in small amounts (around 2%) as cement between grains. The units have varying lateral continuity; most can be traced for tens of meters. Bed forms are often well preserved. Some sand units show small-scale cross bedding and beds being truncated by other turbidites.

Sand and silt show soft sediment deformation in places. Around 17 meters in the stratigraphy is the first appearance of reworked pumice and glass (tuffaceous sediments). The presence of tuffaceous sediments (pumice, pumice fragments, crystals, and glass) in the Kulshan caldera sedimentary sequence indicates the presence of another source material. In this scenario the provenance change is from Nooksack metaconglomerate wall rock to unwelded ignimbrite. This is the only significant provenance change in Kulshan caldera.

15 m thick debris flow creates a near vertical wall of angular clasts of Chilliwack metaconglomerate. Laterally the unit spans out 115 meters. Clasts grade finer both upwards and outwards. The base of the debris flow contains boulders more than a meter in diameter. The larger clasts caused soft sediment deformation in strata beneath. The debris flow is composed of Chilliwack wall rock, though the top is covered with sand and silt.

Section 1 Interpretation

The sequence of sedimentary rocks at the 14 Goat area is not deposited directly on the ignimbrite of Kulshan caldera; therefore, the origin of the 14 Goat area must have a different explanation than that of the sedimentary rocks of Wells Creek area, which are found directly on ignimbrite. According to the geologic map of Hildreth (1996) the sedimentary rocks of the 14 Goat area lie around a secondary ring fault off the main caldera rim. My interpretation is that the 14 Goat area was created shortly after the initial fallout from the Kulshan caldera eruption by a fault along the rim rock creating a scallop shaped basin (with a metaconglomerate Chilliwack basement) on which the sedimentary rocks would be deposited.

The bottom six meters of megabreccia likely represents a short-lived rock fall event. The lack of sorting, stratification, and the instability in the caldera wall are strong pieces of evidence for subaerial deposition. The pebble breccia above the megabreccia indicates the change in environment from subaerial to subaqueous. Kulshan caldera developed into a stable lacustrine environment shortly after the initial collapse. For comparison, according to Nelson et al. (1994), Crater Lake developed maximum water level within 300 years after the initial collapse. This estimate was calculated with present

day precipitation rates, lake volume, input and output rates, and caldera wall stratigraphy. Kulshan caldera's short lived dry depositional record, abundant supply of water from the subglacial eruption and regional ice, and similar volume size to Crater Lake leads me to believe Kulshan had a similar filling rate (less than 300 years).

Turbidites indicate a deep and consistent depositional environment. The repeated layers of laminated sand and silt are similar to turbidite sequences described in other caldera sedimentary sequences (Nelson et al., 1994; Larson and Nelson, 1996; Poppe et al., 1985; Rytuba et al., 1981). Turbidites are common in steep walled lacustrine basins (Reading, 1996) such as those created by caldera subsidence (Larson and Crossey, 2000; Nelson et al., 1994). Later sections show that the steep walls created massive amounts of sediment gravity flows.

The introduction of tuffaceous sediments into Kulshan caldera indicates unwelded ignimbrite was remobilized. I propose ignimbrite was deposited outside the caldera and weathering broke down the ignimbrite into pumice, crystals of plagioclase and hornblende, and fine grained glass (Figure 4 and Figure 5). Above 17 meters in the stratigraphy (excluding debris flows) tuffaceous sediments comprise the greatest component of sedimentation. Deformation of strata is due to resurgent dome uplift and debris flow overburden.

The immense debris flow found above the rhythmite represents a collapse of the caldera rim. Though this is the largest of the debris flows in Kulshan caldera, evidence shows that there were several more of these collapses off the caldera rim and off the domes and lava flows (Hildreth, 1996).

Section 2

Section 2 is the trough cross-bedded sandstone stratigraphy from 20 to 32 meters. Section 2 is located 110 meters west and along strike with Section 1. I repeat meters 20-32 due to vastly different lithologies.

Section 2 is composed of a trough cross-bedded feldspathic arenite (Figure 9). The unit is very well sorted both for grain size and composition (65% plagioclase, 8% lithics, 5% hornblende, 5% biotite, 3% oxides, and 15% glass). Plagioclase crystals are angular and zoned. There are eight meters of exposed trough cross-bedded feldspathic arenite; a glacier covers the base of the section. A moulin in the glacier reveals another 3 meters of cross-bedded feldspathic arenite very similar to that in the outcrop. Small lenses (2 to 7 cm thick and up to 30 cm long) of pumice in fine-grained glassy matrix (tuffaceous) are found throughout the sequence (Figure 4). These small tuffaceous zones cap many of the troughs.

A clastic dike cross cuts the cross-bedded feldspathic arenite. The clastic dike is about 30 cm wide and consists of fine-grained sand to silt laterally grading towards the center of the dike. The silt in the dike was glass that has been altered. This dike continues up into Section 3 (Figure 9 D).

Section 2 Interpretation

The trough cross-bedded feldspathic arenite is a product of fluvial processes. A four-meter wide channel was incised into the lake sediments by a shallow stream. The minute amount of lithic material (compared to lower sections) indicates this stream was

Figure 9. Section 2 20 - 32 meters

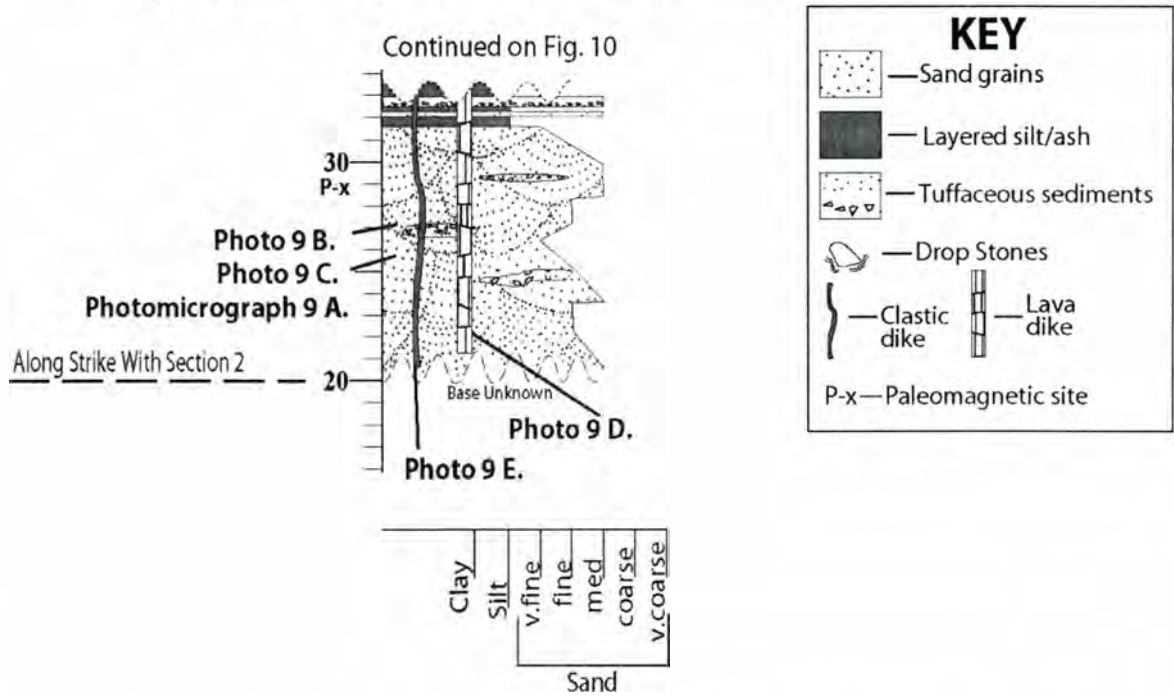


Figure 9. Section 2 is dominated by a trough cross bedded feldspathic arenite from 20 to 32 meters. Photographs are found on the next page.

Figure 9. Section 2 photographs

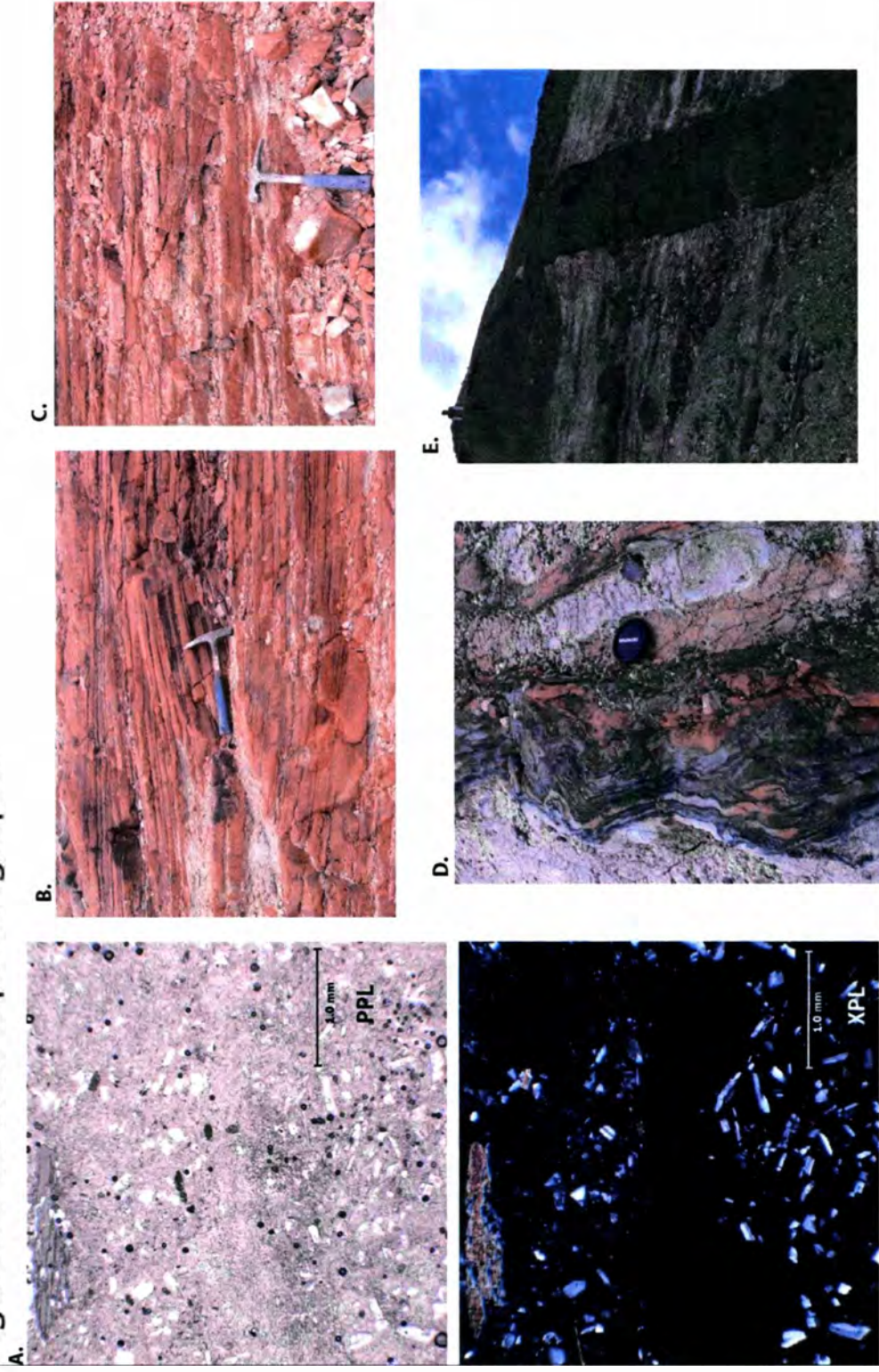


Figure 9 Section 2 photographs. A. Pair of photomicrographs from a tuffaceous zone within the cross bedding, the top is plain polarized light and the bottom is cross polarized light; B. and C. are both of cross bedding in the sandstone; D. is the clastic dike and E. is the andesite dike.

eroding ignimbrite. I interpret the cross-bedding to represent channelized flow in a shallow lacustrine environment. The existence of the clastic dike implies supersaturated sediments were weighted from above (Truswell, 1972), most likely the result of very rapid deposition in a seismically unstable region.

Section 3

In Section 3 turbidites are exposed between meters 50 to 75, with surficial debris obscuring most of the section between meters 32 and 50 (Figure 10). The debris is thick enough that only sandstone beds 30 cm and larger crop out. Ten meters west along strike from the debris covered zone turbidites appear as the dominant sequence; the units have planar beds (2 to 30 cm) of sand and silt. Compared to the turbidites lower in the section there is a greater component of tuffaceous sediment and a lesser component of sediment from wall rock in this section. In a few places granules and pebbles mark the base of turbidites. Well developed rhythmic turbidites crop out between meters 50 and 75. The sand beds in this section are well indurated.

Section 3 Interpretation

Section 3 is composed entirely of turbidites. The consistency of the turbidites suggests a stable and deep lacustrine environment. The turbidites with pebble and granule clasts indicate the continued instability in the caldera wall.

Section 4

Section 4 includes the stratigraphy from 68 to 123 meters (the top) (Figure 11). At 68 meters a well indurated 2 meter thick unit of laminar beds (less than 1 mm to 10 mm) of sand and mud (Figure 11 C) is overlain by an andesite sill. The andesite sill is 3 to 5 meters thick and laterally terminates against the sequence of rhythmical turbidites

Figure 10. Section 3 32 - 75 meters

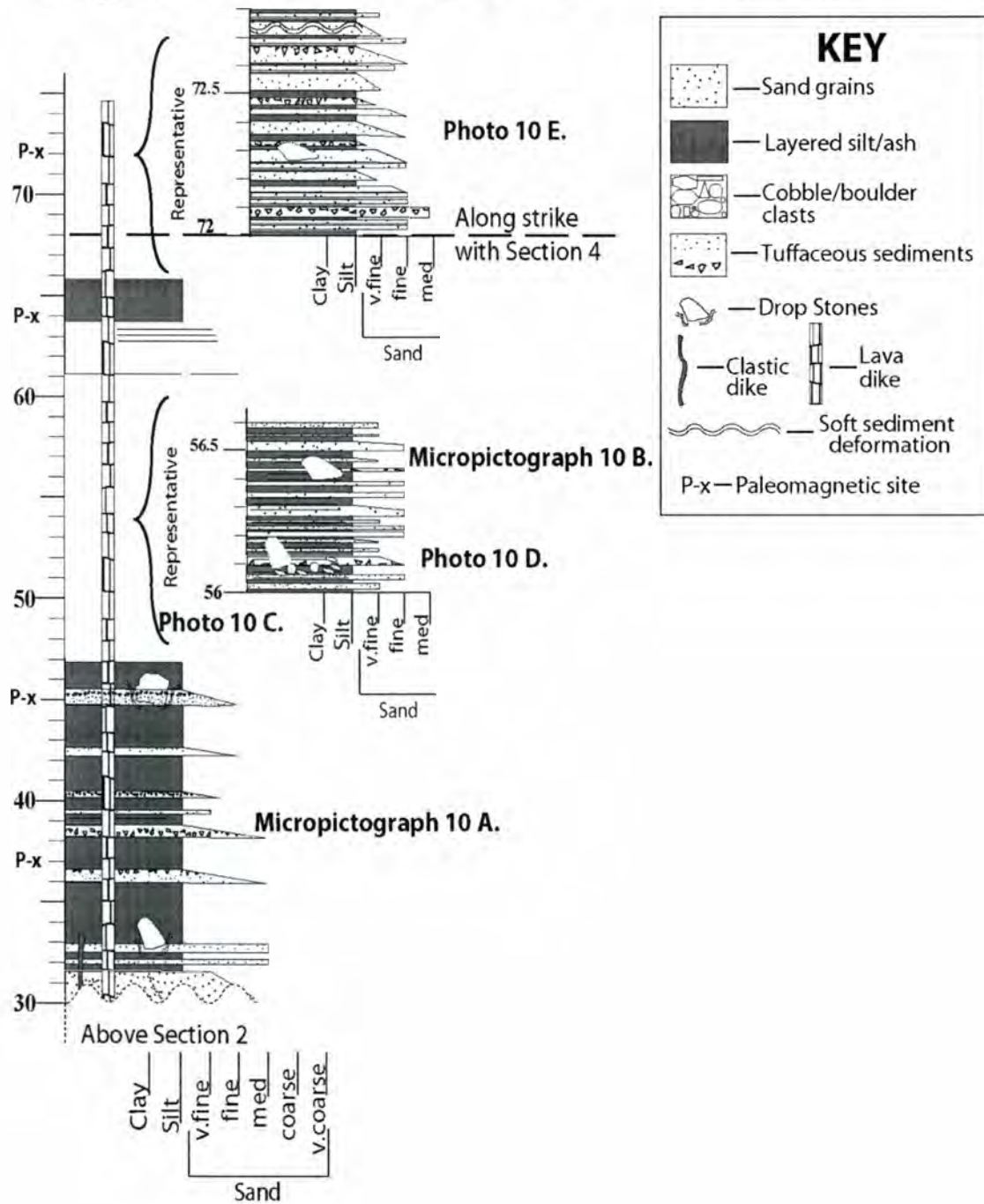


Figure 10. The lower part of Section 3 was mostly covered by debris; however, because turbidites found along strike, 10 meters west, from 32 to 45 meters. I speculate that these meters are rhythmic turbidites. Immediately above this area, at 48 meters, more turbidites appear. Located throughout the section small debris material and dropstones are found. Photographs are found on the next page.

Figure 10. Section 3 photographs

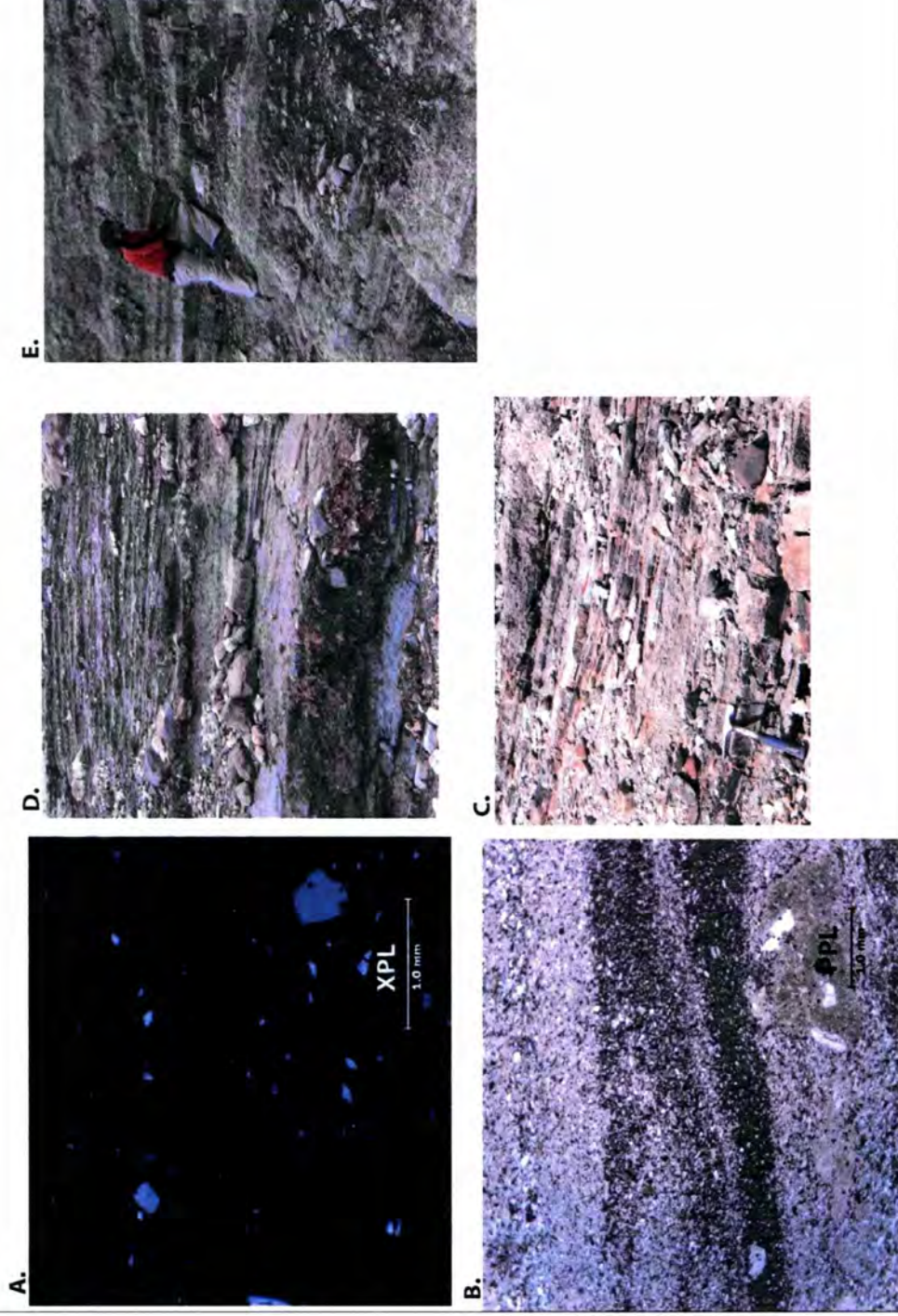


Figure 10 Section 3 photographs. A. and B. are photomicrographs of glass dominated mud/silt found at 45 meters and 64 meters, respectively; C. shows turbidites at 38 meters and 8 meters west of the column; D. is turbidites from about 54 meters; E. is turbidites from 72-77 meters.

described above (Figure 10 E). The andesite sill is a very prominent outcrop amongst the sedimentary rocks. Evidence for this unit being a sill rather than a lava, include soft sediment deformation above and below the sill, the smooth upper contact (Figure 11 B), pepperites, and chilled margins (10 cm) on the upper contact of the lava. The prominence of the sill makes it a marker bed throughout the field area (though the stratigraphic elevation of the sill outside the stratigraphic section is unknown). The unit immediately above the andesite sill consists of repeated beds of sand and mud, identical to the unit below the sill. The laminar beds found within 1.5 meters of the sill are the most indurated sedimentary units found in Kulshan caldera. Sedimentary rocks found within 2 meters of the top of the sill have taken on a green tint; however, thin sections do not show alteration of the grains or matrix.

In addition to the andesite sill, an andesite dike passes within 20 meters of the sill and cross cuts a significant portion of the stratigraphic section (at least meters 20 to 77). The dike appears to continue to Oreamnos Dome. Thin sections of the dike and sill show they have very similar compositions. Sedimentary rocks found within 1 meter of the dike tend to be very well indurated.

Two meters above the lava sill, the units continue with repeated turbidite sequences. These turbidites differ from lower turbidites in that they lack induration and include a greater component of tuffaceous sediment (20% to 50% pumice in sections). Pumice in the tuffaceous beds have normal grading as well as reverse grading, this pattern is caused by variability in pumice size, density, vesicularity, and vesicle interconnectedness (White et al., 2001). Outcrops in this area break easily and are very difficult to sample. Soft sediment deformation is abundant through this section. This

Figure 11. Section 4 photographs

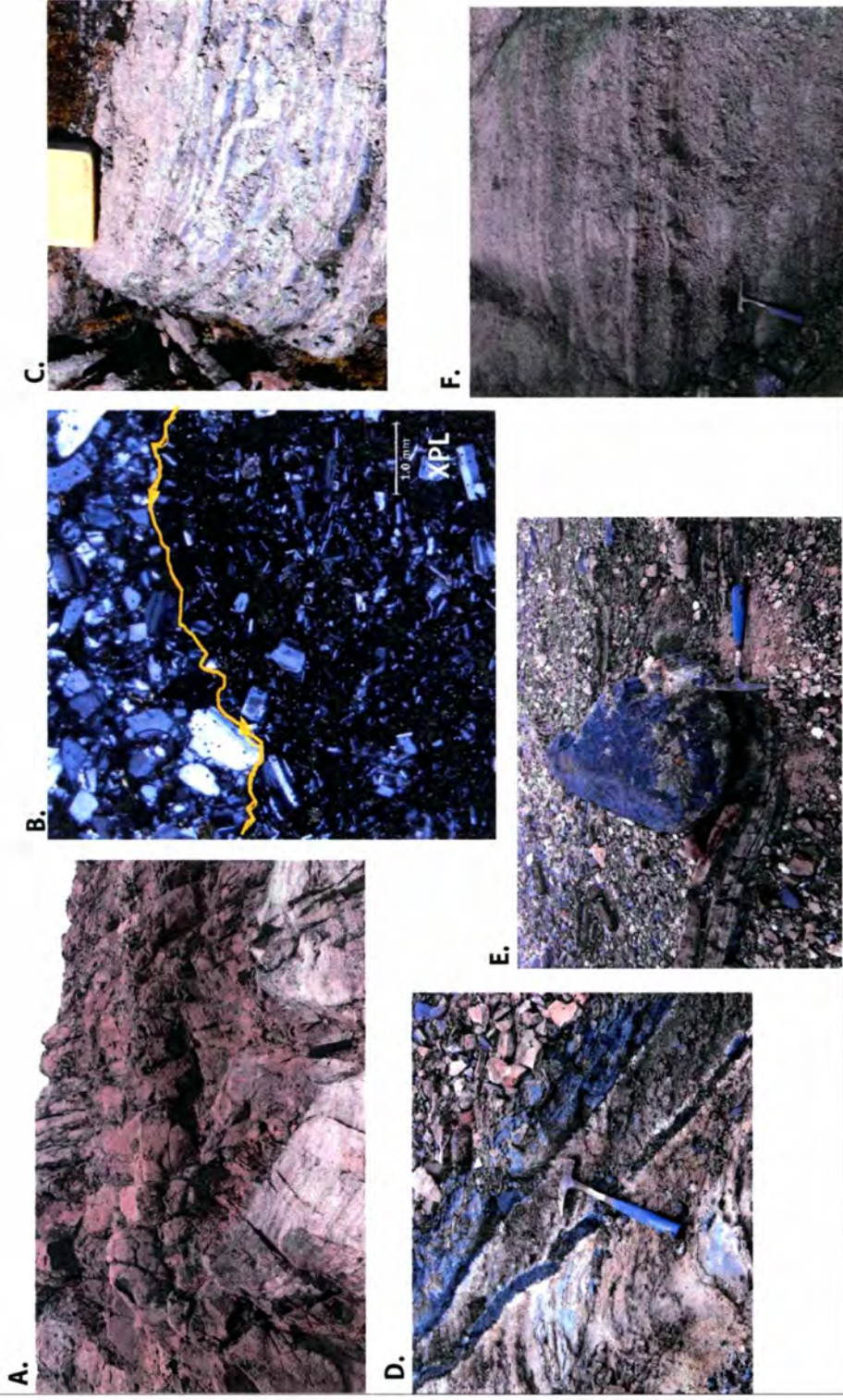


Figure 11 Section 4 photographs. A. is the andesite lava and; B. photomicrographs of the boundary between the sill and sediments, the yellow line delineates the border; C. altered sediments at 78 meters, I interpret the laminar bedding to be varves; D. clastic dikes from about 104 meters; E. a metaconglomerate dropstone, note the deformed underlying layers; F. is the rhythmic turbidites from 109-111 meters.

sequence has several (5 to 6) interconnecting clastic dikes. The clastic dikes contain fine grained sand and mud which show some alteration to clay minerals. The clastic dikes have sand grading to mud laterally towards the center. The dikes are up to 20 cm wide and intertwine throughout an area at least 40 by 40 meters.

This section also has dropstones. These stones occur throughout the stratigraphic column, though they are not as prominent in lower sections. The dropstones are as large as three meters across and as small as 30 cm (the average diameter is less than a meter). The dropstones are most often composed of Chilliwack metaconglomerate, though Nooksack argillite, welded tuff, Lake Ann diorite, and a few other of questionable nature are present as well. The dropstones in Section 4 are accompanied by deformed underlying strata (Figure 11 F). The lack of visible substrata deformation associated with dropstones lower in the stratigraphic column is due to the of exposure.

Section 4 Interpretation

The settling patterns of reworked pumice is difficult to interpret because pumice density varies due to vesicularity and vesicular interconnectedness (White et al., 2000). The dropstones indicate an active ice field. Most of the dropstones are composed of Chilliwack metaconglomerate. Dropstones composed of Lake Ann stock were transported over 5 km and argillite from the Nooksack formation came from over 2 km away. The lack of evidence for a secondary explosive eruption (Hildreth, 1996) and the proximity of Lake Anne stock grandodiorite leaves me to believe that these stones were carried and deposited by ice and not as ballistics.

The clastic dikes found in this section along with the clastic dike found at the base are likely the result of rapid deposition and overburden (sediments, lava or glaciers)

(Truswell, 1972). Overloaded (likely by other sediments lava and glaciers) and saturated sediments were forced into small cracks and filled from the bottom up.

Additional sedimentary structures

Additional sedimentary structures occur within the 14 Goat area but outside the measured section. Near the southern caldera rim is a small section of mudstone containing oscillation ripples and rain drop imprints (Figure 12), this is evidence of a shallow depositional environment. The only shallow environment indicated by the stratigraphy is the fluvial channel. The rain drop imprints and ripple marks are located just above the lava stratigraphically. These are found fairly high stratigraphic sequence; however, since they lie outside the measured stratigraphic section, their exact stratigraphic elevations were not determined. Fossilized grass seeds have been found in finely layered shale within 200 meters of the raindrop imprints (D. Tucker pers comm., 2007). These are the only fossils that have been found in Kulshan caldera.

MAGNETIC STRATIGRAPHY

Twelve paleomagnetic sites with five to seven samples per site were collected to determine the rate of deposition and age of the Kulshan lacustrine environment. Natural remanent magnetization (NRM) results indicate there was little to no coherence of directions within sites. All samples were then thermally demagnetized. Thermal demagnetization results were used to define one to two components of magnetization. Vector plots showing the direction of magnetization, as samples were demagnetized, show well defined signal in most specimens (Figure 13). A Fisher statistical model (Tauxe, 1998) for each site at Kulshan caldera indicates that within-site directional scatter

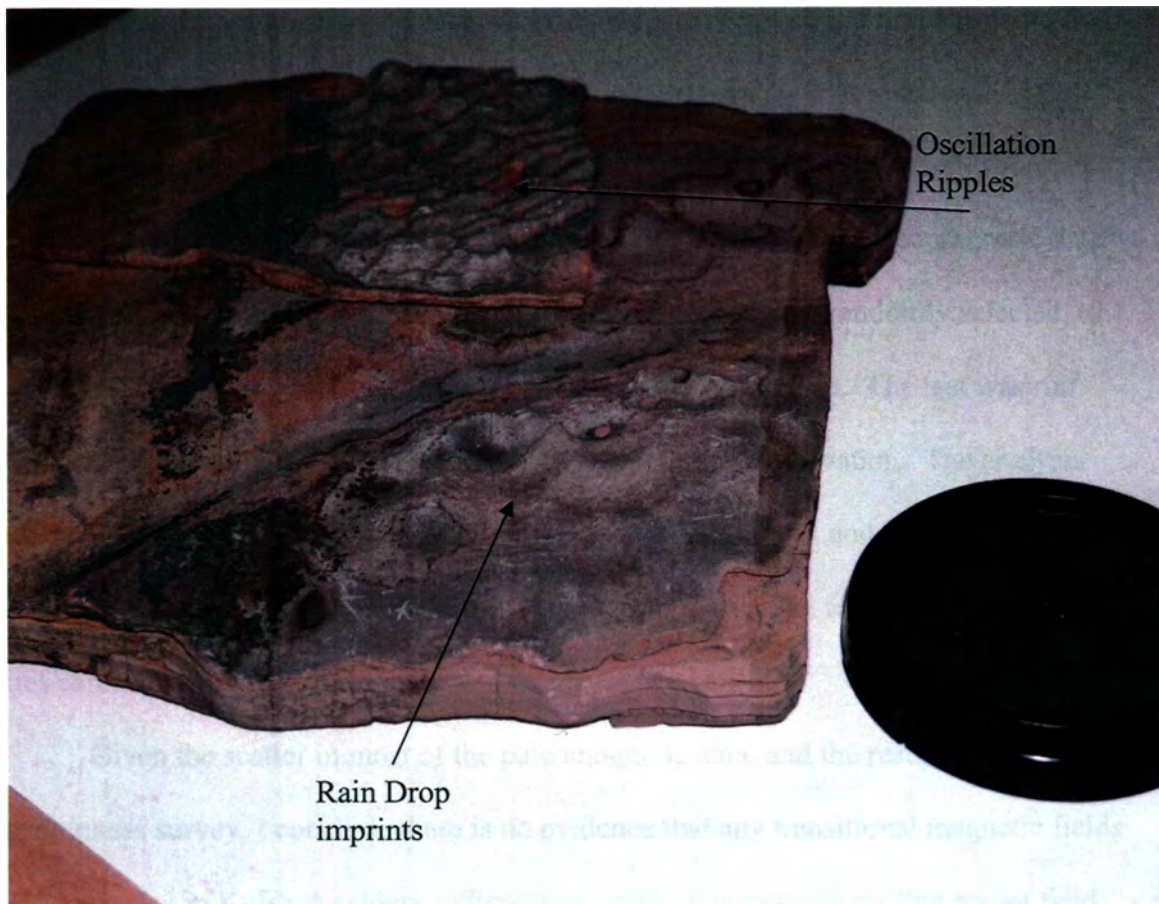


Figure 12. Raindrop imprints and ripple marks appear on the same stone. This was located outside the stratigraphic column of the 14 Goat lake area but still within the 14 Goat area.

is high, as indicated by the low k values (Table 1). Despite this scatter, it was apparent that for some sites the polarity of the geomagnetic field at the time of magnetization could be determined. In the second analysis of the data, we presumed that the most reliable remanent magnetization for stratigraphic interpretations was likely acquired early and represented by the high temperature magnetic components (275° - 600° C). The high temperature analysis showed that site Pks039 (45 m) indicated a reverse polarity, while sites Pks066 (72 m) and Pks099 (105 m) (Figure 14) indicated normal polarity. If site Pks039 (45 m) is reversed and Pks066 (72 m) is normal then the samples below the height of 45 m would be reversed and the samples above 72 m would be normal,

implying that the sedimentary rocks at Kulshan caldera recorded the transition into the Jaramillo magnetic normal subchron. However, the remaining 9 sites showed mixed polarities. The wide range of directional scatter in sites Pks039 (45 m) and Pks066 (72 m) does not convey strong reliability. Using a randomness test for paleomagnetic data developed by Watson (1956), all high temperature samples were randomly selected, to see if any of the sites could provide directions that are not random. The test was run twice to see if there was any grouping of nonrandom sites by elevation. The analysis results (Table 1) reveal that sites Pks093 (99 m), Pks058 (66 m), and Pks024 (30 m) can be considered nonrandom. The analysis results from the second test confirmed that all sites can be considered random.

Given the scatter in most of the paleomagnetic data, and the results of the randomness survey, I conclude there is no evidence that any transitional magnetic fields were recorded in Kulshan caldera sedimentary units. It is more likely that recent field overprints (lightning or hydrothermal alteration) created additional fields resembling transitional deposits.

Anisotropy of magnetic susceptibility (AMS)

The bulk susceptibility measurements of the AMS (k -bulk) (Table 2) from Kulshan caldera show that magnetite controls the magnetic fabric. The minimum axes of susceptibility (k_{\min}) (Table 2) (Figure 15) were fit using bootstrap method confidence ellipses (Constable and Tauxe, 1990). Sites Pks031, Pks039, Pks058, Pks074, Pks082, Pks099 have tight groupings that have minimum susceptibility (k_{\min}) ellipses vertical to subvertical (k_{\min}). A physical characteristic associated with this type of grouping in AMS data is the settling of grains from quiet water. The Sites Pks009, Pks015, Pks024, Pks066

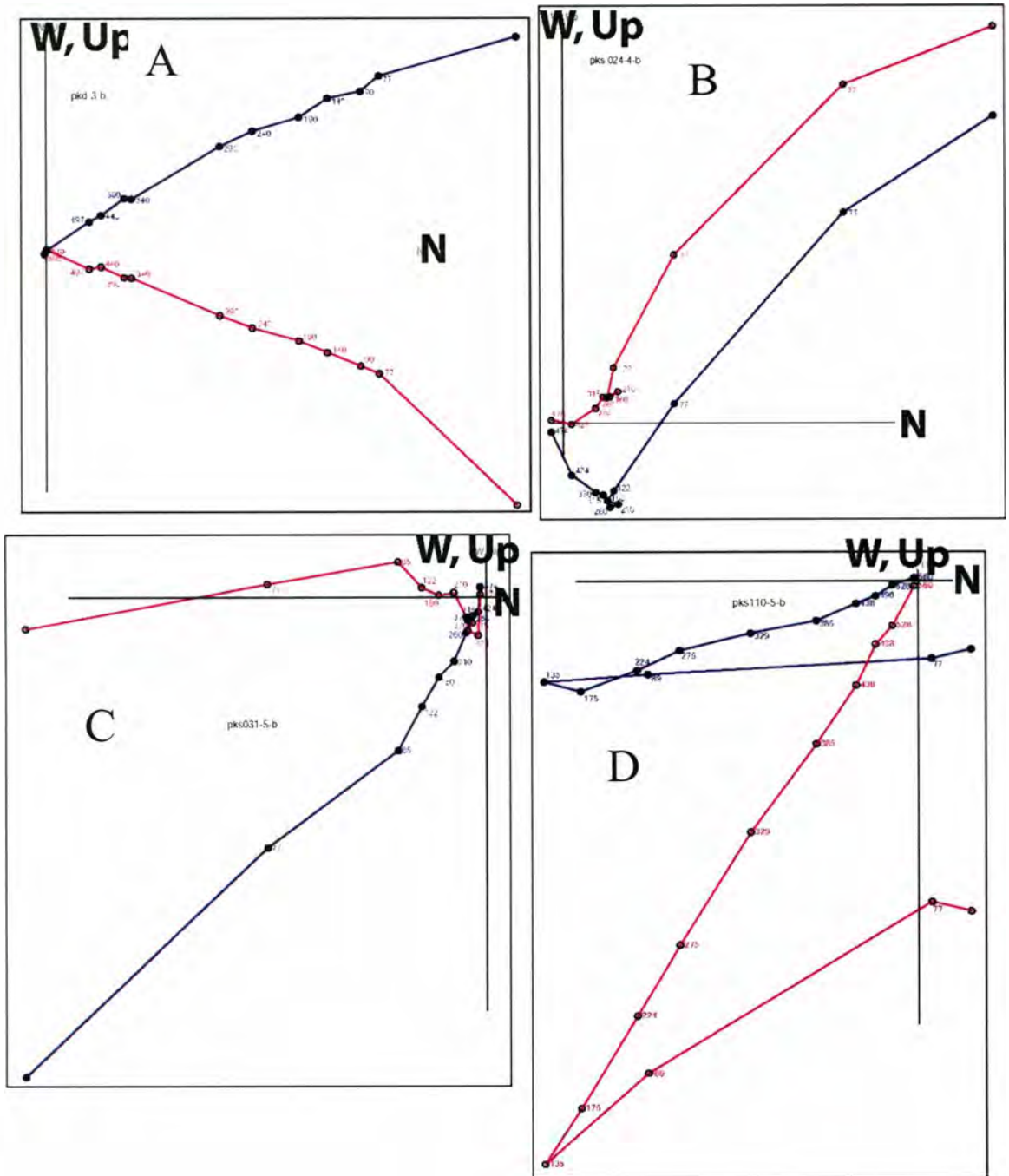


Figure 13. Orthogonal plots showing the direction of magnetization as specimens are thermally demagnetized to the origin. Each plot represents one type of lithology tested during this study. A. is from the andesite dike; B. is tuffaceous sediment from 30 meters; C. is siltstone from 38 meters; D. is sandstone from 116 meters. The plots show only one component of magnetization.

Paleomagnetic directions of high temperature phases
in sedimentary rocks at Kulshan caldera

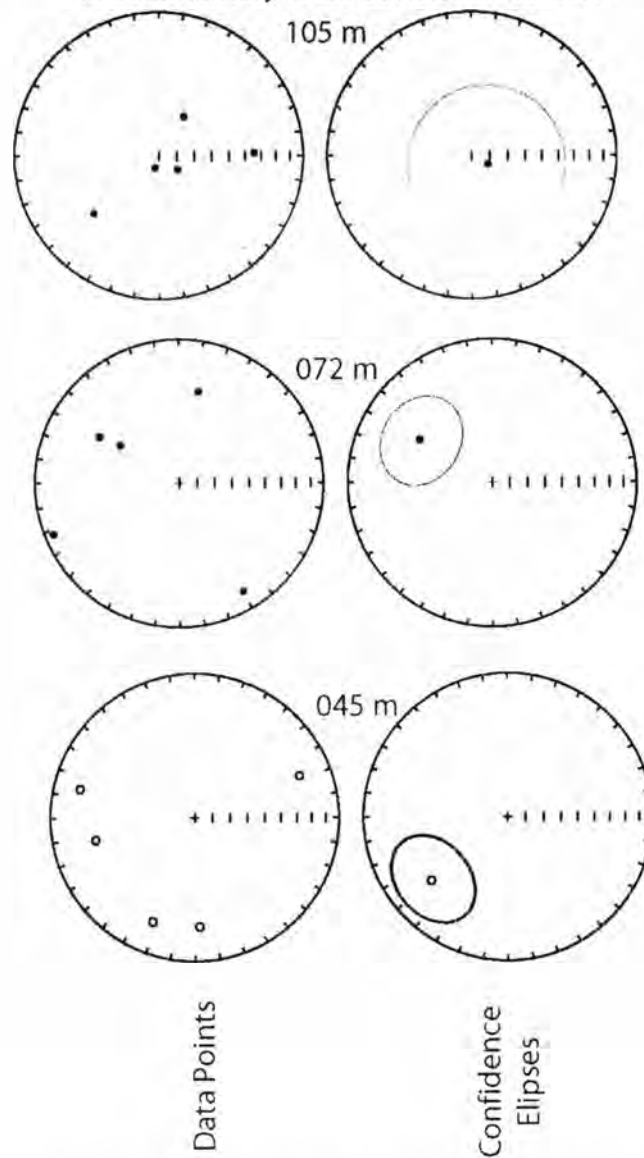


Figure 14. High temperature components are plotted on equal area projections for individual specimen representing each sample in the site. Closed circles are downward directions, open circles are upward projections. High degree of scatter in the directions, and a Watson (1957) randomness survey led me to determine there is no transition recorded in the rocks at Kulshan caldera

and Pks105 have a small degree of striation which has implication for paleocurrent directions and small degrees of flow.

All but two specimens from Kulshan caldera have a Flinn-k value less than 1 (Housen et al., 1993); therefore, AMS ellipsoids of all sites from Kulshan caldera are oblate. The maximum axes of susceptibilities (k_{max}) (Table 2) (Figure 15) are well grouped in sites Pks039 (southeast), Pks066 (southeast), Pks082 (east-northeast), Pks099 (east), the remaining sites are scattered.

A closer look at all sites with quiet water AMS and their remanent magnetization I can determine if post-depositional slumping caused errors or if post-depositional alteration caused error in the paleomagnetism (Schwehr and Tauxe, 2003).

Cryptoslumping is evident if sites with grouped K_{max} have less grouping in remanent magnetizations, compared to sites with poorly grouped K_{max} . Though the connection can be hard to make because the remanent magnetizations for Kulshan caldera are greatly scattered, it is apparent that the closest grouped remanent magnetizations from Kulshan caldera (Pks039, Pks066 and Pks099) all have well grouped K_{max} (Figure 16). Therefore, it was not cryptoslumping that caused the scatter in magnetizations, but instead post-depositional alteration (i.e. lightning).

AGE

Constraining the age of the lacustrine environment in Kulshan caldera is beneficial for detailing Kulshan history and ice sheet distribution in the North Cascades. Hildreth et al. (2004) determined the Kulshan caldera period of volcanism spanned the Jaramillo normal subchron (1.072 - .988 Ma) (Gradstein et al., 2004)). As noted in the magnetic stratigraphy section of this paper, the sedimentary rocks of Kulshan caldera do

not clearly delineate the Jaramillo subchron. Hildreth et al. (2004) indicate the rhyodacitic lava of Camp Kiser (0.992 ± 0.014 Ma), the last of the Kulshan era lavas, lies on top of the lacustrine sedimentary rocks. Since the Kulshan lacustrine environment is stratigraphically bounded by Kulshan era ignimbrite and lavas, sedimentation is limited from 1.149 ± 0.010 to 0.992 ± 0.014 Ma. The lacustrine environment of Kulshan caldera lasted no longer than 157 ka, with a minimum rate of deposition of 79 cm/ka. Arguments could be made for shorter duration estimate if one assumes that Oreamnos Dome (1.127 ± 0.012 Ma) (Hildreth et al., 2004) erupted after most of the sediments accumulated. Because there is no direct evidence of debris flows or dropstones from Oreamnos Dome, it is possible to suggest that the lacustrine environment ended before Oreamnos Dome erupted. This estimate suggests the duration of the lacustrine environment at 22 ka and a rate of sedimentation of 560 cm/ka.

DISCUSSION

Though the number of calderas found in the Cascade volcanic range during the Quaternary is anomalously low compared to other continental arcs of similar range and composition, at least three calderas preserve post-collapse sedimentary records. Crater Lake, OR, Hannegan caldera, WA (Tucker et al., 2007), and Kulshan caldera all have some record of lacustrine sediments. Of the three, Kulshan caldera has the best detailed stratigraphy and sedimentology. Though Crater Lake has had several studies conducted on the sediments only 150 cm of core have been recovered and studied.

The eruption of Kulshan caldera is similar to the record of Crater Lake: both are located in the Cascade volcanic range, both ejected about 55 km^2 of ignimbrite from small sized calderas (Kulshan: 4.5×8 km and Crater Lake: 8×10 km), and both basins

Table 1. Paleomagnetic Data and Randomness survey

Site Name	Elevation	Samples	N	k	Ro	</>	R	RANDOM
TEST ONE								
Pks110	116 m	5	5	0.668	3.609	>	1.2922	RANDOM
Pks099	105 m	5	10	1.881	5.104	>	4.3831	RANDOM
Pks093	99 m	5	15	1.691	6.251	<	6.8156	
Pks082	88 m	5	20	1.041	7.218	>	6.9041	RANDOM
Pks074	80 m	5	25	0.594	8.07	>	6.4712	RANDOM
Pks066	72 m	5	30	0.539	8.84	>	7.6361	RANDOM
Pks058	66 m	4	36	0.782	9.684	<	10.6946	
Pks039	45 m	5	41	0.875	10.335	>	8.6168	RANDOM
Pks031	38 m	6	45	0.201	10.827	>	10.7709	RANDOM
Pks024	30 m	5	48	0.335	11.182	<	12.3457	
Pks015	21 m	4	52	FAIL	11.639	<	12.0845	
Pks009	15m	3		FAIL	FAIL		FAIL	FAIL
TEST TWO								
Pks009	15m	3		FAIL	FAIL		FAIL	FAIL
Pks015	21 m	4	5	FAIL	3.609	>	1.7926	RANDOM
Pks024	30 m	5	8	0.335	4.565	>	1.6085	RANDOM
Pks031	38 m	6	12	0.201	5.591	>	3.6573	RANDOM
Pks039	45 m	5	17	0.875	6.655	>	2.8146	RANDOM
Pks058	66 m	4	23	0.782	7.74	>	4.1143	RANDOM
Pks066	72 m	5	28	0.539	8.54	>	7.6437	RANDOM
Pks074	80 m	5	33	0.594	9.272	>	5.3874	RANDOM
Pks082	88 m	5	38	1.041	9.949	>	4.8991	RANDOM
Pks093	99 m	5	43	1.691	10.584	>	7.3837	RANDOM
Pks099	105 m	5	48	1.881	11.182	<	11.4673	
Pks110	116 m	5	53	0.668	11.75	>	11.4668	RANDOM

Table 2. AMS Data

Specimen	K-bulk	K max	Dec Max	Inc Max	K min	Dec Min	Inc Min	Flinn	L	P	F
pk009-2-a	9.33E-03	1.074	207	26	0.881	42	63	0.15	1.03	1.22	1.19
pk009-3-a	6.39E-03	1.093	160	2	0.857	273	84	0.18	1.04	1.28	1.23
pk009-5-a	7.15E-03	1.068	175	25	0.888	42	55	0.13	1.02	1.20	1.18
pk009-5-b	9.12E-03	1.069	173	21	0.881	41	59	0.10	1.02	1.21	1.19
pk015-1-a	7.84E-03	1.039	257	0	0.939	349	78	0.18	1.02	1.11	1.09
pk015-1-b	6.61E-03	1.033	182	12	0.940	18	77	0.07	1.01	1.10	1.09
pk015-2-a	6.73E-03	1.034	188	3	0.943	71	84	0.11	1.01	1.10	1.09
pk015-2-b	9.94E-03	1.035	228	5	0.944	120	76	0.17	1.01	1.10	1.08
pk015-4-a	9.01E-03	1.043	293	7	0.933	150	81	0.19	1.02	1.12	1.10
pk015-4-b	9.80E-03	1.045	289	4	0.924	147	85	0.12	1.01	1.13	1.12
pk015-5-a	6.98E-03	1.025	297	0	0.958	29	82	0.12	1.01	1.07	1.06
pk015-5-b	7.19E-03	1.041	219	8	0.925	15	81	0.06	1.01	1.13	1.12
pk015-3-a	7.41E-03	1.030	51	10	0.951	208	79	0.13	1.01	1.08	1.07
pk015-3-b	6.61E-03	1.037	337	10	0.930	212	72	0.04	1.00	1.12	1.11
pk024-1-a	2.05E-03	1.057	232	5	0.901	101	82	0.09	1.01	1.17	1.16
pk024-1-b	1.65E-03	1.071	43	1	0.870	181	89	0.05	1.01	1.23	1.22
pk024-2-a	9.17E-04	1.040	265	1	0.967	359	67	1.75	1.05	1.08	1.03
pk024-2-b	1.03E-03	1.023	239	6	0.963	57	84	0.17	1.01	1.06	1.05
pk024-3-a	2.20E-03	1.100	314	18	0.855	134	72	0.24	1.05	1.29	1.22
pk024-4-a	4.14E-03	1.042	274	37	0.925	139	43	0.07	1.01	1.13	1.12
pk024-4-b	4.53E-03	1.047	255	29	0.930	139	38	0.25	1.02	1.13	1.10
pk024-4-c	4.35E-03	1.047	286	47	0.925	133	40	0.15	1.02	1.13	1.11
pk024-5-a	6.73E-04	1.035	176	18	0.960	329	70	0.63	1.03	1.08	1.05
pk024-5-b	1.26E-03	1.044	151	36	0.945	323	54	0.48	1.03	1.10	1.07
pk024-3-b	1.62E-03	1.103	323	18	0.848	148	72	0.22	1.05	1.30	1.24
pk024-5-c	1.97E-03	1.056	37	2	0.921	218	88	0.28	1.03	1.15	1.11
pk031-1-a	2.98E-03	1.056	25	12	0.914	232	77	0.19	1.02	1.16	1.13
pk031-2-a	4.35E-03	1.066	251	17	0.911	63	73	0.34	1.04	1.17	1.12
pk031-2-b	4.13E-03	1.064	255	17	0.910	78	73	0.29	1.04	1.17	1.13
pk031-2-c	4.90E-03	1.065	243	16	0.901	65	74	0.21	1.03	1.18	1.15
pk031-3-a	8.24E-04	1.028	246	4	0.961	11	84	0.32	1.02	1.07	1.05
pk031-3-b	7.71E-04	1.029	105	2	0.949	1	83	0.10	1.01	1.09	1.08
pk031-3-c	7.51E-04	1.034	248	5	0.953	38	84	0.35	1.02	1.09	1.06

Table 2 continued

Specimen	K-bulk	K max	Dec Max	Inc Max	K min	Dec Min	Inc Min	Flinn	L	P	F
pk031-4-a	1.07E-03	1.077	191	3	0.862	355	86	0.06	1.01	1.25	1.23
pk031-4-b	1.88E-03	1.078	177	3	0.887	59	83	0.24	1.04	1.22	1.17
pk031-5-a	1.23E-02	1.081	125	10	0.879	303	80	0.22	1.04	1.23	1.18
pk031-5-b	1.10E-02	1.077	128	9	0.879	278	80	0.17	1.03	1.23	1.19
pk031-6-a	9.92E-04	1.039	84	3	0.935	329	83	0.12	1.01	1.11	1.10
pk031-6-b	9.57E-04	1.043	80	2	0.929	338	82	0.13	1.01	1.12	1.11
pk031-1-b	2.86E-03	1.040	96	16	0.940	247	72	0.23	1.02	1.11	1.09
pk039-a-1	1.39E-03	1.043	338	0	0.929	246	84	0.14	1.02	1.12	1.11
pk039-1-b	6.67E-04	1.063	11	2	0.892	234	88	0.10	1.02	1.19	1.17
pk039-1-c	1.03E-03	1.061	55	2	0.890	182	87	0.06	1.01	1.19	1.18
pk039-2-a	2.69E-03	1.055	109	2	0.910	7	81	0.13	1.02	1.16	1.14
pk039-2-b	1.98E-03	1.067	93	0	0.895	360	82	0.17	1.03	1.19	1.16
pk039-3-a	1.58E-03	1.047	107	10	0.935	353	66	0.31	1.03	1.12	1.09
pk039-3-b	7.58E-04	1.056	121	17	0.910	343	67	0.15	1.02	1.16	1.14
pk039-4-a	1.10E-03	1.084	115	14	0.872	304	76	0.19	1.04	1.24	1.20
pk039-4-b	8.31E-04	1.078	108	12	0.889	291	78	0.27	1.04	1.21	1.16
pk039-4-c	8.10E-04	1.068	130	17	0.896	296	73	0.20	1.03	1.19	1.16
pk039-5-a	1.95E-03	1.066	208	14	0.896	15	75	0.16	1.03	1.19	1.16
pk039-5-b	2.07E-03	1.057	164	13	0.896	10	75	0.05	1.01	1.18	1.17
pk039-5-c	1.87E-03	1.065	196	11	0.888	11	79	0.10	1.02	1.20	1.18
pk058-1-a	5.46E-04	1.074	182	7	0.895	50	80	0.28	1.04	1.20	1.15
pk058-1-b	5.42E-04	1.077	168	3	0.887	57	83	0.23	1.04	1.21	1.17
pk058-1-c	5.51E-04	1.071	166	4	0.894	46	83	0.21	1.03	1.20	1.16
pk058-2-a	1.20E-03	1.035	284	6	0.950	62	82	0.28	1.02	1.09	1.07
pk058-2-b	1.23E-03	1.038	295	7	0.950	102	83	0.41	1.03	1.09	1.07
pk058-2-c	1.22E-03	1.040	271	4	0.955	95	86	0.64	1.03	1.09	1.05
pk058-3-a	9.61E-04	1.041	207	11	0.944	44	78	0.34	1.03	1.10	1.08
pk058-3-b	9.40E-04	1.038	223	10	0.942	13	78	0.21	1.02	1.10	1.08
pk058-4-a	1.70E-03	1.079	86	5	0.857	225	83	0.06	1.01	1.26	1.24
pk058-5-a	2.01E-03	1.094	275	20	0.867	100	70	0.27	1.05	1.26	1.20
pk058-5-b	1.87E-03	1.087	276	23	0.875	105	66	0.26	1.05	1.24	1.19
pk058-5-c	1.82E-03	1.087	276	21	0.878	106	69	0.27	1.05	1.24	1.18
pk058-5-d	1.98E-03	1.084	292	21	0.866	99	68	0.15	1.03	1.25	1.21

Table 2 Continued

Specimen	K-bulk	K max	Dec Max	Inc Max	K min	Dec Min	Inc Min	Flinn	L	P	F
pk066-1-a	3.31E-03	1.125	92	9	0.821	312	78	0.23	1.07	1.37	1.29
pk066-1-b	3.23E-03	1.126	95	8	0.828	316	80	0.29	1.08	1.36	1.26
pk066-2-a	5.08E-03	1.113	109	11	0.816	345	70	0.12	1.04	1.37	1.31
pk066-2-b	5.79E-03	1.104	109	4	0.829	5	74	0.12	1.04	1.33	1.29
pk066-2-c	7.27E-03	1.115	116	17	0.817	340	68	0.14	1.04	1.36	1.31
pk066-3-a	3.21E-03	1.096	346	11	0.856	156	79	0.20	1.05	1.28	1.23
pk066-4-a	3.71E-03	1.095	4	11	0.858	215	77	0.20	1.05	1.28	1.22
pk066-5-a	3.15E-03	1.088	202	10	0.864	17	80	0.18	1.04	1.26	1.21
pk066-5-b	2.79E-03	1.092	195	9	0.853	358	80	0.15	1.04	1.28	1.24
pk066-5-c	2.76E-03	1.098	197	7	0.845	12	83	0.15	1.04	1.30	1.25
pk074-1-a	2.78E-02	1.014	273	1	0.980	3	5	0.28	1.01	1.04	1.03
pk074-1-b	1.18E-02	1.042	252	62	0.922	344	1	0.04	1.01	1.13	1.12
pk074-1-c	1.10E-02	1.039	305	80	0.937	152	9	0.15	1.01	1.11	1.09
pk074-2-a	4.69E-03	1.032	83	9	0.944	293	79	0.10	1.01	1.09	1.09
pk074-2-b	4.08E-03	1.040	349	0	0.935	259	84	0.15	1.02	1.11	1.10
pk074-2-c	4.06E-03	1.040	46	5	0.922	208	85	0.02	1.00	1.13	1.13
pk074-3-a	4.93E-03	1.051	201	3	0.919	83	83	0.18	1.02	1.14	1.12
pk074-3-b	4.63E-03	1.055	347	3	0.919	94	80	0.23	1.03	1.15	1.12
pk074-3-c	5.81E-03	1.071	359	2	0.896	113	84	0.24	1.04	1.20	1.15
pk074-4-a	4.56E-03	1.068	279	30	0.888	132	56	0.13	1.02	1.20	1.18
pk074-5-a	1.24E-02	1.041	9	5	0.923	222	85	0.03	1.00	1.13	1.12
pk074-5-b	5.91E-03	1.072	26	3	0.874	243	86	0.08	1.02	1.23	1.21
pk074-5-c	6.37E-03	1.045	61	3	0.916	276	86	0.04	1.01	1.14	1.14
pk074-4-b	5.74E-03	1.069	257	21	0.888	131	57	0.15	1.03	1.20	1.17
pk082-1-a	6.96E-03	1.077	262	7	0.903	82	83	0.43	1.06	1.19	1.13
pk082-1-b	8.48E-03	1.082	239	13	0.879	76	76	0.23	1.04	1.23	1.18
pk082-2-a	9.66E-03	1.135	41	10	0.802	242	79	0.21	1.07	1.42	1.32
pk082-2-b	8.27E-03	1.089	48	11	0.854	254	78	0.12	1.03	1.28	1.24
pk082-2-c	6.40E-03	1.050	88	22	0.938	253	68	0.46	1.04	1.12	1.08
pk082-3-a	6.31E-03	1.044	63	12	0.943	257	77	0.41	1.03	1.11	1.07
pk082-3-b	7.95E-03	1.051	83	6	0.921	291	83	0.20	1.02	1.14	1.12
pk082-4-a	7.84E-03	1.054	320	9	0.905	194	74	0.08	1.01	1.17	1.15
pk082-4-b	9.68E-03	1.059	295	8	0.888	176	73	0.03	1.01	1.19	1.19

Table 2 Continued

Specimen	K-bulk	K max	Dec Max	Inc Max	K min	Dec Min	Inc Min	Flinn	L	P	F
pk082-4-c	1.92E-02	1.073	297	7	0.864	184	72	0.04	1.01	1.24	1.23
pk082-5-a	6.76E-03	1.050	297	9	0.903	160	78	0.02	1.00	1.16	1.16
pk082-5-b	8.56E-03	1.065	339	14	0.888	159	76	0.10	1.02	1.20	1.18
pk082-5-c	1.68E-02	1.075	344	14	0.866	157	76	0.07	1.02	1.24	1.22
pk093-1-a	1.27E-02	1.096	345	11	0.856	156	79	0.20	1.05	1.28	1.23
pk093-1-b	1.38E-02	1.095	347	10	0.860	159	80	0.22	1.05	1.27	1.22
pk093-2-a	5.28E-03	1.074	299	2	0.901	188	85	0.35	1.05	1.19	1.14
pk093-2-b	5.84E-03	1.082	295	1	0.891	191	86	0.35	1.05	1.21	1.15
pk093-3-a	4.78E-03	1.085	109	6	0.881	7	64	0.28	1.05	1.23	1.17
pk093-3-b	4.86E-03	1.090	108	5	0.885	8	64	0.41	1.06	1.23	1.16
pk093-4-a	1.23E-02	1.090	72	14	0.873	293	72	0.26	1.05	1.25	1.19
pk093-4-b	1.27E-02	1.097	69	13	0.865	291	73	0.28	1.06	1.27	1.20
pk093-4-c	1.19E-02	1.092	70	14	0.868	286	73	0.25	1.05	1.26	1.20
pk093-4-d	1.24E-02	1.094	71	13	0.867	294	73	0.26	1.05	1.26	1.20
pk093-5-a	4.67E-03	1.086	89	2	0.886	355	58	0.35	1.06	1.23	1.16
pk093-5-b	4.40E-03	1.084	81	1	0.885	350	58	0.30	1.05	1.23	1.17
pk099-1-a	3.14E-03	1.008	223	3	0.988	11	87	0.21	1.00	1.02	1.02
pk099-1-b	3.30E-03	1.008	30	3	0.988	168	86	0.20	1.00	1.02	1.02
pk099-2-a	6.92E-03	1.089	29	4	0.865	267	83	0.20	1.04	1.26	1.21
pk099-3-b	1.83E-03	1.024	56	41	0.967	211	47	0.35	1.02	1.06	1.04
pk099-4-a	3.31E-03	1.019	97	9	0.965	243	79	0.08	1.00	1.06	1.05
pk099-4-b	3.68E-03	1.022	298	5	0.959	61	82	0.04	1.00	1.07	1.06
pk099-5-a	3.80E-03	1.033	2	8	0.951	207	81	0.26	1.02	1.09	1.07
pk099-5-b	3.88E-03	1.029	23	10	0.956	206	80	0.22	1.01	1.08	1.06
pk099-5-c	3.56E-03	1.019	4	5	0.971	191	85	0.24	1.01	1.05	1.04
pk110-1-b	6.14E-04	1.026	208	41	0.963	9	48	0.27	1.01	1.07	1.05
pk110-1-a	5.90E-04	1.027	206	39	0.966	10	50	0.49	1.02	1.06	1.04
pk110-2-a	3.77E-03	1.004	356	32	0.995	153	55	0.67	1.00	1.01	1.01
pk110-2-b	3.79E-03	1.004	348	35	0.995	162	55	0.47	1.00	1.01	1.01
pk110-2-c	3.41E-03	1.003	357	31	0.996	156	58	0.51	1.00	1.01	1.01
pk110-3-a	7.42E-04	1.034	138	27	0.970	320	63	1.35	1.04	1.07	1.03
pk110-3-b	7.50E-04	1.016	155	23	0.980	343	66	0.46	1.01	1.04	1.03
pk110-4-a	7.42E-04	1.042	127	11	0.956	351	75	0.81	1.04	1.09	1.05

Table 2 Continued

Specimen	K-bulk	K max	Dec Max	Inc Max	K min	Dec Min	Inc Min	Flinnk	L	P	F
pk110-4-b	7.03E-04	1.032	144	18	0.966	359	69	0.78	1.02	1.04	1.02
pk110-4-c	7.47E-04	1.017	159	0	0.983	66	83	0.95	1.01	1.06	1.05
pk110-5-a	1.19E-03	1.024	245	7	0.966	138	66	0.27	1.01	1.06	1.05
pk110-5-b	1.25E-03	1.025	30	8	0.965	139	65	0.29	1.02	1.05	1.04
pk110-5-c	1.19E-03	1.023	11	11	0.971	139	72	0.44	1.02	1.06	1.03
pk110-5-d	1.14E-03	1.026	22	6	0.971	126	67	0.75	1.02	1.04	1.02

contain a significant sedimentation history. Nelson et al. (1994) described a model for post-caldera collapse and sedimentation. Phase 1 is represented by the initial collapse of the caldera roof, which creates the ring fault and the basin for sedimentation. Phase 2 is represented by subaerial deposition of ignimbrite and debris fans from caldera walls, which create the basin floor; wide ranging volcanism continues through this period. Phase 3 is a period of subaqueous sedimentation of flat-lying lake turbidites and pollen- and diatom-rich muddy sediment covering growing domes; this period is still rife with volcanism. Phase 4 is a period of continued subaqueous rapid sedimentation without volcanism. Kulshan caldera fits reasonably well into this model. The initial 1000 m of ignimbrite (Hildreth, 1996) and the bottom six meters of Kulshan sedimentary stratigraphy represent the subaerial component after the initial ring fault collapse. After the subaerial rock falls, Kulshan experienced subaqueous sedimentation with varying amounts of volcanism (dome building, lava flows and sill and dike intrusions). The final stage of the model differs from the record at Kulshan caldera. Dates from Crater Lake indicate that volcanism subsided ca. 3 ka after the initial collapse (Bacon and Lanphere, 2006); Kulshan caldera volcanism continued for ca. 150 ka (Hildreth et al., 2004). The sediments indicate Kulshan caldera experienced subaqueous sedimentation. Yet Phase 4 (sedimentation without volcanism) is disputed by the fact that Camp Kiser lava sits atop the sediments, indicating Kulshan caldera never experienced the final phase.

On the basis of present day precipitation rates, known porous layers on the caldera rim, and no additional inputs, Bacon et al. (2002) estimated that Crater Lake had a filling time of 300 yrs after the initial collapse. This study proposes that Kulshan caldera had a similar filling rate, if not faster. A subglacial eruption, heavy precipitation (assuming

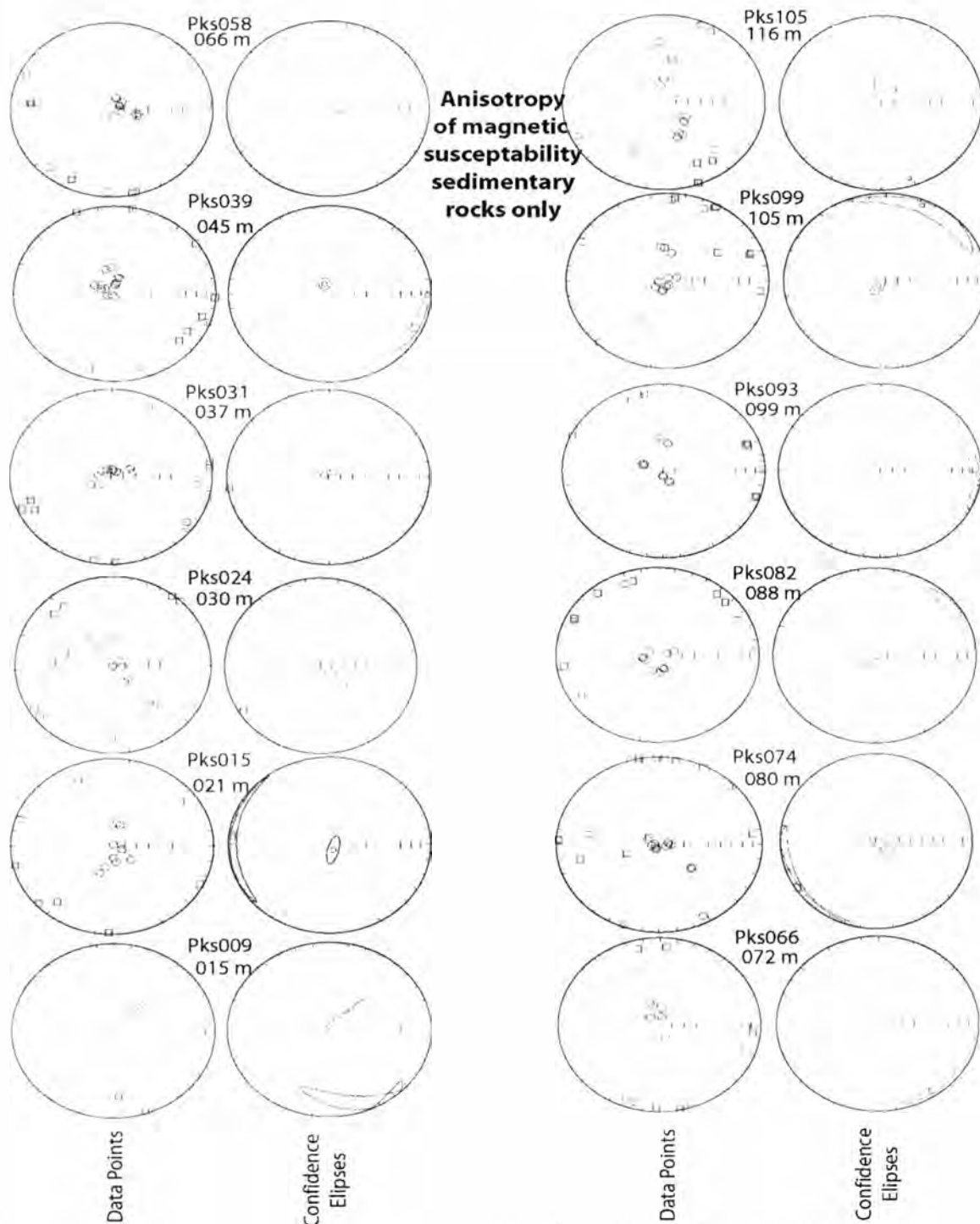


Figure 15. Bootstrap confidence ellipses around the data points indicate the minimum susceptibility (circles) is close to vertical, implying quiet water settling. Wide degree of scatter in the maximum susceptibility (squares) for most sites also implies quiet water settling. In the sites where the squares are grouped NRM measurement help to determine if there was slumping after deposition.

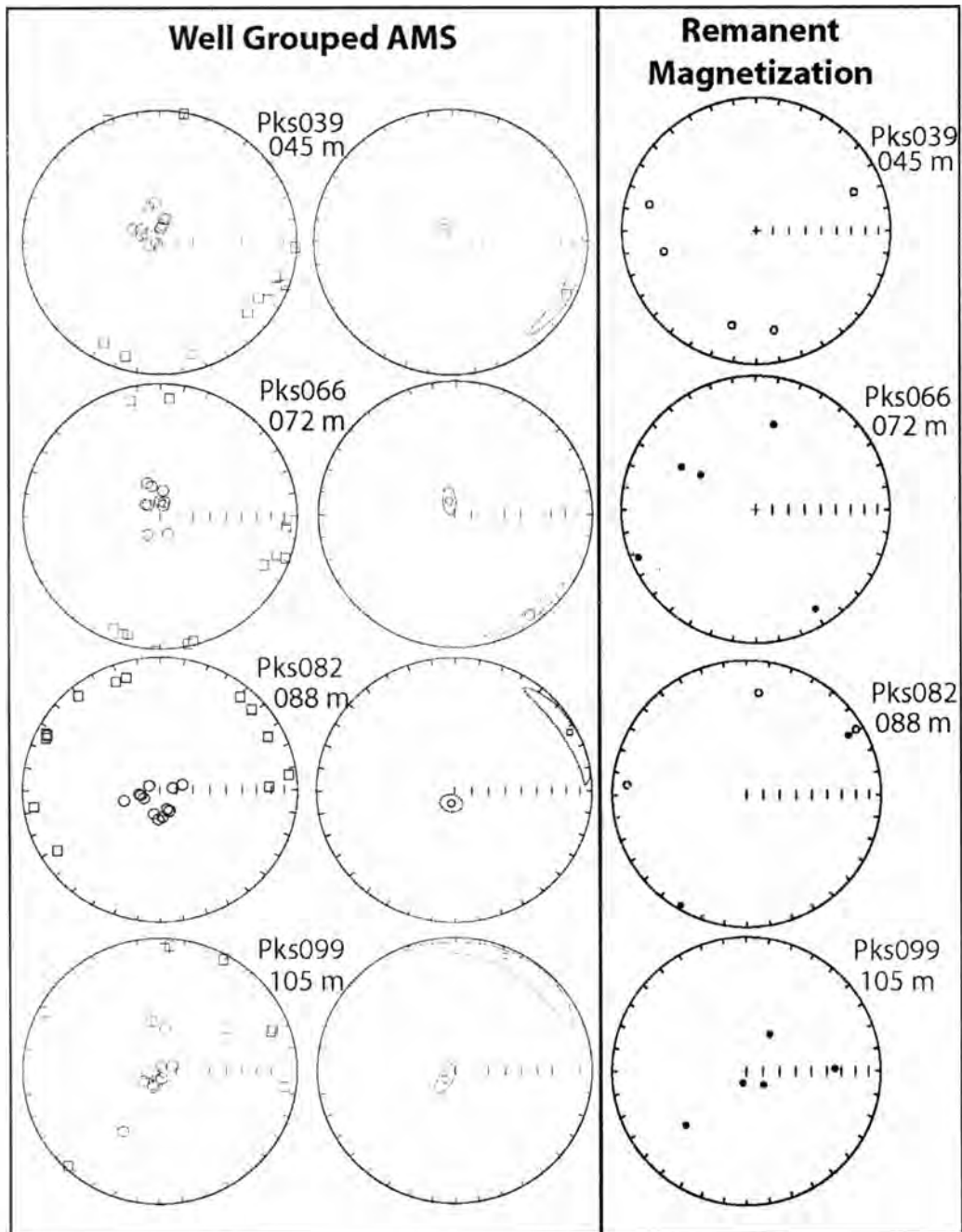


Figure 16. Comparing the well-grouped maximum susceptibilities to the grouping of NRM's can indicate post-depositional slumping. In Kulshan caldera, the remanent magnetizations of sites Pks039, Pks066 and Pks099 have three of the best groupings of all the sites; therefore, it is not post-depositional slumping that caused the NRM scatter but most likely lightning.

similar rates of precipitation as today), and melting of rim glaciers during volcanism all indicate that Kulshan caldera likely filled rapidly.

Stratigraphy and sedimentology from Crater Lake were analyzed by Nelson et al. (1994). Cores (1.5 m) with diatomaceous and pollen rich mud were retrieved from submerged domes and the central platform. Geophysical surveys indicate flat-lying turbidites cover the deeper basins and debris fans lie as aprons near the caldera wall. The sedimentary units of Kulshan caldera have remarkable likeness to the geophysical results of Crater Lake. Units from the sedimentary sequence in the Wells Creek area are akin to the deposits found on the central platform of Crater Lake. Carbon dates from Crater Lake indicate a rate of sedimentation of around 7 cm/ka (center platform) and 246-1007 cm/ka (near slopes). The lower limits on the rates of sedimentation at Kulshan caldera (80 cm/ka) is an order of magnitude greater than central platforms of Crater Lake and an order of magnitude less than the rates of sedimentation on the debris aprons of Crater Lake.

Similar to Crater Lake in Oregon, the Holocene Laguna de Ayarza (4 x 6.5 km), Guatemala still has a lake residing within the caldera rim and sampling was done through nine meter cores and geophysical analysis (Poppe et al., 1985). The results were akin to Crater Lake results; 170 m of sediment has accumulated since the initial eruption 23 kya. This results in a sedimentation rate of 7 m/ka. Turbidites dominate the top nine meters and unfaulted flat-lying sediments are the only noticeable features from seismic surveys. Also, similar to Crater Lake, the cores revealed biota in the form of diatoms. Mineralogy of sediments show hydrothermal alteration has transformed much of the silt and fine-grained ash to clay.

Cores and geophysical data from the $23,100 \pm 500$ years B.P. 18 x 12 km Lake Atitlan, Guatemala reveal similar traits to Crater Lake (Newhall et al., 1987), types and rates of sedimentation depend greatly on water depth and distance from the source. Turbidites, rainfall seasonal varves, and deltaic deposits all are found in 9.8 m cores. Diatoms gastropods and plant detritus are forms of biota described in the cores. Estimations for the rate of sedimentation are 0.5 cm/yr. Though Lake Atitlan is significantly larger than Kulshan, it serves as an analogous depositional environments.

In the cases of Lake Taupo, New Zealand and Creede caldera, Colorado, size does matter in terms of sedimentary environment. Taupo caldera could more properly be described as a large lake with a volcano residing inside. Smith (1991) and Riggs et al. (2001) described the detailed stratigraphy and sedimentology from Taupo's most recent eruption at 181 AD, indicating rafted pumice and wave-dominated shoreline deposits as well as stream flow into a fast-rising, followed by a fast-receding Lake Taupo. Kulshan's deep basin and steep caldera walls make it a completely different basin type than Taupo. Basin topography is the greatest factor for determining good analogous calderas.

Creede caldera, part of the Oligocene San Juan volcanic belt of southwest Colorado, is a 15 x 18 km caldera with a large resurgent dome in the center and a moat of sedimentary rocks surrounding the dome (Larson and Nelson, 2000; Larson and Crossey, 1996). The lithofacies of Creede caldera include ash flow tuffs, ash fallout, alluvial fans, breccias, lake turbidites, deltas, and laminar lake beds. Creede caldera experienced turbidite deposits intermixed with debris flows consisting primarily of tuffaceous sediments (Heiken et al., 2000). Laminated carbonate deposits found between beds of lacustrine tuffaceous sediments are interpreted as precipitates from lake water. Secondary hydrothermal alteration has changed much of the originally deposited mineralogy. Two

features that make Creede caldera sedimentary sequence different from calderas in my study are the presence of travertine and carbonate deposits.

Kulshan caldera fits the model and depositional environments seen in other small (<10km) calderas (Crater Lake, Lake Atitlan, and Lagune de Ayarza). The most significant difference between Kulshan caldera and other calderas is the apparent lack of fossils or trace fossils.

The existence of glaciers/ice was the second biggest difference between Kulshan caldera and analogous calderas. Besides creating an inhospitable environment for plants to grow, the melting of ice into Kulshan caldera lake resulted in dropstones found throughout the sequence. Glaciers are a vast source of water during times of melt and would have added much to the water supply. Hildreth (1996) also speculates that glaciers carved out the northern rim of the caldera. This could have very well marked the end of the lacustrine environment at Kulshan caldera.

Future work around the Wells Creek basin could provide information about the degree of hydrothermal alteration towards the center of the caldera. Understanding contact relationships between sediments and post-caldera lava domes should yield tighter age constraints and a better picture of the depositional environments. A project looking at the paleomagnetic signature of the sediments of the Wells Creek area may reveal information about the duration of transitions and age of the lacustrine environment at Kulshan caldera.

References

- Bacon, C.R., and Lanphere, M.L. 2006. Eruptive history and geochronology of Mount Mazama and the Crater Lake region, Oregon. *Geological Society of America Bulletin*, **118**: 1331–1359.
- Bacon, C.R., Gardner, J.V., Mayer, L.A., Buktenica, M.W., Dartnell, P., Ramsey D.W., & Robinson, J.E. 2002. Morphology, volcanism, and mass wasting in Crater Lake, Oregon. *Geological Society of America Bulletin* **114**(6): 675–692.
- Clement, B. 2004. Dependence of the duration of geomagnetic polarity reversal on site latitude. *Nature*, **428**, 637–640.
- Gibbard, P. and van Kolfshoten, T. 2004 The Pleistocene and Holocene Epochs Chapter 22 *In*, A Geologic Time Scale 2004. *Edited by* Gradstein, F., Ogg, J., and Smith, A. Cambridge University Press, Cambridge, 589.
- Gradstein, F., Ogg, J., and Smith, A. 2004. A geologic time scale 2004. Cambridge University Press, Cambridge, 598p.
- Heiken, G., Krier, D., McCormick, T., and Snow, G. 2000. Intracaldera volcanism and sedimentation- Creede Caldera, Colorado. *In* Ancient Lake Creede: Its volcano-tectonic setting, history of sedimentation, and relation to mineralization in the Creede Mining District. *Edited by* Bethke, P.M., and Hay, R.L. Geological Society of America Special Paper, **346**, 127–157.
- Hildreth, W. 1996. Kulshan caldera: a Quaternary subglacial caldera in the North Cascades, Washington. *Geological Society of America Bulletin*, **108**, 786–793.
- Hildreth, W., Fierstein, J., and Lanphere, M. 2003. Eruptive History and Chronology of the Mount Baker volcanic field, Washington. *Geological Society of America Bulletin*, **115**, 729-765.
- Hildreth, W., Lanphere, M.A., Champion, D.E., and Fierstein, J. 2004. Rhyodacites of the Kulshan caldera, north Cascades of Washington: Postcaldera lavas that span the Jaramillo. *Journal of Volcanology and Geothermal Research*, **130**, 227–264.
- Housen, B., Richter, C. and van der Pluijm, B.A. 1993. Composite magnetic anisotropy fabrics: experiments, numerical models, and implications for the quantification of rocks fabrics. *Tectonophysics*, **220**, 1–12.
- Larson, D. and Crossey, L.J. 1996. Depositional environments and paleolimnology of an ancient caldera lake: Oligocene Creede Formation, Colorado. *Geologic Society of America Bulletin*, **108**, 526-544.

- Larsen, D., and Nelson, P.H. 2000. Stratigraphy, correlation, depositional setting, and geophysical characteristics of the Oligocene Snowshoe Mountain Tuff and Creede Formation in two cored boreholes. *In* Ancient Lake Creede: Its volcano-tectonic setting, history of sedimentation, and relation to mineralization in the Creede Mining District. *Edited by* Bethke, P.M., and Hay, R.L. Geological Society of America Special Paper, **346**, 159–178.
- Nelson, C.H., Bacon, C.R., Robinson, S.W., Adam, D.P., Bradbury, J.P., Barber, J.H. Jr., Schwartz, D., and Vagenas, G. 1994. The volcanic, sedimentologic and paleolimnologic history of the Crater Lake caldera floor, Oregon: Evidence for small caldera evolution. *Geological Society of America Bulletin*, **106**, 684–704.
- Newhall, C.G., Paull, C.K., Bradbury, J.P., Higuera-Grundy, A., Poppe, L.J., Self, S., Bonar Sharpless, N., and Ziagos, J. 1987. Recent Geologic History of Lake Atitlan, a caldera lake in Western Guatemala. *Journal of Volcanology and Geothermal Research*, **33**, 81-107.
- Opdyke, N.D., and Channell, J.E.T. 1996. *Magnetic stratigraphy*. Academic Press, San Diego, California, 341 p.
- Poppe, L.J., Paull, C.K., Newhall, C.G., Bradbury, J.P., and Ziagos, J. 1985. A geophysical and geological study of Laguna de Ayarza, a Guatemalan caldera lake. *Journal of Volcanology and Geothermal Research*, **25**, 125–144.
- Reading, H. G. 1996. *Sedimentary environments: Processes, facies and stratigraphy*. Elsevier, New York, 544 p.
- Riggs, N.R., Ort, M.H., White, J.D.L., Wilson, C.J.N., Houghton, B.F. and Clarkson, R. 2001. Post-1.8-ka marginal sedimentation in Lake Taupo, New Zealand: effects of wave energy and sediment supply in a rapidly rising lake. *In* *Volcaniclastic Sedimentation in Lacustrine Settings* *Edited by* J.D.L. White and N.R. Riggs. International Association Sedimentologists Special Publication, **30**, pp. 151–178.
- Rytuba, J.J., Minor, S.A., McKee, E.H. 1981. Geology of the Whitehorse caldera and caldera fill-deposits, Malheur County, Oregon. United States Geologic Survey Open-File Report, **81-1092**, 1-19.
- Schweher, K. and Tauxe, L. 2003. Characterization on soft-sediment deformation: detection of cryptoslumps using magnetic methods. *Geology*, **31**, 203-206.
- Singer, B., Hoffman, K.A., Coe, R.S., Brown, L.L., Jicha, B.R., Pringle, M.S., and Chauvin A. 2005. Structural and temporal requirements for geomagnetic field reversal deduced from lava flows. *Nature*, **434**, 633–636.
- Smith, R.C.M. 1991. Post-eruption sedimentation on the margin of a caldera lake, Taupo Volcanic Centre, New Zealand. *Sedimentary Geology*. **74**, 89–138.

Tauxe, L. 1998. *Paleomagnetic Principles and Practice*. Kluwer Academic Publishers, Dordrecht, The Netherlands. 277 p.

Truswell, J.A. 1972. Sanstone sheet and related intrusions from Coffee Bay, Transkei, South Africa. *Journal of Sedimentary Petrology*, **42**, 578-593.

Tucker, D., Hildreth, W., Ullrich, T., Friedman, R. 2007. Geology and complex collapse mechanisms of the 3.72 Ma Hannegan Caldera, north Cascades, Washington, USA. *Geologic Society of America Bulletin*, **119**, 329-342.

Watson, G.S. 1956. A test for randomness of directions. *Royal Astronomical Society Monthly Notes, Geophysical Supplement*, **7**, 160–161.

Westgate, J. A., Easterbrook, D. J., Naeser, N. D., and Carson, R. J. 1987. Lake Tapps Tephra: An early Pleistocene stratigraphic marker in the Puget lowland, Washington. *Quaternary Research*, **28**, 340–355.

White, J.D.L., Manville, V., Wilson, C.J.N., Houghton, B.F., Riggs, N.R. and Ort, M. 2001. Settling and deposition of 181 AD Taupo pumice in lacustrine and associated environments . *In Volcaniclastic Sedimentation in Lacustrine Settings Edited by J.D.L. White and N.R. Riggs*. International Association Sedimentologists Special Publication, **30**, pp. 141–150.

APPENDIX A

MAGNETIC STRATIGRAPHY

Full Methods

Magnetic stratigraphy is the process of analyzing the magnetic record of samples collected through a stratigraphic sequence. In the most idealized magnetic stratigraphy project, sites within a horizon would correlate statistically and result in a magnetic polarity and magnetic direction and inclination. These horizons would then be stacked according to their stratigraphy and compared to known magnetic polarities and dates could then be applied. In the best-case scenario the horizons would also be selected in six meter intervals as to most accurately portray the magnetic record without having too many missing intervals.

The geology of Kulshan caldera immediately lent itself to several difficulties. Below is a lithological description of each horizon sampled in Kulshan caldera. Information from this data is the spacing interval, the medium for magnetic minerals, potential strength of magnetization, and coherence of cementation. The first letter describes its assumed age (P- Pleistocene), the second letter describes the location (k- Kulshan), the third letter is a description of the rock type (s- sedimentary, d- dike, l-lava, nd- near dike), and if there is a fourth symbol, it describes the location in terms of stratigraphy (i.e. 009- 9 meters up section, add six meters (8 for pks072) for a correction made after sample- 15 meters).

Pkd- This is a series of five cores taken vertically from a lava dike. They were all taken between 24 meters and 37 meters. There is no data taken describing the lateral location of sampling in the dike. Cores were very solid.

Pknd- This is a series of five cores taken from a sand and tuffaceous unit less than .5 meters from the dike. Here we hoped to see if the samples collected here have recorded the dike intrusion over the initial deposition. Cores were very solid.

Pks009- These cores came from a sandstone layer. The layer was found a few meters above the basement breccia. This rock has a significant proportion of clastic sand grains. The next most abundant grain is plagioclase feldspar, and thirdly hornblende. The matrix is mostly glassy but shades of calcite can be found filling small spaces. These cores had a hard cementation but broke frequently along planar laminations. This was chosen to be the first site because it is the first unit where predominant grains are clastic, and all are sand grain in size.

Pks015- These cores come from a sandstone layer that still has high proportions of clastic grains but far less than Pks009; they also have higher percents of plagioclase than Pks009. The amount of hornblende is similar to Pks015. Cores were solid.

Pks024- These cores were taken from a tuffaceous unit. There were pumice clasts up to 2 cm down to 1 mm. The pumice clasts were matrix supported. The matrix was glass and comprised significant portions of the samples. Cores were solid.

Pks031- Cores were taken from a sandstone layer. The sandstone is predominantly plagioclase, there are similar percentages of hornblende as previous sandstones and small amounts of biotite. The matrix is glass with calcite filling cracks.

Pks039- Cores were taken from a well-lithified siltstone layer. The grains are too small to be classified but they appear to be mostly glass.

Pks058- Cores were taken from a well-lithified siltstone layer. The grains are too small to be classified but they appear to be mostly glass. The gap of 19 meters here between horizons was due to a large gap of rhythmites, where sand units were not thick enough for coring.

Pks066- Cores were taken from a sandstone layer. It is similar in composition to Pks031, predominantly plagioclase.

PkI066- These cores came from an andesite lava sill.

Pks074- Cores were taken from a very well-lithified sandstone layer. This unit rests on top of the lava sill. It seems that alteration from the lava sill made the unit more coherent than the rest. Its composition is similar to the other non-clastic dominated sandstones. There is a green color to the cores.

Pks080- Cores were taken from a well-lithified siltstone layer. The grains are too small to be classified but they appear to be mostly glass.

Pks093- Cores were taken from a sandstone layer. It is similar in composition to Pks031, predominantly plagioclase. Cores were solid.

Pks099- Cores were taken from a sandstone layer. It is similar in composition to Pks031, predominantly plagioclase. The cores are very brittle.

Pks110- Cores were taken from a sandy unit composed predominantly of plagioclase grains. The sand here is a small unit sitting in a larger field of gravely pumaceous silt. The cores are very brittle.

The process for determining magnetic stratigraphy began by collecting oriented field samples. Wilderness restrictions in Kulshan caldera prevented the collections of samples using the conventional drilling methods. Paleomagnetic statistical models require 5 to 7 samples per stratigraphic horizon (or site) (Tauxe, 1998). I collected 76 coherent oriented blocks representing 13 stratigraphic horizons (including an andesite sill), one andesite dike site, and one near dike site. The maximum distance between horizons is 15 meters and the minimum distance is six meters.

The samples were drilled with a nonmagnetic drill to obtain one core per sample. The cores were then marked and cut with a nonmagnetic diamond saw blade. Samples were marked according the standards set at the Pacific Northwest Paleomagnetic laboratory. Each specimen was tested for magnetic susceptibility on a Kappabridge KLY-3. Samples were then stored in a magnetically shielded room. Before demagnetization each specimen was soaked in liquid nitrogen for twenty minute intervals as many as two times to remove variable remanent magnetization (VRM). Two sets of samples were created to determine whether alternating field (AF) demagnetization or thermal demagnetization would give the best results for determining magnetic stratigraphy. The first half of the test group specimens were subjected to the alternating magnetic field demagnetizer and subsequently measured in the magnetometer. The alternating field (AF) test specimens were subjected to increasing intensities in magnetic fields of 2.5, 5, 7.5, 10, 15, 20, 25, 35, 45, 60, 75, 90, 110, 130, 155, 180, 200 mT. After specimens were subjected to a degree of AF, remanent magnetizations was measured using a 2-G 755 DC SQUID cryogenic magnetometer. The second half of the test group was subjected to thermal demagnetization for 20 minutes in a magnetically shielded

custom built oven, subsequently cooled for 20 minutes, and then their remanent magnetizations were measured at increasing temperature intervals that ran from 77 degrees Celsius to 600 degrees Celsius.

Subsequent results from AF and thermal demagnetization were compared and analyzed for coherency among the two test groups. It was apparent that thermal demagnetization gave the specimen a smoother transition between increasing steps and provided a better chance at missing any potential magnetic field changes. The remaining specimens were demagnetized and analyzed using the thermal demagnetization techniques described above.

The results for both the paleomagnetic test and the AMS can be seen in the journal thesis. The entire set of data, plots, and tables can be found the Data Repository found in the back of this thesis.

APPENDIX B

PLAGIOCLASE COMPOSITIONS

Four samples from different elevations were sent to the GeoAnalytical lab at Washington State University. Dr. Scott Cornelius performed the analysis looking at the compositions of plagioclase grains. The grains are zoned but no preference was taken towards a particular sampling site. I assumed random sampling of enough grains would negate the possible zoning effects. Table B 1 shows compositions from plagioclase at 21 meters. Table B 2 shows compositions from plagioclase at 31 meters. Table B 3 shows compositions from plagioclase at 88 meters. Table B 4 shows compositions from plagioclase at 100 meters. Percent anorthite was calculated on an Excel document titled norm4. This file along with all data for the plagioclase composition can be found in the data repository

Table B 1. Plagioclase compositions from 21 meters.

PKS 15	Line Numbers	SiO ₂		BaO		Al ₂ O ₃		Fe ₂ O ₃		CaO		Na ₂ O		K ₂ O		Oxide Totals		% Anorthite		% Albite		% Orthoclase			
		Oxide	Percents	Oxide	Percents	Oxide	Percents	Oxide	Percents	Oxide	Percents	Oxide	Percents	Oxide	Percents	Oxide	Percents	Oxide	Percents	Oxide	Percents	Oxide	Percents	Oxide	Percents
	175	58.48	0.07	26.22	0.25	7.55	7.08	0.39	100.03	37.45	58.97	2.30													
	176	60.30	0.10	24.97	0.25	6.28	7.50	0.54	99.95	31.60	63.46	3.19													
	177	57.78	0.07	26.67	0.29	7.93	6.70	0.33	99.77	39.50	56.69	1.95													
	178	59.63	0.03	25.19	0.29	6.46	7.70	0.50	99.80	32.40	64.96	2.95													
	179	59.39	0.10	25.75	0.25	7.06	7.03	0.44	100.02	35.70	59.49	2.60													
	180	59.81	0.08	25.23	0.29	6.52	7.57	0.51	100.02	32.40	63.58	3.01													
	181	53.82	0.06	29.04	0.30	10.79	5.18	0.24	99.43	54.10	42.89	1.41													
	182	56.33	0.05	27.73	0.33	8.97	6.13	0.33	99.86	44.70	51.87	1.95													
	183	60.44	0.07	24.44	0.23	5.69	7.97	0.56	99.39	28.50	66.76	3.31													
	184	50.16	0.05	31.83	0.50	14.03	3.60	0.12	100.29	70.60	27.30	0.71													
	185	58.65	0.12	25.95	0.28	7.27	7.14	0.43	99.86	36.10	60.10	0.18													
	186	59.14	0.06	24.98	0.23	6.52	7.42	0.66	99.00	33.10	61.50	3.90													
	187	51.47	0.03	30.35	0.31	12.44	4.26	0.16	99.02	62.70	34.58	0.95													
	188	59.30	0.08	25.95	0.29	7.04	7.20	0.41	100.28	35.10	61.00	2.42													
	189	59.59	0.11	25.57	0.25	6.65	7.46	0.47	100.11	33.00	63.10	2.77													
	190	53.41	0.08	29.72	0.35	11.67	5.15	0.17	100.55	58.30	38.67	1.00													
	191	57.59	0.04	26.62	0.25	7.99	6.80	0.36	99.66	39.90	56.36	2.13													
	192	50.21	-0.02	31.85	0.36	13.65	3.78	0.13	99.95	69.20	28.39	0.77													
	193	53.10	0.05	29.79	0.45	11.53	4.71	0.20	99.83	57.50	39.85	1.82													
	194	56.74	-0.01	26.99	0.28	8.58	6.21	0.29	99.08	43.30	52.55	1.72													
	195	60.37	-0.03	24.65	0.22	5.88	7.97	0.58	99.65	29.60	65.50	3.43													
	196	57.12	-0.01	27.08	0.42	8.60	6.46	0.28	99.95	42.50	54.40	1.65													
	197	58.80	0.03	26.00	0.32	7.27	7.17	0.44	100.04	36.10	60.10	2.60													

Table B 2. Plagioclase compositions from 31 meters.

PKS 24	Line Numbers	SiO2		BaO		Al2O3		Fe2O3		CaO		Na2O		K2O		Oxide Totals		% Anorthite		% Albite		% Orthoclase			
		Oxide	Percents	Oxide	Percents	Oxide	Percents	Oxide	Percents	Oxide	Percents	Oxide	Percents	Oxide	Percents	Oxide	Percents	Oxide	Percents	Oxide	Percents	Oxide	Percents	Oxide	Percents
	198	60.62	0.06	24.94	0.25	6.05	7.68	0.53	100.13	30.30	65.00	3.20													
	199	56.08	0.01	27.30	0.27	9.11	6.31	0.26	99.33	45.70	50.70	1.60													
	200	58.82	0.06	25.90	0.27	7.01	7.08	0.45	99.58	35.40	60.00	2.70													
	201	60.98	0.02	24.70	0.23	5.97	7.66	0.51	100.08	30.10	64.80	3.10													
	202	60.61	0.10	24.36	0.25	5.56	8.07	0.60	99.55	28.00	67.00	3.60													
	203	52.80	0.00	30.12	0.34	11.86	4.64	0.19	99.96	59.20	38.30	1.30													
	204	56.53	0.01	27.03	0.24	8.68	6.28	0.32	99.09	43.30	53.20	1.90													
	205	59.21	0.14	25.12	0.24	6.61	7.28	0.47	99.09	33.40	61.60	2.80													
	206	57.70	0.02	26.36	0.22	7.75	7.09	0.38	99.52	39.10	56.40	2.20													
	207	54.56	0.05	27.40	0.67	9.54	5.65	0.34	98.22	48.60	47.20	2.00													
	208	57.23	0.03	26.79	0.26	7.96	6.58	0.41	99.26	40.10	55.70	2.40													
	209	58.99	0.09	25.81	0.25	6.91	7.29	0.51	99.86	34.60	61.20	3.01													
	210	60.01	0.12	24.79	0.24	6.12	7.60	0.52	99.40	30.80	64.30	3.10													
	211	54.83	0.03	28.04	0.38	9.80	5.87	0.27	99.23	49.70	46.50	1.60													
	212	59.49	0.06	25.23	0.31	6.60	7.56	0.53	99.77	33.10	62.40	3.20													
	213	59.32	0.00	25.59	0.26	7.08	7.29	0.45	99.98	35.00	61.50	2.60													
	214	58.28	0.11	26.12	0.26	7.54	6.97	0.43	99.72	37.50	58.73	2.50													
	215	60.99	0.12	24.27	0.26	5.51	7.98	0.64	99.77	27.60	67.50	3.80													
	216	59.05	0.05	25.54	0.25	6.78	7.33	0.51	99.51	33.90	61.70	3.00													
	217	52.20	0.04	30.06	0.54	12.31	4.35	0.14	99.64	61.30	36.40	0.80													
	218	59.18	0.05	25.68	0.22	6.92	7.27	0.48	99.79	34.50	61.50	2.80													
	219	59.52	0.14	25.09	0.25	6.48	7.33	0.49	99.29	32.80	62.00	3.00													
	220	54.29	0.02	28.92	0.29	10.71	5.32	0.22	99.76	53.30	43.80	1.30													

Table B 3. Plagioclase compositions from 88 meters

PKS 82	Line Numbers	SiO ₂		BaO		Al ₂ O ₃		Fe ₂ O ₃		CaO		Na ₂ O		K ₂ O		Oxide Totals		% Anorthite		% Albite		% Orthoclase	
		Oxide	Percents	Oxide	Percents	Oxide	Percents	Oxide	Percents	Oxide	Percents	Oxide	Percents	Oxide	Percents	Oxide	Percents	Oxide	Percents	Oxide	Percents	Oxide	Percents
	231	59.69	0.07	25.32	0.29	6.56	7.39	0.51	99.84	32.90	63.00	3.00											
	232	54.70	0.04	28.76	0.50	10.67	5.12	0.22	100.00	53.50	43.40	1.30											
	233	58.90	0.12	26.43	0.27	7.51	6.67	0.43	100.34	38.40	56.50	2.50											
	234	59.40	0.09	25.30	0.26	6.92	7.19	0.40	99.55	34.70	61.00	2.50											
	235	60.43	0.07	24.55	0.23	5.85	7.66	0.57	99.36	29.70	65.00	4.00											
	236	48.54	-0.01	31.95	0.56	14.44	3.07	0.14	98.69	73.90	24.00	1.00											
	238	61.12	0.09	24.75	0.25	5.76	7.64	0.60	100.19	29.40	65.00	4.00											
	239	59.48	-0.03	25.39	0.25	6.97	6.94	0.48	99.48	35.70	59.00	3.00											
	240	60.54	0.12	24.73	0.27	5.98	7.71	0.66	100.00	30.00	65.30	4.00											
	247	59.10	0.06	26.00	0.28	6.97	7.00	0.50	99.91	35.50	60.00	3.00											
	248	52.92	0.01	29.91	0.27	11.96	4.52	0.19	99.78	59.40	38.00	1.30											
	249	61.09	0.08	24.17	0.26	5.59	7.36	1.22	99.78	29.60	63.00	7.00											
	250	60.05	0.09	25.33	0.30	6.54	7.15	0.50	99.96	33.60	61.00	3.00											
	251	55.11	0.04	28.32	0.48	10.08	5.29	0.26	99.59	51.30	45.00	2.00											
	253	57.62	0.09	26.80	0.30	8.10	6.47	0.39	99.78	41.00	55.00	3.00											
	254	58.22	0.07	26.16	0.32	7.66	6.94	0.47	99.84	38.30	58.00	3.00											
	255	60.77	0.10	24.79	0.25	6.07	7.42	0.64	100.02	31.10	63.00	4.00											
	256	59.02	0.10	26.04	0.30	7.42	6.90	0.46	100.24	37.30	59.00	3.00											
	257	60.31	0.05	24.95	0.29	6.28	7.46	0.72	100.06	31.70	63.00	4.00											
	258	59.69	0.00	25.34	0.25	6.77	7.18	0.47	99.69	34.30	61.00	3.00											
	259	53.49	0.10	29.27	0.35	11.47	4.70	0.24	99.63	57.40	40.00	2.00											
	261	60.82	0.09	24.69	0.28	5.92	7.58	0.99	100.38	30.10	64.00	6.00											
	262	58.48	0.06	25.41	0.29	7.60	7.03	0.39	99.26	36.80	59.00	2.00											

Table B 4. Plagioclase compositions from 100 meters.

PKS 93	Line Numbers	SiO2 Oxide Percents	BaO Oxide Percents	Al2O3 Oxide Percents	Fe2O3 Oxide Percents	CaO Oxide Percents	Na2O Oxide Percents	K2O Oxide Percents	Oxide Totals	% Anorthite	% Albite	% Orthoclase
	263	60.18	0.02	25.30	0.32	6.45	7.94	0.38	100.58	32.00	67.00	2.00
	264	60.86	0.08	24.68	0.23	5.83	7.38	0.58	99.65	30.40	63.00	3.00
	265	58.41	0.07	26.13	0.29	7.29	6.83	0.45	99.46	37.10	58.00	3.00
	266	60.25	0.03	24.95	0.24	6.39	7.20	0.52	99.58	32.90	61.00	3.00
	267	59.54	0.06	25.55	0.24	7.08	7.03	0.47	99.95	35.80	60.00	3.00
	268	59.89	0.10	25.66	0.28	6.90	7.03	0.44	100.29	35.20	60.00	3.00
	269	61.39	0.10	24.37	0.28	5.55	7.84	0.72	100.25	28.10	66.00	4.00
	270	60.49	0.06	24.74	0.27	5.99	6.92	1.18	99.65	32.40	59.00	7.00
	271	59.97	0.06	25.27	0.25	6.73	7.29	0.47	100.03	33.80	62.00	3.00
	272	60.93	0.02	24.90	0.22	6.15	7.50	0.57	100.28	31.20	64.00	3.00
	273	56.63	0.03	27.27	0.36	8.95	6.02	0.31	99.58	45.10	51.00	2.00
	274	58.41	0.12	26.45	0.30	7.84	6.52	0.38	100.02	39.90	55.00	2.00
	275	60.38	0.09	24.87	0.30	6.22	7.43	0.49	99.79	31.60	63.00	3.00
	276	59.99	0.09	25.19	0.27	6.68	7.30	0.51	100.02	33.60	62.00	3.00
	277	57.92	0.03	26.54	0.28	8.08	6.69	0.43	99.96	40.10	57.00	3.00
	278	61.51	0.00	24.03	0.22	5.65	7.79	0.60	99.80	28.60	66.00	4.00
	279	61.07	0.07	24.36	0.32	5.92	7.53	0.60	99.88	30.30	64.00	4.00
	280	59.08	0.00	25.62	0.26	7.49	7.02	0.42	99.88	37.10	59.00	2.00
	281	58.82	0.04	26.16	0.26	7.01	6.76	0.47	99.53	36.40	57.00	3.00
	282	60.08	0.06	24.88	0.22	5.90	7.74	0.81	99.68	30.20	64.00	5.00
	283	58.48	0.04	25.89	0.25	7.05	6.89	0.52	99.13	36.10	58.00	3.00
	284	60.88	0.03	24.51	0.25	5.71	7.86	0.59	99.82	28.60	67.00	3.00
	285	60.44	0.11	24.92	0.20	6.12	7.25	1.19	100.23	31.80	61.00	7.00
	286	60.08	0.08	25.07	0.27	6.48	7.42	0.53	99.93	32.60	63.00	3.00

APPENDIX C

PETROGRAPHY

Sample Number

Pks015-2

Locality:

21 meters on strat column
Kulshan caldera sedimentary
unit

Rock Type:

Lithic Arenite

**Megascopic
Description**

Color

Dark Gray to green

Grain size

Coarse to medium sand

Induration

Good

Sedimentary structures

Normal grading

**Microscopic
Descriptions**

Mineral percentage

Plagioclase- 45%	glass/pumice/ash	Lithics- 40%
Biotite-	Hornblende- 5%	Calcite- 5% secondary
Oxides- 1%	Glass Matrix- 5%	

Textures

Rounding

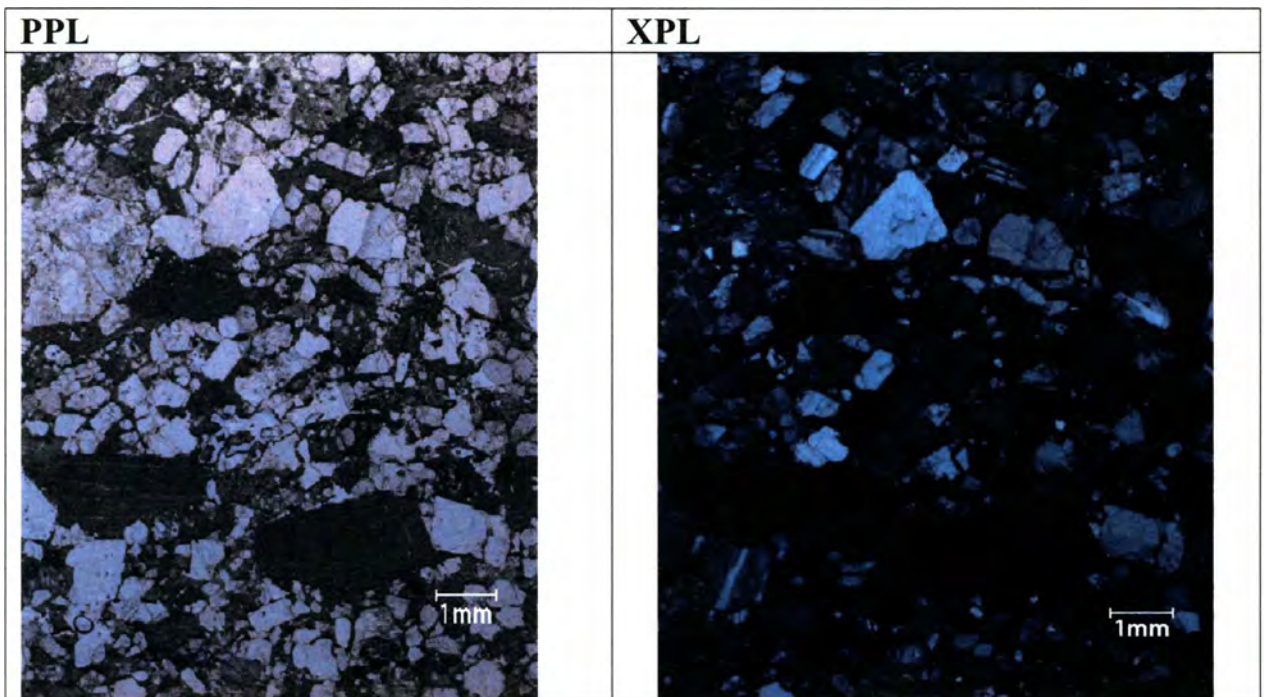
Angular

grain to grain relations

grain supported

Sorting

Good sorting



Sample Number

Pks024-5-b

Locality:30 meters on strat column
Kulshan caldera sedimentary
unit**Rock Type:**

Feldspathic wacke

**Megascopic
Description****Color**

Blue grey with off white

Grain sizeMud, sand, and pumice from
2cm-<1mm**Induration**

Good

Sedimentary structuresBedding in pumice with
some grading**Microscopic
Descriptions****Mineral percentage**

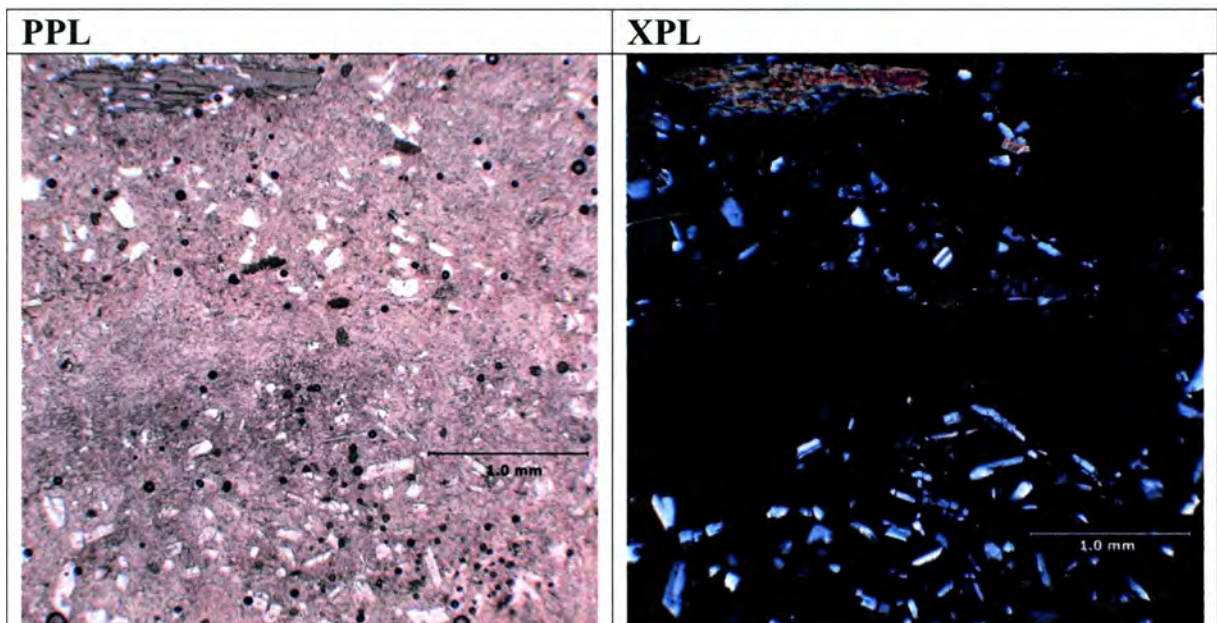
Plagioclase- 20% up to 40% in sand layers	pumice- 40%	Lithics
Biotite	Hornblende- 5%	Calcite
Oxides- 2%	Glass Matrix- 25%	

Textures**Rounding**Angular/
Pumice subangular**grain to grain relations**

Sand

Sorting

Poor



Sample Number

Pks031-3-t

Locality:37 meters on strat column
Kulshan caldera sedimentary
unit**Rock Type:**

Pumaceous wacke

**Megascopic
Description****Color**

Brown

Grain size

Sand

Induration

Good

Sedimentary structures

Bedding

**Microscopic
Descriptions****Mineral percentage**

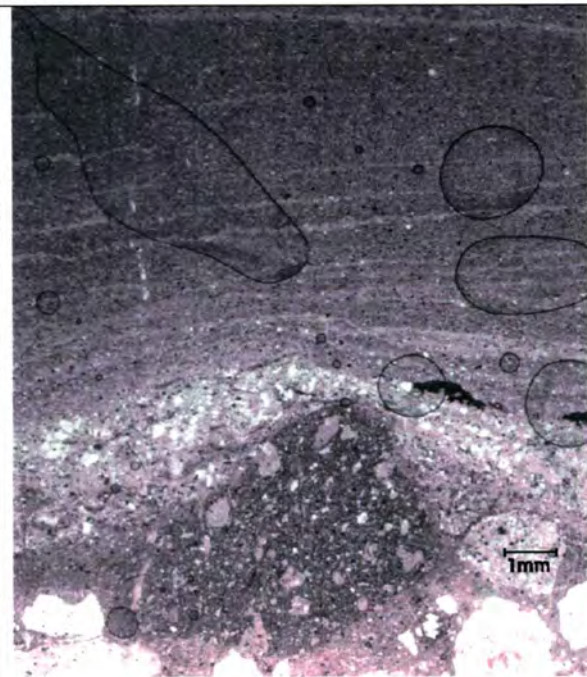
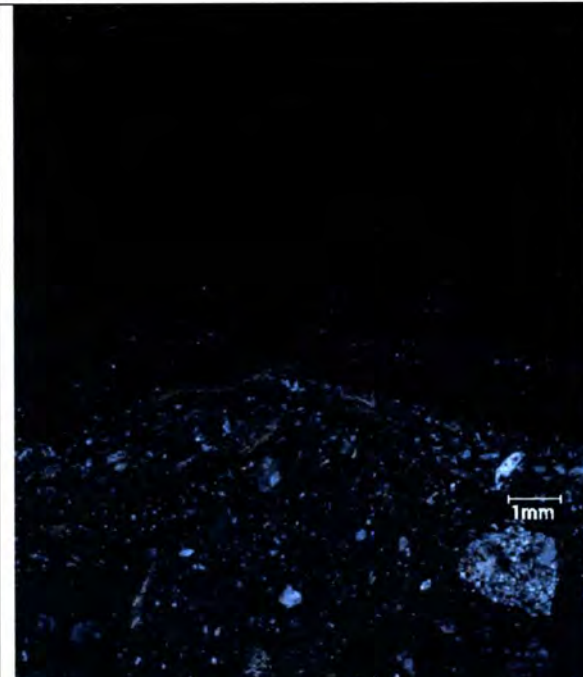
Plagioclase- 45%	pumice- 30%	Lithics- 5%
Biotite	Hornblende- 5%	Calcite
Oxides- 2%	Glass Matrix- 15%	

Textures**Rounding**Angular/
Pumice subangular**grain to grain relations**

in sand beds grain to grain

Sorting

Poor sorting

PPL**XPL**

Sample Number
Pks039-4

Locality:
45 meters on strat column
Kulshan caldera sedimentary
unit

Rock Type:
Feldspathic wacke

**Megascopic
Description**

Color
Brown to tan

Grain size
Silt to fine sand

Induration
Medium

Sedimentary structures
Laminated bedding

**Microscopic
Descriptions**

Mineral percentage

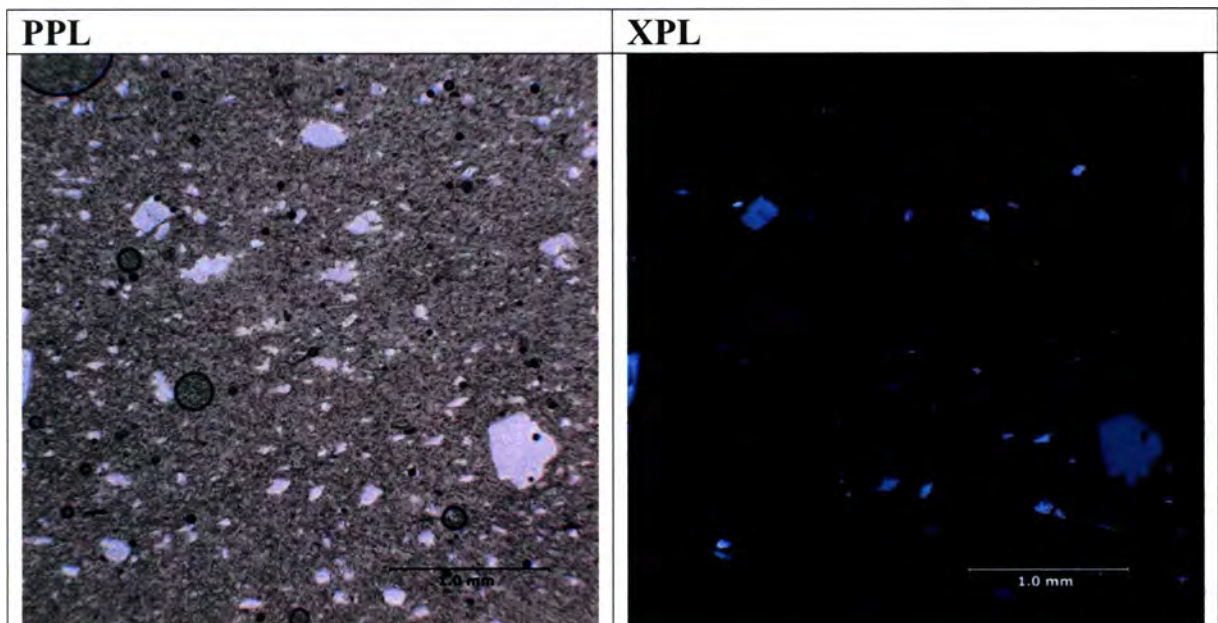
Plagioclase- 35%	Pumice	Lithics- 5%
Biotite	Hornblende- 10%	Calcite
Oxides	Glass Matrix- 50%	

Textures

Rounding
angular

grain to grain relations
matrix supported

Sorting
Poor sorting



Sample Number

Pks058-3

Locality:64 meters on strat column
Kulshan caldera sedimentary
unit**Rock Type:**

Feldspathic wacke

**Megascopic
Description****Color**

Tan

Grain size

Fine sand and silt

Induration

Poor

Sedimentary structures

Laminar bedding

**Microscopic
Descriptions****Mineral percentage**

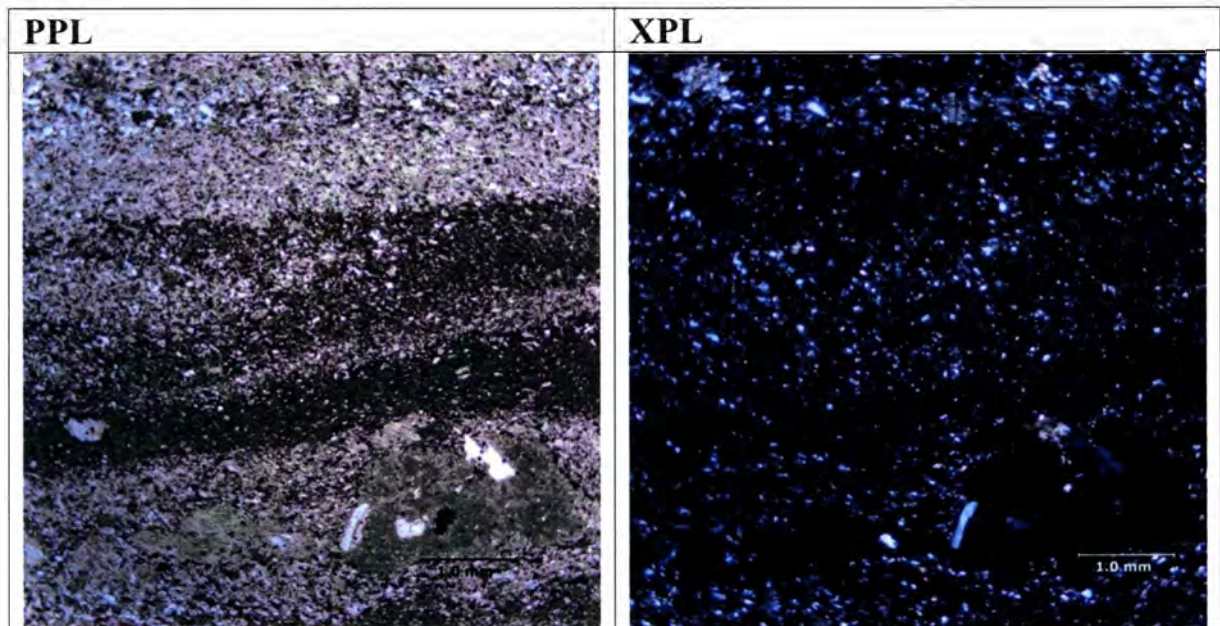
Plagioclase- 30%	pumice- 15%	Lithics- 10%
Biotite	Hornblende- 8%	Calcite
Oxides- 3%	Glass Matrix- 35%	

Textures**Rounding**angular/
pumice subangular**grain to grain relations**

Grain to grain supported

Sorting

Poor sorting



Sample Number

Pks066-2

Locality:66 meters on strat column
Kulshan caldera sedimentary
unit**Rock Type:**

Feldspathic/Lithic arenite

**Megascopic
Description****Color**

Brown

Grain size

Medium sand

Induration

Good

Sedimentary structures

Planar bedding

**Microscopic
Descriptions****Mineral percentage**

Plagioclase- 50%	glass/pumice/ash	Lithics- 15%
Biotite	Hornblende- 25%	Calcite
Oxides- 3%	Glass Matrix- 5%	

Textures**Rounding**

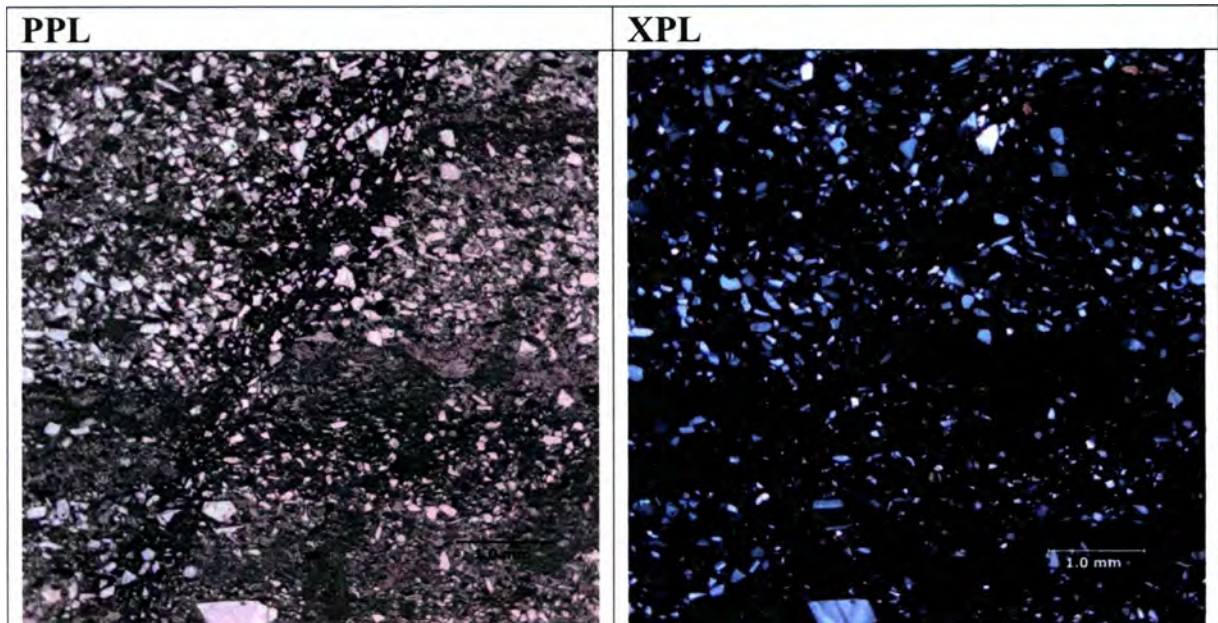
Angular grains

grain to grain relations

Grain supported

Sorting

Medium sorting



Sample Number

Pk1066-3

Locality:72 meters on strat column
Kulshan caldera sedimentary
unit**Rock Type:**

Andesite Sill

**Megascopic
Description****Color**

red brown

Crystal size

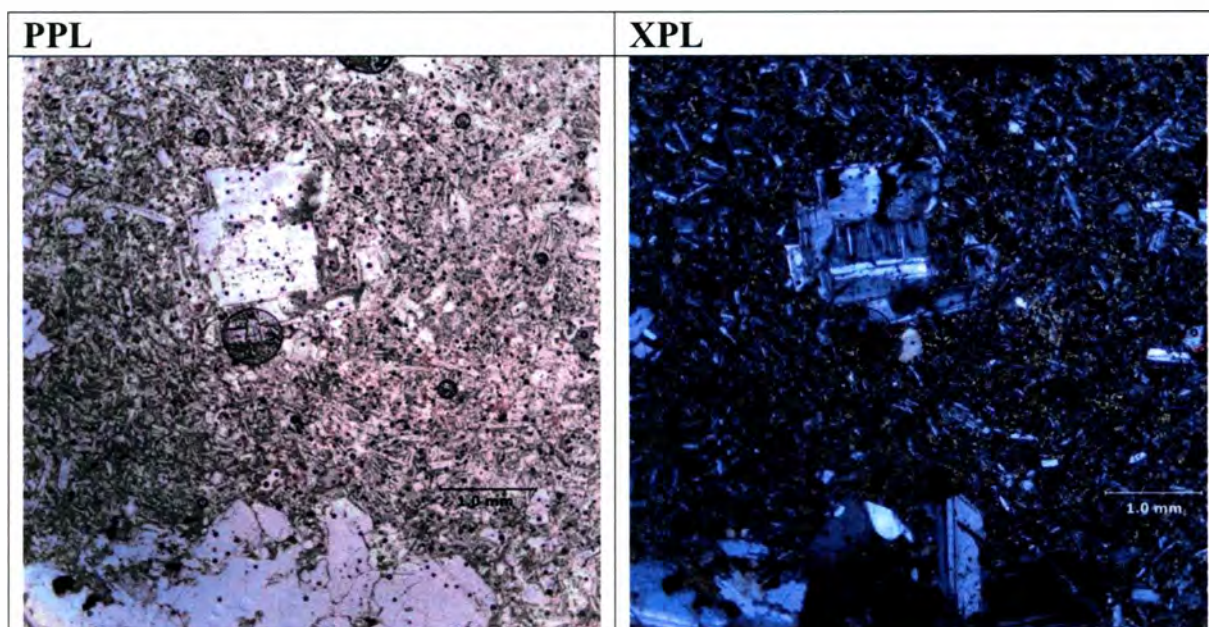
Up to 3mm

Structures

No crystal growth pattern

**Microscopic
Descriptions****Mineral percentage**

Plagioclase- 50%++	Pumice	Lithics
Biotite	Hornblende- 25%	Calcite
Oxides	Glass Matrix- 25%	



Sample Number

Pks073-5-t

Locality:80 meters on strat column
Kulshan caldera sedimentary
unit**Rock Type:**

Lithic wacke

**Megascopic
Description****Color**

White/green/grey

Sedimentary structures

Planar bedding

Grain size

Medium to coarse sand

Induration

Well lithified

**Microscopic
Descriptions****Mineral percentage**

Plagioclase- 50%	Pumice	Lithics- 20%
Biotite	Hornblende- 15%	Calcite
Oxides	Glass Matrix- 10%	

Textures**Rounding**

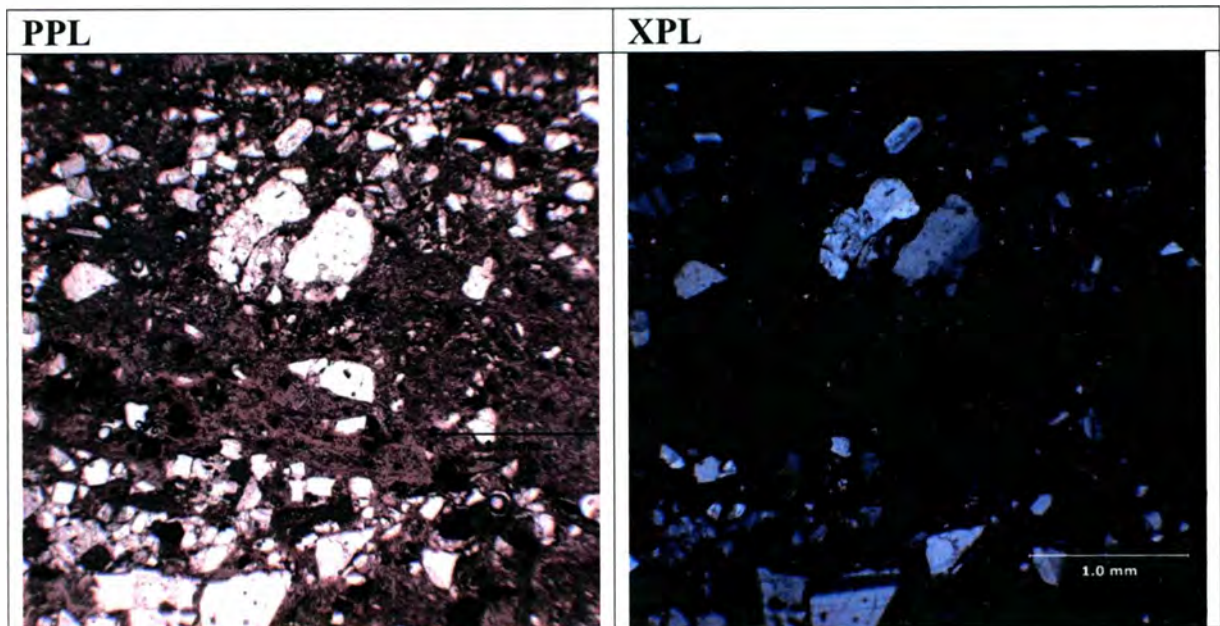
Angular

grain to grain relations

Grain supported

Sorting

Well sorted



Sample Number

Pks073-5-m

Locality:

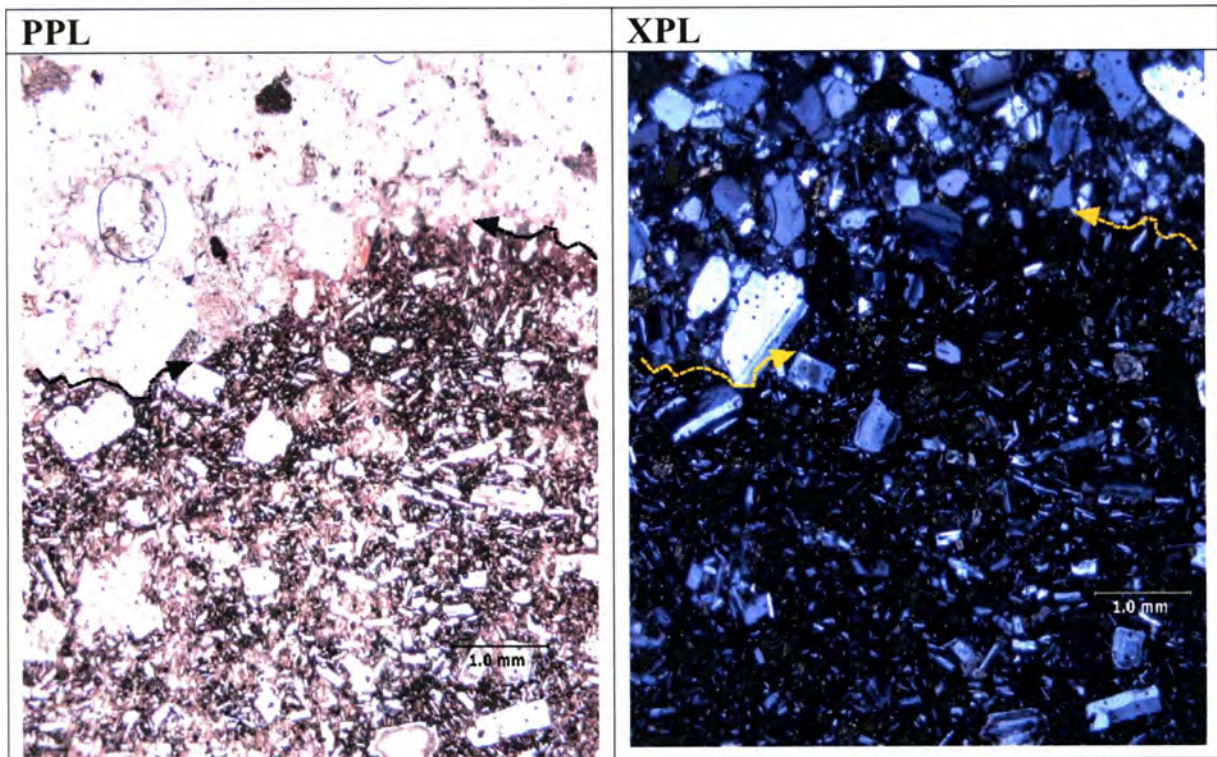
80 meters on strat column
Kulshan caldera sedimentary
unit

Rock Type:

Andesite sand interaction

Sedimentary Structures

This is a thin section of lava sill and sedimentary rocks interaction. Note the crystal size compared to Sample Pkl 66-3. There is a comparable zone of cooling found the upper lava of this thin section.



Sample Number

Pks093-4

Locality:99 meters on strat column
Kulshan caldera sedimentary
unit**Rock Type:**

Lithic/Feldspathic wacke

**Megascopic
Description****Color**

Buff

Grain size

Medium sand

Induration

Good

Sedimentary structures

Laminar bedding

**Microscopic
Descriptions****Mineral percentage**

Plagioclase- 40%	Pumice- 10%	Lithics- 25%
Biotite	Hornblende- 10%	Calcite
Oxides- 5%	Glass Matrix- 10%	

Textures**Rounding**

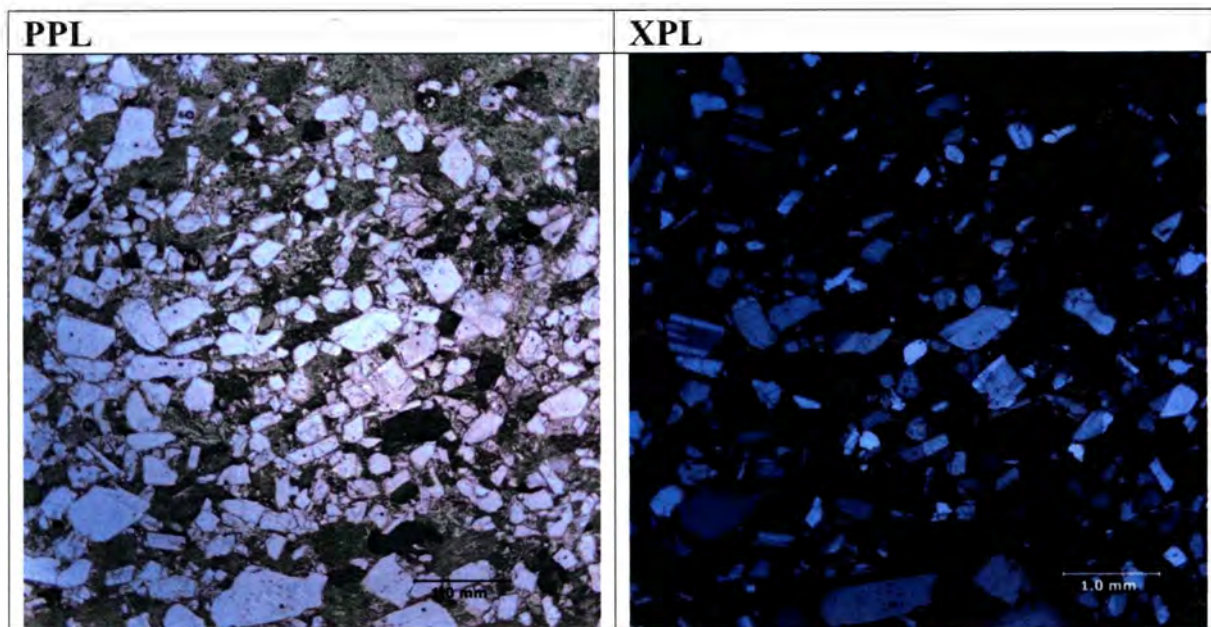
Angular

grain to grain relations

Grain supported

Sorting

Good sorting



Sample Number

Pks099-3-b

Locality:105 meters on strat column
Kulshan caldera sedimentary
unit**Rock Type:**

Feldspathic wacke

**Megascopic
Description****Color**

tan to light brown

Sedimentary structuresLaminar bedding 4 mm-
<1 mm silt beds usually
smaller**Grain size**

Fine grained sand to silt

Induration

Medium

**Microscopic
Descriptions****Mineral percentage**

Plagioclase- 35%	glass/pumice/ash	Lithics- 10%
Biotite	Hornblende- 15%	Calcite
Oxides- 3%	Matrix- 35% glass	

Textures**Rounding**

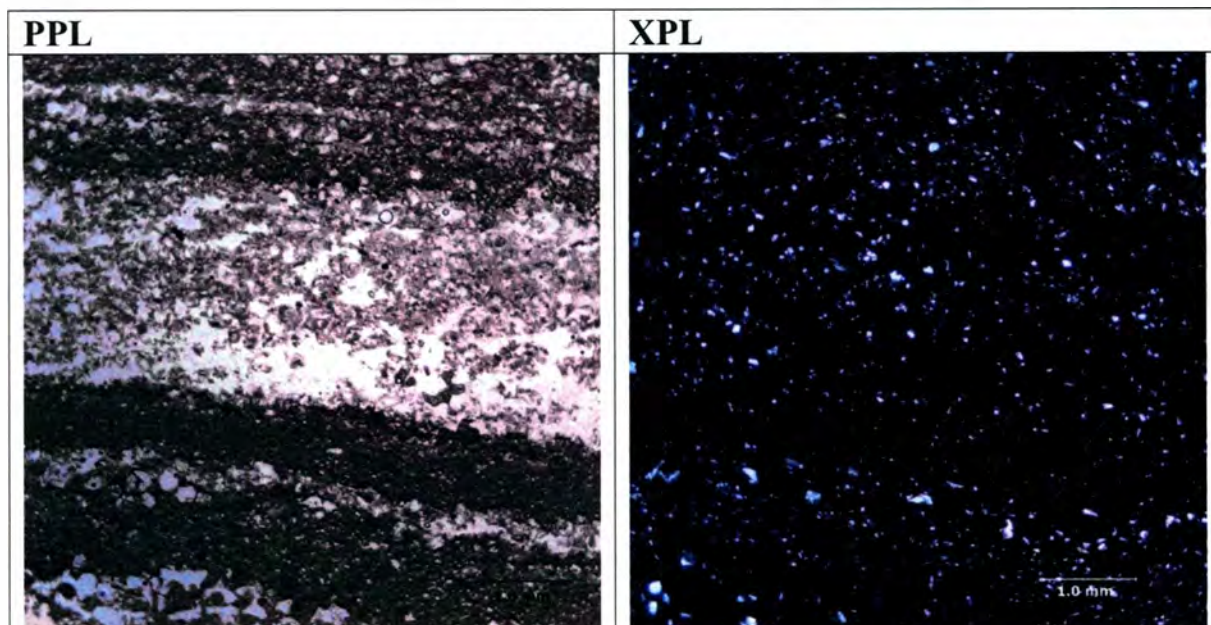
Angular

grain to grain relations

Grain supported

Sorting

good sorting



Sample Number

Pks110-2-b

Locality:116 meters on strat column
Kulshan caldera sedimentary
unit**Rock Type:**

Feldspathic/lithic wacke

**Megascope
Description****Color**

Brown and light brown

Sedimentary structures

Laminated beds

Grain size

Fine sands

Induration

Good

**Microscopic
Descriptions****Mineral percentage**

Plagioclase- 45%	pumice- 15%	Lithics- 25%
Biotite	Hornblende- 10%	calcite
Oxides- 3%	matrix	

Textures**Rounding**

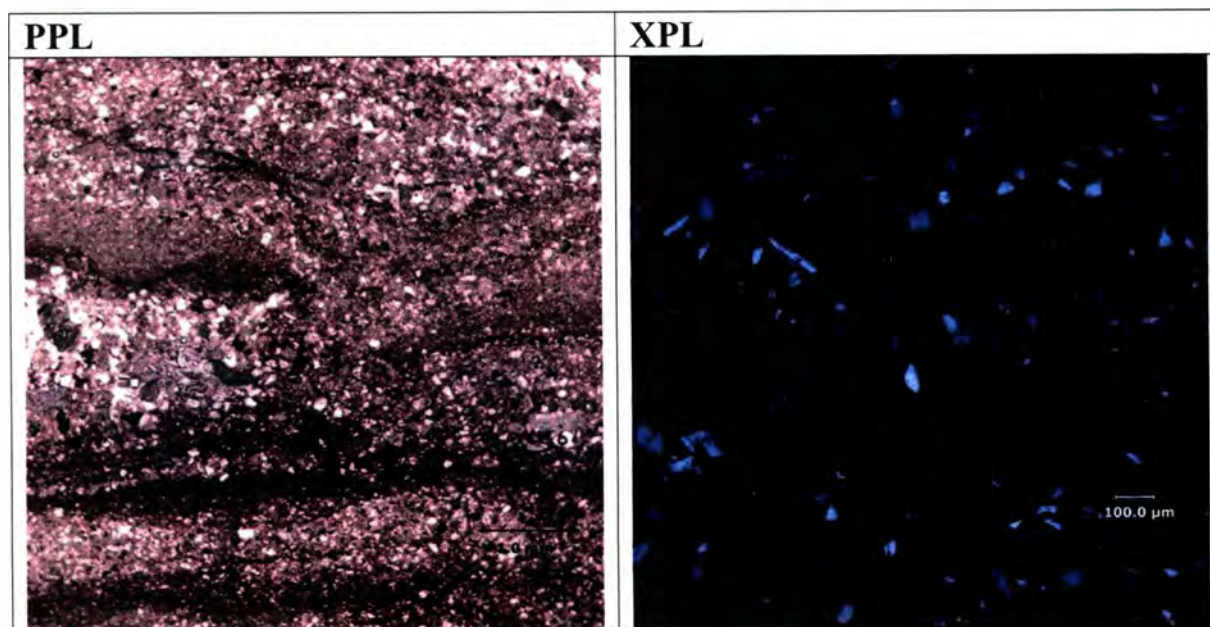
Angular

grain to grain relations

Grain supported

Sorting

poor sorting



Sample Number

Pkcd-2

Locality:20-40 meters on strat column
Kulshan caldera sedimentary
unit**Megascopeic
Description****Color**Light brown to dark
brown**Grain size**

Fine sand to mud

Induration

Poor

Sedimentary structures

This came from a clastic dike. There are vertical beds of mud, silt, and sand. Grading however is not is typical flow patterns but instead, all layers are variously interspersed throughout the dike.

Megascopeic**Mineral percentage**

Plagioclase- 45%	pumice-	Lithics- 20%
Biotite	Hornblende-	Calcite
Oxides- 5%	Matrix- 35%	

Textures**Rounding**

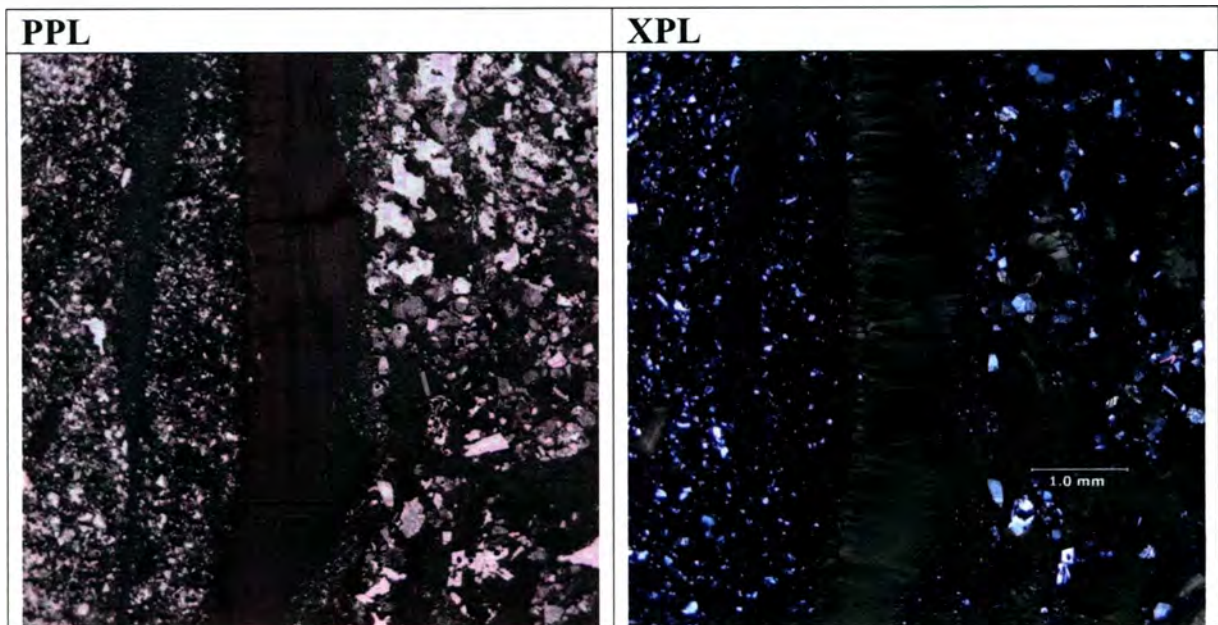
Angular

grain to grain relations

Grain supported

Sorting

poor sorting



Sample Number

Pkd 2-t

Locality:Dike is found from
21-70 meters Kulshan caldera
sedimentary unit**Rock Type:**

Andesite dike

**Megascopic
Description****Color**

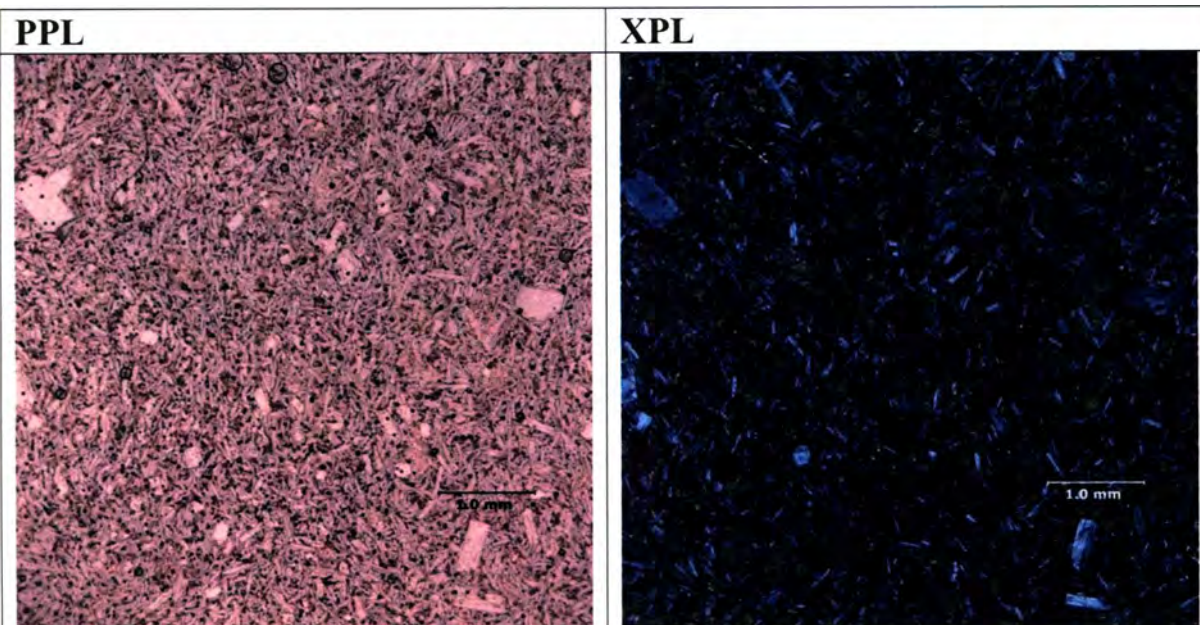
red brown

Crystal size

Up to 2mm

StructuresCrystal growth is in the
same direction as flow**Microscopic
Descriptions****Mineral percentage**

Plagioclase- 50%++	Pumice	Lithics
Biotite	Hornblende- 25%	Calcite
Oxides	Glass Matrix- 25%	



APPENDIX D

AGE

After the failed attempt to determine the dates or rates of sedimentation of the lacustrine environment at Kulshan caldera using paleomagnetism, I tried dating the andesite sill to possibly add another constraint. The sill does not give a definitive age but it possibly constrain the age more than the 0.992 ± 0.014 Ma lava of Camp Kiser. I crushed and separated out hornblende minerals in the clean lab at the Pacific Centre for Isotopic and Geochemical Research at the University of British Columbia. Using the Laser-Equipped Noble Gas Mass Spectrometer (Micromass VG 5400), Dr. Tom Ullrich analyzed the $^{40}\text{Ar}/^{39}\text{Ar}$ ratio in the hornblendes in order to date the lavas.

The equation for Hornblende is $\text{Ca}_2(\text{Mg,Fe,Al})_5(\text{Al, Si})_8\text{O}_{22}(\text{OH})_2$. ^{40}Ar often replaces Ca_2 in the equation. Samples of hornblende from the sill at Kulshan caldera were dated and their results (Table D 1 and Figure D 1) indicate that there was not enough ^{40}Ar in the hornblende to reduce the error. The sample came back with an age of $1.02 \pm .45$ Ma, which is a date with an error of 45%. It is most probable to presume that ^{40}Ar likely went preferentially into plagioclase rather than hornblende (Dr. Tom Ullrich, pers. comm.). The shear percent of plagioclase in the sill helps to prove this interpretation. This is the reason plagioclase was dated in previous studies (Hildreth, 1996; Hildreth et al., 2004).

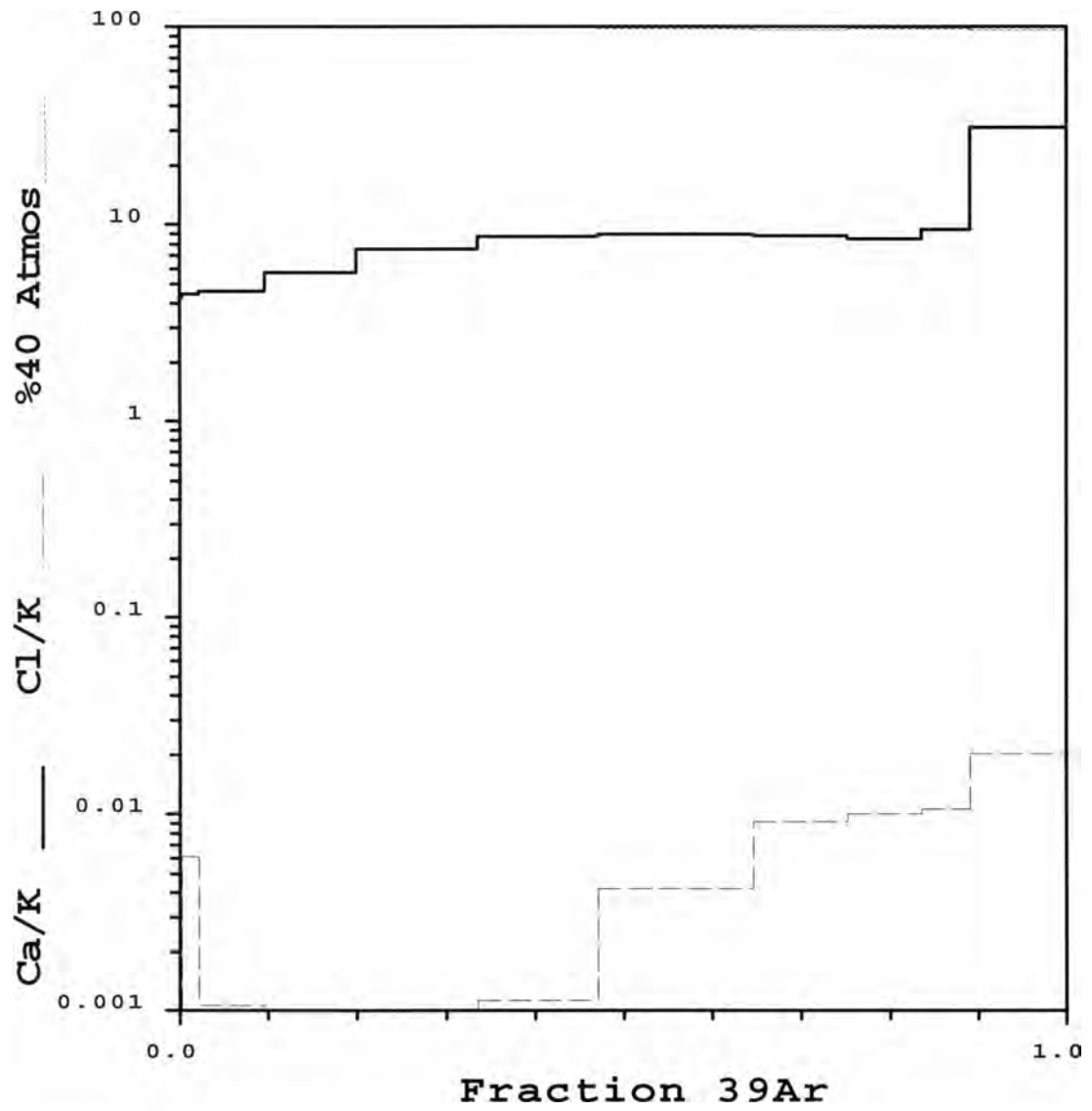


Figure D 1. Plateau age for hornblende from Kulshan caldera is 1.02 ± 0.45 Ma

APPENDIX E

Maps

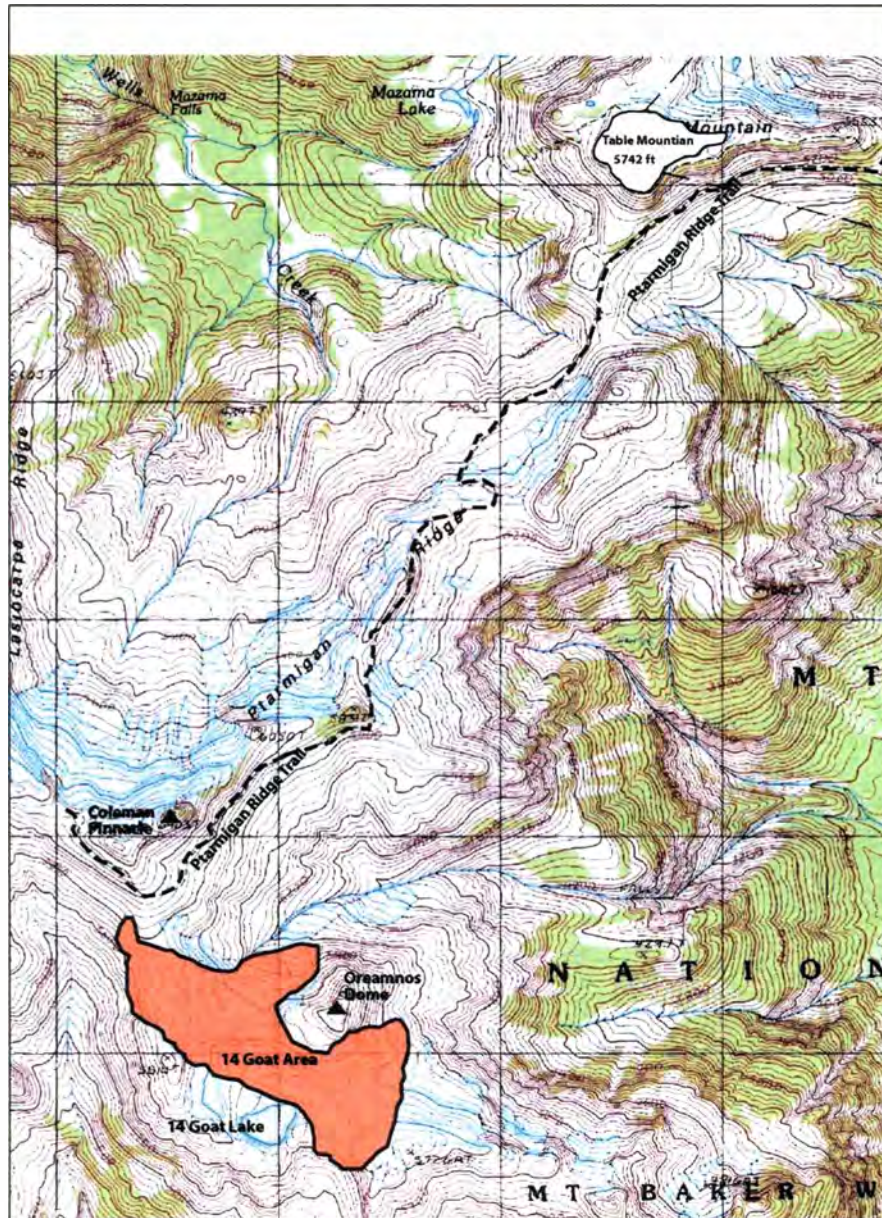


Figure E 1 Map of the trail from Artist Point to 14 Goat area. It is 5 miles from the parking lot to the 14 Goat lake. The trail is referred to as the Ptarmigan Ridge Trail and is a very easy hike through alpine meadows between both Mount Baker and Shuksan.

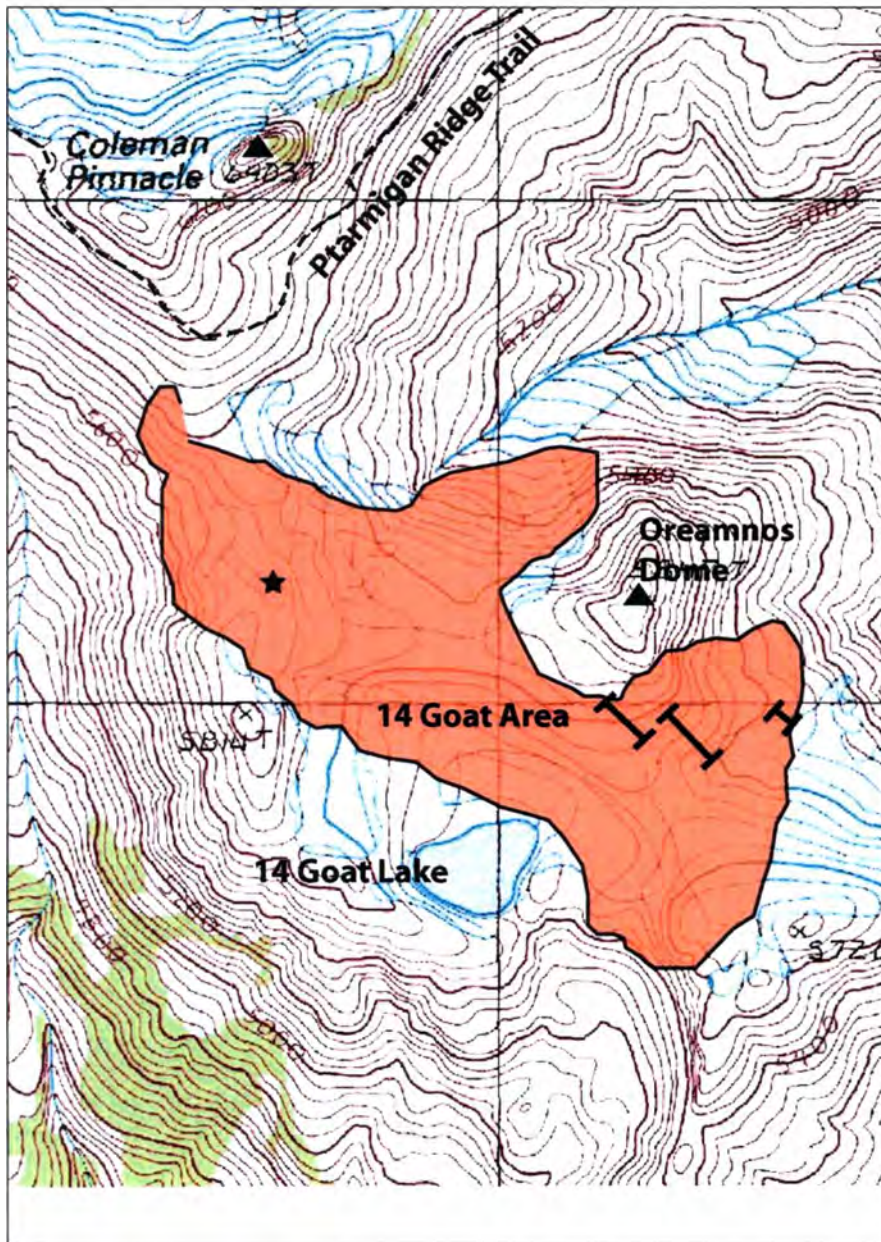


Figure E 2. Is a topographic map of the 14 Goat area and the locations of the section lines for the stratigraphic column. Additionally the star denotes the location of the raindrop imprints and ripplemarks. The UTM coordinates can be found in Table E 1.

Table E 1 UTM Coordinates collected on NAD83

	X (meters)	Y (meters)
Section 1 bottom	593,606.202	5,407,026.057
Section 1 top	593,568.085	5,407,039.160
Section 2 bottom	593,410.852	5,406,892.647
Section 3 top	593,347.720	5,407,020.101
Section 4 bottom	593,281.015	5,406,924.808
Section 4 top	593,208.355	5,407,003.425
Raindrops and ripples	592,554.407	5,407,233.319

REFERENCE

United States Geological Survey. 1989. Shuksan Arm- 7.5 min. topographic quadrangle, Reston, Virginia, 1989.